# A Two Parameter Approach To Elastic-Plastic Fracture Mechanics.

By

Abderrahmane Nekkal.

Submission for the degree of
MSc.

Department of Mechanical Engineering.
University of Glasgow.

Scotland.

January 1991.



ProQuest LLC.
789 East Eisenhower Parkway
P.O. Box 1346
Ann Arbor, MI 48106 – 1346

# Contents

## Aknowledgement

I wish to express my gratitude to my supervisor Prof. J. W. Hancock, for his valuable guidance and continuous help throughout this work.

My gratitude is extended to Hibbitt, Karlsson and Sorensen for access to Abaqus under academic licence. I am also indebted to Mr A. Torry and Mr N. Flaherty for their assistance in the experimental work and to Mr Al-Ani for his valuable help. Many thanks are due to the Algerian Goverment for their financial support throughout the period of my study.

Last but not least, I would like to thank my mother, sisters and my friends for their continuous moral support.

Abstract

The work presented in this thesis establishes techniques for the implementation of two parameter fracture mechanics. Two parameter fracture mechanics is based on the characterisation of elastic-plastic crack tip fields by the crack tip opening displacement (C.T.O.D) or equivalently by the J-contour integral introduced by Rice (1968), and the elastic T-stress which is the non-singular term in the Williams expansion (1957). In order to establish failure criteria in the form of a C.T.O.D-T fracture locus, it was necessary to design and analyse specimens which were capable of producing a range of T-stresses. An eccentrically loaded single edge crack bar was used to produce a range of bending to tension ratios on the ligament. Linear elastic finite element analyses established the relationship between the T-stress and the applied loading. Subsequent non-linear finite element analyses established techniques for the measurement of J and hence C.T.O.D.

Experiments were carried out to evaluate the C.T.O.D and corresponding T-stresses on a Carbon-Manganese steel designated 50D under B.S 4360. These experiments were performed at a range of low temperatures to verify both the validity of linear elastic fracture mechanics and the extent to which a single parameter fracture criterion could be used . At temperatures at which single parameter characterisation was not valid, the newly developed two parameter characterisation in the form of C.T.O.D-T locus was introduced together with available test results from a similar steel but different geometry. The experimental results verified

the applicability of the technique.

In order to extend finite element techniques to realistic engineering defects, it was necessary to develop techniques to evaluate T for semi-elliptical defects. Stress intensity factors K and T-stresses were determined using a line spring analysis for semi-elliptical cracks in a chosen geometry under pure bending for a range of crack depth to thickness ratios.

# 1 Introduction

Fracture mechanics is a branch of engineering which is concerned with maintaining the integrity of structures which contain cracks or flaws. The objective is the prediction of the behaviour of defects in large, complex structures based on results obtained from small, simple laboratory tests which quantify the critical combinations of stress and crack size.

Fracture mechanics can be divided into two areas; linear elastic fracture mechanics (henceforth L.E.F.M) and elastic-plastic fracture mechanics (henceforth E.P.F.M). L.E.F.M attempts to define the conditions when a crack extends by providing a description of the elastic stress and strain fields local to the crack tip. Under valid L.E.F.M conditions, fracture occurs at stresses appreciably below the yield stress when a body is largely elastic, and non-linear effects such as plasticity are neglected. L.E.F.M is subject to geometric restrictions which are based on the requirement that plasticity is restricted to a small zone at the crack tip. When plasticity at the crack tip becomes significant, the use of L.E.F.M is invalidated. The restriction of L.E.F.M. can be relaxed by E.P.F.M concepts. Elastic-plastic fracture parameters were developed in the 1960's notably by Rice (1968) and Hutchinson (1968). As a result, elastic-plastic stress fields can be characterised by either the crack tip opening displacement or the J contour integral. The fields are characterised by a single dominant parameter, J, if the dimensions of a given specimen are satisfied. These requirements are particularly severe for deep cracks in tension and for shallow

cracks in general. Recent work by Hancock and co-workers (Al-Ani and Hancock 1991), (Betegón and Hancock 1990), (Du and Hancock 1990) and (Sumpter and Hancock 1990) showed that the effect of the second term in the Williams (1957) expansion (denoted T) controls the crack tip constraint, and can be used in combination with either the C.T.O.D or J as a two parameter fracture criterion. The two parameter approach significantly relaxes the restrictions associated with single parameter fracture mechanics.

In the present work, following a literature review of elementary mechanics given in Section 2, the basis of L.E.F.M is discussed in Section 3. In order to establish a suitable method for the determination of L.E.F.M parameters (K and T) under plane strain conditions, simple finite element techniques were used and compared with available published solutions. This is described in Section 4. To obtain the relationship between T and applied loadings, finite element analyses under plane strain elastic conditions were necessary. In Section 5, E.P.F.M is reviewed as an introduction to the design of a simple specimen geometry to generate a range of T-stresses as described in Section 6. The same geometry was analysed under elastic-plastic conditions using finite element techniques to relate J to the applied loadings, as outlined in Section 7. In addition, laboratory experiments were carried out based on the geometry chosen in the finite element calculations to evaluate the critical crack tip opening displacement of a carbon-manganese steel designated 50D under B.S 4360, and its relation to T at low temperatures as detailed in Section 8. Finally, elastic analyses were performed for semi-elliptical surface cracks for a chosen geometry subject to pure

bending, for which K and T were determined. Section 9 describes the techniques used to evaluate these parameters, and comparison of the evaluated stress intensity factors is made with available published solutions.

# 2 Stress and Strain

## 2.1 Stress

The concept of stress is fundamental to mechanics, and describes the way in which forces are transmitted through a solid body. To illustrate this, consider the isolated, prismatic element shown in Fig 2.1 subject to arbitrary forces in a cartesian system of axes (x,y,z). If the element is small enough, these forces may be considered to be distributed uniformly over each face. Given that the force $\underline{F}$ is a vector with components $F_j$ then the stress on any particular face is then defined as the component of the force $F_j$ divided by the appropriate area $A_i$ :

$$\sigma_{ij} = \lim \frac{F_j}{A_i} \qquad 2.1$$

The stresses $\sigma_{ij}$ acting on planes whose normals are parallel to the coordinate axes are known as the components of the stress tensor and are illustrated in Fig 2.1. The convention is that i and j may be x, y or z. The first index (i) refers to the direction of the normal to the plane on which the stress acts, and the second index (j) refers to the direction of the force components. Thus the component $\sigma_{zy}$ arises from a force in the z direction which acts on a plane whose normal is in the y direction. The stress $\sigma_{ij}$ is positive if the force acts in the positive j direction on a plane whose outward normal points in the positive i direction. Under such definition, all of the stresses illustrated in Fig 2.1 are positive.

## 2.2 Equilibrium Equations

The components of the stress tensor cannot be specified arbitrarily. For a static body, the requirement that the forces be in equilibrium imposes certain conditions on these stress components. From moment equilibrium conditions the stress tensor is necessarily symmetric :

$$\sigma_{ij} = \sigma_{ji} \quad (i,j = x, y \text{ or } z) \qquad 2.2$$

and from force equilibrium considerations the components of the stress tensor must satisfy the equations :

$$\frac{\partial \sigma_{xx}}{\partial x} + \frac{\partial \sigma_{yx}}{\partial y} + \frac{\partial \sigma_{zx}}{\partial z} + \beta_x = 0$$

$$\frac{\partial \sigma_{xy}}{\partial x} + \frac{\partial \sigma_{yy}}{\partial y} + \frac{\partial \sigma_{zy}}{\partial z} + \beta_y = 0 \qquad 2.3$$

$$\frac{\partial \sigma_{xz}}{\partial x} + \frac{\partial \sigma_{yz}}{\partial y} + \frac{\partial \sigma_{zz}}{\partial z} + \beta_z = 0$$

where $\beta_x$, $\beta_y$ and $\beta_z$ are body forces. Equations 2.3 are known as the equilibrium equations.

In the absence of body forces, these equations may simply be written as :

$$\sigma_{ij,\, x_j} = 0 \qquad 2.4$$

where the comma denotes differentiation, and the three axes $x_j$ are identified with x, y, z.

## 2.3 Strain

The concept of strain is used to specify the way in which a solid, continuous body deforms when it is subjected to stress. Deformation represents a change of geometry due to the relative displacement of points in the body excluding those due to rigid body motion. The state of strain at a point in a body is specified by the components of the strain tensor. These components give the normal and shear strains for infinitesimal line elements originally parallel to the coordinate axes. They are defined in terms of the components of the displacement vector $u_i$ :

$$e_{xx} = \frac{\partial u_x}{\partial x} \quad ; \quad e_{yy} = \frac{\partial u_y}{\partial y} \quad ; \quad e_{zz} = \frac{\partial u_z}{\partial z}$$

$$e_{xy} = \frac{1}{2}\left(\frac{\partial u_x}{\partial y} + \frac{\partial u_y}{\partial x}\right) ; e_{xz} = \frac{1}{2}\left(\frac{\partial u_x}{\partial z} + \frac{\partial u_z}{\partial x}\right) ; e_{yz} = \frac{1}{2}\left(\frac{\partial u_y}{\partial z} + \frac{\partial u_z}{\partial y}\right)$$

2.5

Symmetry of the strain tensor further requires that :

$$e_{xy} = e_{yx} \quad ; \quad e_{xz} = e_{zx} \quad ; \quad e_{yz} = e_{zy} .$$

More compactly, the strain may be defined for small deformations as :

$$e_{ij} = \frac{1}{2}\left(u_i , x_j + u_j , x_j\right) \qquad 2.6$$

where the comma denotes partial differentiation.

The components $e_{xx}$ , $e_{yy}$ and $e_{zz}$ are the normal strains which

represent the changes in length per unit length of infinitesimal line elements in the x, y and z directions, respectively. Normal strains are positive for extensions. The strain components $e_{ij}$ ( $i \neq j$ ) are the shear strains. Physically the shear strain can be considered to represent one half the change of angle between two infinitesimal line elements originally parallel to the $x_i$ and $x_j$ axes. Shear strains are positive for a decrease in the right angle between any two positive ( or negative ) coordinate axes as illustrated in Fig 2.2

## 2.4 Compatibility

Eliminating the displacements $u_i$ from the strain-displacement equation (2.6) gives the compatibility relations, which ensure that the displacements and strains are consistent. In cartesian-coordinates these equations are :

$$\frac{\partial^2 e_{xx}}{\partial y^2} + \frac{\partial^2 e_{yy}}{\partial x^2} = 2 \frac{\partial^2 e_{xy}}{\partial x \partial y}$$

$$\frac{\partial^2 e_{yy}}{\partial z^2} + \frac{\partial^2 e_{zz}}{\partial y^2} = 2 \frac{\partial^2 e_{yz}}{\partial y \partial z} \qquad 2.7$$

$$\frac{\partial^2 e_{zz}}{\partial x^2} + \frac{\partial^2 e_{xx}}{\partial z^2} = 2 \frac{\partial^2 e_{xz}}{\partial z \partial x}$$

## 2.5 Stress/Strain Relationship in Elastic Solids

The tensile bar illustrated in Fig 2.3, subject to a normal stress $\sigma_{xx}$, will experience a corresponding direct strain $e_{xx}$. For linear elastic small strain reversible deformation, the stress is proportional to strain and the constant of proportionality is Young's modulus E.

$$e_{xx} = \frac{1}{E}\sigma_{xx} \qquad (\sigma_{yy} = \sigma_{zz} = 0) \tag{2.8}$$

The associated transverse strains $e_{yy}$ and $e_{zz}$ are defined through Poisson's ratio $\upsilon$ such that :

$$e_{yy} = e_{zz} = -\upsilon e_{xx} = -\frac{\upsilon}{E}\sigma_{xx} \qquad (\sigma_{yy} = \sigma_{xx} = 0) \tag{2.9}$$

The stress/strain relations for an isotropic, linear elastic body can now be written in the form :

$$e_{xx} = \frac{1}{E}[\sigma_{xx} - \upsilon(\sigma_{yy} + \sigma_{zz})]$$

$$e_{yy} = \frac{1}{E}[\sigma_{yy} - \upsilon(\sigma_{xx} + \sigma_{zz})]$$

$$e_{zz} = \frac{1}{E}[\sigma_{zz} - \upsilon(\sigma_{xx} + \sigma_{yy})] \tag{2.10}$$

$$e_{xy} = \frac{1}{2G}\sigma_{xy} \quad ; \quad e_{xz} = \frac{1}{2G}\sigma_{xz} \quad ; \quad e_{yz} = \frac{1}{2G}\sigma_{yz}$$

where G is the shear modulus related to Young's modulus and Poisson's ratio by :

$$G = \frac{1}{2} \frac{E}{(1+\upsilon)} \qquad 2.11$$

A more general relation between the stress tensor $\sigma_{ij}$ and the strain tensor $e_{kl}$ is given by the fourth order stiffness tensor Cijkl :

$$\sigma_{ij} = C_{ijkl}\, e_{kl} \qquad 2.12$$

It may be noted that $C_{ijkl}$ involves 81 elastic constants. Both the stress and strain tensors are symmetric ($\sigma_{ij} = \sigma_{ji}$ and $e_{ij} = e_{ji}$ ), and only six values of stress are related to six values of strain, so that at most 36 elastic constants will be involved. Furthermore, from arguments based upon strain energy, it may be shown that for an isotropic material compliances such as $C_{1211}$ are zero, so that the maximum number of elastic constants reduce to 21. The most general form of Hooke's Law contains 21 elastic constants. Equation (2.15) may also be written in terms of the compliance tensor $S_{ijkl}$ :

$$e_{ij} = S_{ijkl}\, \sigma_{ij} \qquad 2.13$$

where $S_{ijkl}$ is again a symmetric fourth order tensor with properties of symmetry involving 21 independent components.

## 2.6 Plane Stress/Plane Strain

Many engineering problems are essentially two dimensional in nature and can be idealised as either plane stress or plane strain. Plane stress with respect to the x, y plane is defined by the condition :

$$\sigma_{zz} = \sigma_{xz} = \sigma_{yz} = 0$$

In plane strain deformation the displacements are restricted to the plane. This allows plane strain to be described in terms of the strains :

$$e_{zz} = e_{xz} = e_{yz} = 0$$

## 2.7 Stress Functions

The problem of determining the stress and strain distribution in a body subject to arbitrary prescribed boundary conditions, can now be stated as a search for stress distributions which satisfy the equilibrium equations, and strain distributions which satisfy the compatibility condition. The stresses and strains must be connected by the stress-strain relations, and both must satisfy the appropriate boundary conditions.

The problem can be further reduced for linear elastic deformation in a way proposed by Airy (1862) for two dimensional problems. The stress-strain relations may be substituted into the compatibility equations, enabling them to be expressed in terms of stresses. Now consider an analytic function $\phi$ from which the stresses may be defined in the absence of body forces as :

$$\sigma_{xx} = \frac{\partial^2 \phi}{\partial x^2}$$

$$\sigma_{yy} = \frac{\partial^2 \phi}{\partial y^2}$$

$$\sigma_{xy} = - \frac{\partial^2 \phi}{\partial x \partial y}$$

2.14

Direct substitution shows that the equilibrium relations are satisfied, while substitution in the compatibility relations expressed in terms of stresses shows that compatibility is satisfied by the biharmonic equation :

$$\nabla^2 ( \nabla^2 \phi ) = 0 \qquad 2.15$$

The function $\phi$ may be real or complex. As an illustration, the method proposed by Westergaard (1952) is summarised. This is particularly useful for bodies containing cracks. The co-ordinates (x,y) are combined as the real and imaginary components of a complex number z :

$$z = x + iy \qquad 2.16$$

Stress functions are now analytical functions of z which satisfy the biharmonic subject to appropriate boundary conditions. The stresses can be derived as shown by Dugdale and Ruiz (1971)in the form :

$$\sigma_{xx} = \text{Re } \phi (z)'' - y \text{ Im } \phi (z)''$$

$$\sigma_{yy} = \text{Re } \phi (z)'' + y \text{ Im } \phi (z)''$$

$$\sigma_{xy} = - y \text{ Re } \phi (z)''$$

2.17

Here Re, Im denote the real and imaginary parts of the function

and the prime " ' " denotes differentiation with respect to z.
As an example which is relevant to the present work, consider a central crack in an infinite sheet subject to bi-axial tension. The crack lies in the x-axis in the region -a > r > a. Westergaard (1952), has given an appropriate stress function in the form :

$$\phi(z)' = \sigma (z^2 - a^2)^{\frac{1}{2}} \qquad 2.18$$

from which differenciation gives :

$$\phi(z)'' = \sigma z (z^2 - a^2)^{-\frac{1}{2}} \qquad 2.19$$

$$\phi(z)''' = -\sigma z^2 (z^2 - a^2)^{-3/2} \qquad 2.20$$

The stress field can now be found from equations 2.17. However, it is simpler to restrict interest to the plane directly ahead of the crack tip for which y=o. The imaginary parts now disappear and give :

$$\sigma_{xx} = \text{Re}\ \phi(z)'' = \frac{\sigma x}{\sqrt{(x^2 - a^2)}} \qquad 2.21$$

where $\sigma_{yy}=0$.
Changing co-ordinates to the crack tip, r=x-a :

$$\sigma_{xx} = \sigma_{yy} = \frac{\sigma (r+a)}{\sqrt{(r^2 + 2ar)}} \qquad 2.22$$

For small distances r << a :

$$\sigma_{xx} = \sigma_{yy} = \frac{\sigma a}{\sqrt{2ar}} = \sigma \sqrt{\frac{a}{2r}} \qquad 2.23$$

As r tends to zero, there is a stress singularity at the crack tip. This is discussed in the next section (Section 3).

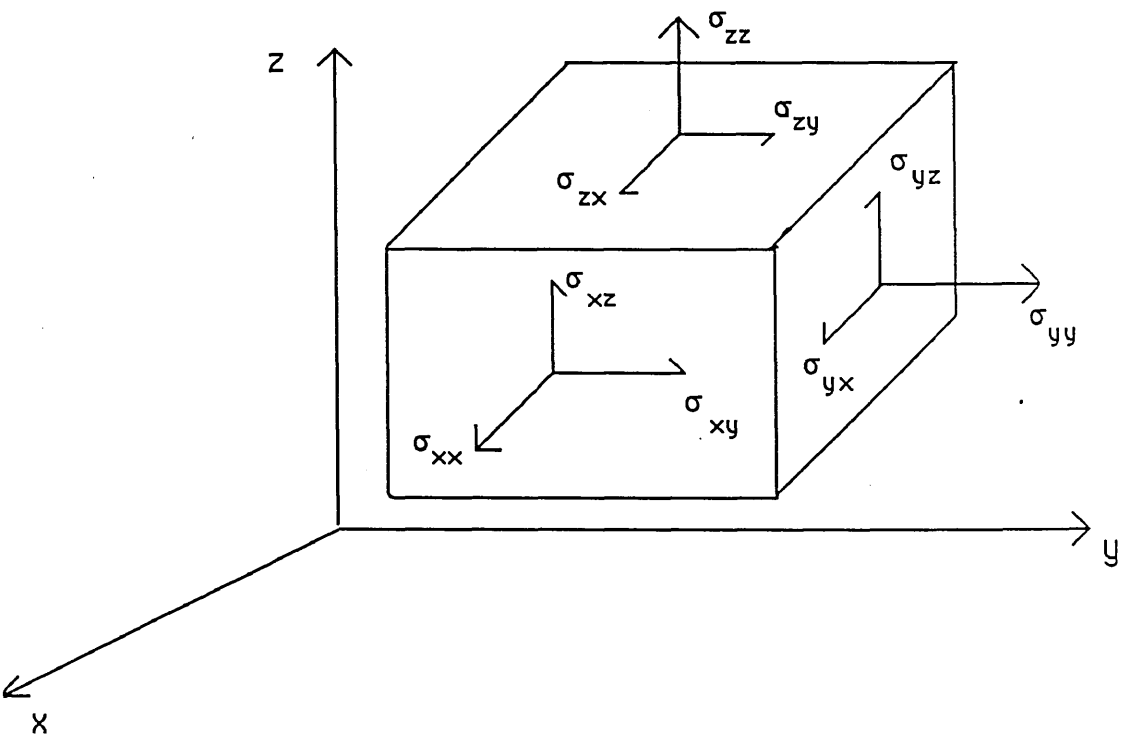


Stress components referred to cartesian axes.

Fig 2.1

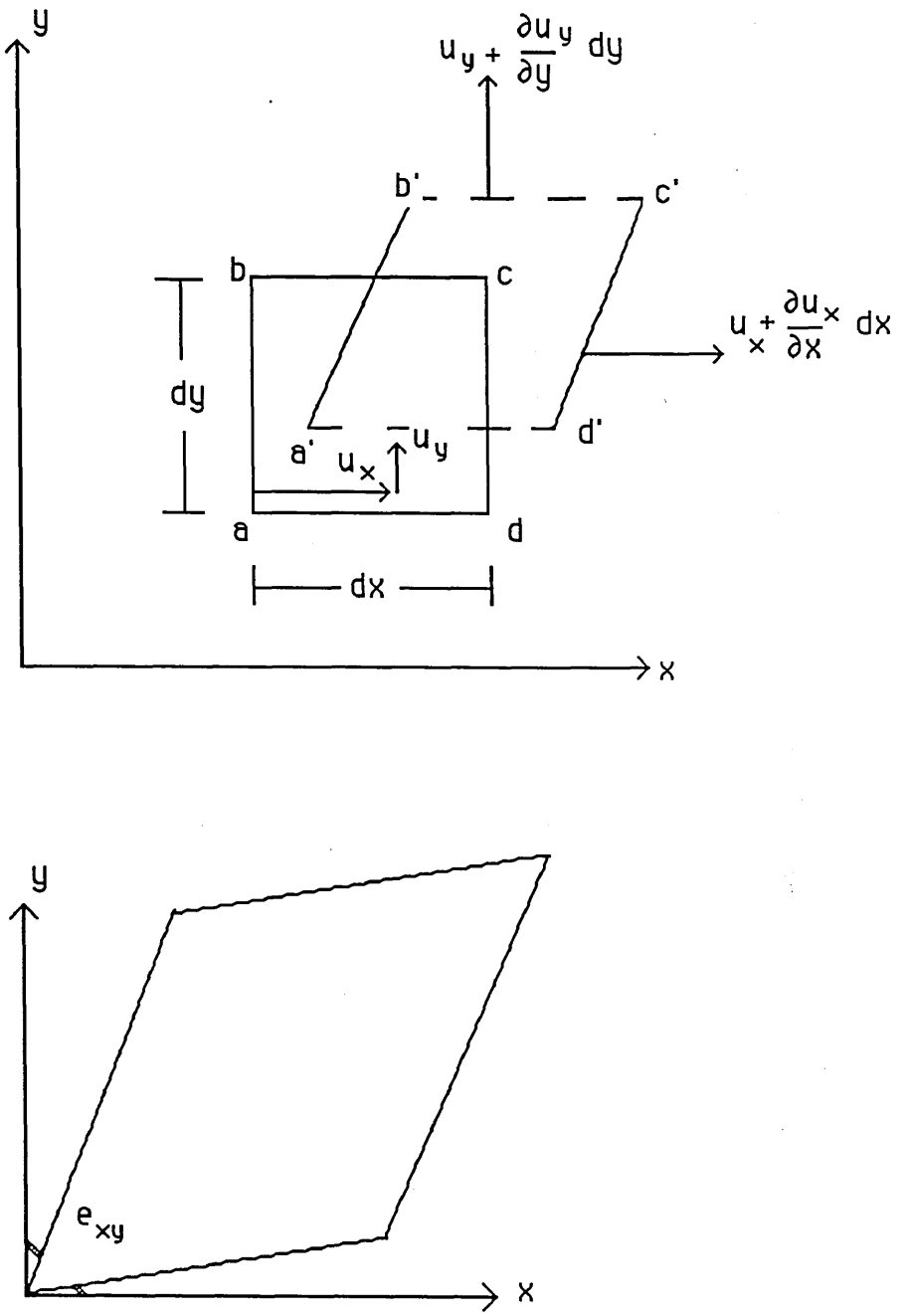





Displacements and strains referred to cartesian axes.

Fig 2.2

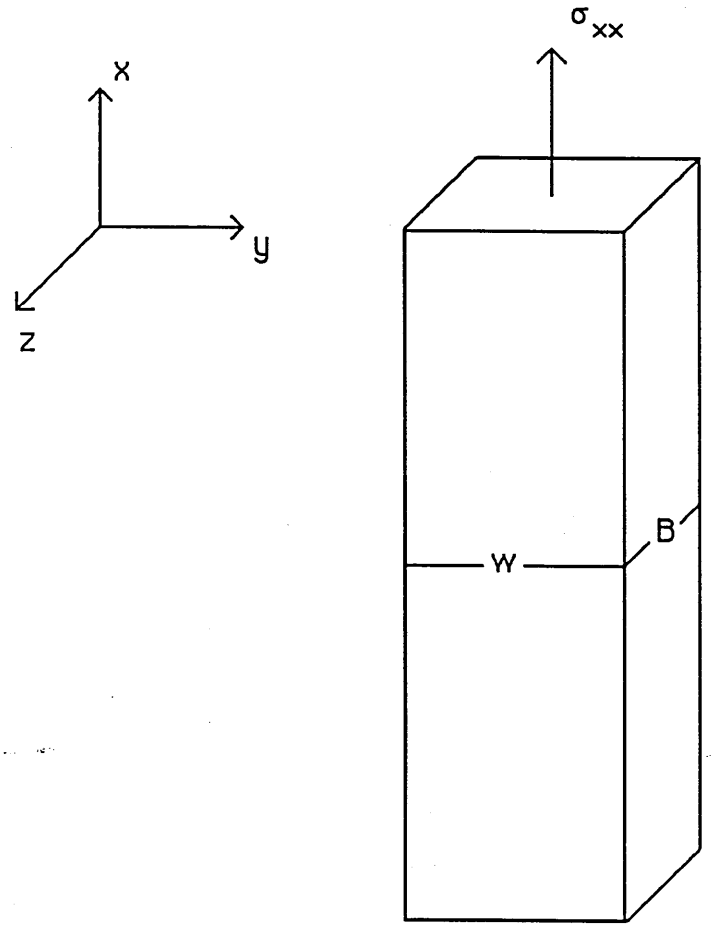


Tensile bar subject to a normal stress $\sigma_{xx}$.

Fig 2.3

# 3 Linear elastic fracture mechanics

## 3.1 Introduction

Linear elastic fracture mechanics (henceforth LEFM) attempts to define the conditions when a crack extends by providing a description of the stress and strain fields local to crack tip. The origins of fracture mechanics lie in Griffith's energy criterion (1921) for the propagation of pre-existing cracks. Griffith's criterion is based on the concept that a crack can propagate when the elastic energy released during crack extension is equal to or higher than the surface energy required to create the newly formed crack surface. The elastic energy released by introducing a slit of length 2a and unit thickness into a body under fixed grip conditions is given by :

$$w_e = \pi a^2 \frac{\sigma^2}{E'} \qquad 3.1$$

where $\sigma$ is the stress applied and

$$E' = E \qquad \text{for plane stress}$$

$$E' = \frac{E}{1-\upsilon^2} \qquad \text{for plane strain}$$

The surface energy required to create the total crack surface is :

$$w_s = 4a\gamma \qquad 3.2$$

where $\gamma$ is the surface energy per unit area. Crack extension is assumed to occur when the potential energy U(a) is stationary or

decreases

$$U(a)= w_s(a)-w_e(a) \qquad 3.3$$

Hence:

$$\frac{dU}{da} = 0 = 4\gamma - 2\pi a \frac{\sigma^2}{E'} \qquad 3.4$$

which leads to :

$$\sigma\sqrt{\pi a} = \sqrt{2\gamma E'} \qquad 3.5$$

Equation 3.5 can be written in the form :

$$K = \sqrt{E' G} \qquad 3.6$$

where :

$$K = \sigma\sqrt{\pi a} \qquad 3.7$$

and :

$$G = 2\gamma \qquad 3.8$$

Here, K is a parameter called the stress intensity factor which has units of $N/m^{-3/2}$, and G is known as the strain energy release rate. Irwin (1952) showed that G, the elastic energy release rate, could be regarded as a force tending to cause crack extension. The importance of Eq 3.6 lies in the convenience of calculating stress intensity factors for cracks in complex geometric structures. Section 4 discusses in detail the evaluation of stress intensities using numerical methods, with particular emphasis on finite element techniques.

The stress intensity factor K, may be regarded as a scale factor that accounts for the presence of a crack as it affects the stresses in the vicinity of the crack tip. There are three modes of loading, which are illustrated in Fig 3.1. Mode1, in which the crack

is loaded by tension perpendicular to the faces; mode 2 or the edge-sliding mode is characterised by displacements in which the crack surfaces slide over one another perpendicular to the leading edge of the crack, and finally mode 3 or the anti-plane strain mode in which the crack surfaces slide with respect to one another parallel to the leading edge. The significance of K in any of these modes can be seen by expanding the stress field in cylindrical coordinates (r, $\theta$) about the crack tip following the work of Williams (1957) :

$$\sigma_{ij} = A_{ij}(\theta)r^{-0.5} + B_{ij}(\theta) + C_{ij}(\theta)r^{0.5} + \text{------} \qquad 3.9$$

The first term in the expansion is singular at the crack tip, whereas the remaining terms are finite and bounded. Neglecting the higher order terms, the asymptotic elastic stress field of a symmetrical loaded mode1 crack can be described by the leading term in the series, in the form :

$$\sigma_{ij} = \frac{K}{\sqrt{2\pi r}} f(\theta) \qquad 3.10$$

It is now observed that when r tends to zero the stresses become infinite. The stress intensity factor can thus be regarded as a measure of the strength of the inverse square root stress singularity at the crack tip. In linear elastic fracture mechanics, the stress intensity factor K must be proportional to the external load applied. In addition, for an infinite plate subjected to uniaxial tension the only characteristic dimension is the crack length. Hence, from dimensional considerations, K must also be proportional to the square root of the crack length. The familiar form for a Griffith's crack is :

$$K = \sigma \sqrt{\pi a} \qquad 3.11$$

Following Westergaard (1939), the in-plane stress components for mode1 can be written for both plane stress and plane strain by neglecting higher order terms as :

$$\sigma_{yy} = \frac{K}{\sqrt{2\pi r}} \cos\frac{\theta}{2} \left( 1 + \sin\frac{\theta}{2} \sin\frac{3\theta}{2} \right)$$

$$\sigma_{xx} = \frac{K}{\sqrt{2\pi r}} \cos\frac{\theta}{2} \left( 1 - \sin\frac{\theta}{2} \sin\frac{3\theta}{2} \right) \qquad 3.12$$

$$\tau_{xy} = \frac{K}{\sqrt{2\pi r}} \sin\frac{\theta}{2} \cos\frac{\theta}{2} \cos\frac{3\theta}{2}$$

$$\sigma_{zz} = \upsilon \left( \sigma_{xx} + \sigma_{yy} \right) \quad , \quad \tau_{xz} = \tau_{yz} = 0$$

And for plane stress :

$$\sigma_{zz} = 0 \qquad ; \quad \tau_{xz} = \tau_{yz} = 0$$

The corresponding plane strain displacements are given as :

$$u = \frac{K}{G} \sqrt{\frac{r}{2\pi}} \cos\frac{\theta}{2} \left( 1 - 2\upsilon + \sin^2\frac{\theta}{2} \right)$$

$$v = \frac{K}{G} \sqrt{\frac{r}{2\pi}} \cos\frac{\theta}{2} \left( 2 - 2\upsilon - \cos^2\frac{\theta}{2} \right) \qquad 3.13$$

$$w = 0$$

Equations 3.12 and 3.13 have been written for the case of plane strain (that is, w=0 ) but can be changed to the plane stress case by replacing Poisson's ratio $\upsilon$ with $\upsilon/(1+\upsilon)$ in the in-plane displacement equations and by taking $\sigma_z=0$ to determine the out of plane displacement w. To evaluate w, the out of plane strain is integrated with respect to z. Using $e_{zz}$ from Eqs 2.5 and 2.10 and $\sigma_{xx}$, $\sigma_{yy}$ from Eq 3.12 gives the following form of the displacement w for plane stress conditions :

$$w = -2\,\frac{\upsilon}{E}\,\frac{K}{\sqrt{2\pi r}}\cos\frac{\theta}{2}\,Z \qquad 3.14$$

For mode 2 deformation, the stress components are :

$$\sigma_{xx} = \frac{K_2}{\sqrt{2\pi r}}\sin\frac{\theta}{2}\left(2 + \cos\frac{\theta}{2}\cos\frac{3\theta}{2}\right)$$

$$\sigma_{yy} = \frac{K_2}{\sqrt{2\pi r}}\sin\frac{\theta}{2}\cos\frac{\theta}{2}\cos\frac{3\theta}{2}$$

$$\tau_{xy} = \frac{K_2}{\sqrt{2\pi r}}\cos\frac{\theta}{2}\left(1 - \sin\frac{\theta}{2}\sin\frac{3\theta}{2}\right)$$

3.15

$$\sigma_{zz} = \upsilon\,(\sigma_{xx} + \sigma_{yy}) \qquad \text{for plane strain}$$

$$\sigma_{zz} = 0 \qquad \text{for generalised plane stress}$$

the corresponding displacements are :

$$u = \frac{K_2}{8G}\sqrt{\frac{2r}{\pi}}\left[(2\kappa + 3)\sin\frac{\theta}{2} + \sin\frac{3\theta}{2}\right)]$$

$$v = \frac{K_2}{8G}\sqrt{\frac{2r}{\pi}}\left[ ( 3 - 2\kappa ) \cos\frac{\theta}{2} - \cos\frac{3\theta}{2} \right]$$

$w = 0$ for plane strain

$$w = -\frac{\upsilon}{E}\int ( \sigma_{xx} + \sigma_{yy} ) dz$$ for generalised plane stress

3.16

Here, $\kappa = 3 - 4\upsilon$ for plane strain

$\kappa = 3 - \upsilon / 1 - \upsilon$ for generalised plane stress

For mode 3 deformation, the stress components are :

$$\sigma_{xx} = \sigma_{yy} = \sigma_{zz} = \tau_{xy} = 0$$

$$\tau_{xz} = -\frac{K_3}{\sqrt{2\pi r}} \sin\frac{\theta}{2}$$

$$\tau_{yz} = \frac{K_3}{\sqrt{2\pi r}} \cos\frac{\theta}{2}$$

3.17

The corresponding displacements are :

$$u = v = 0$$

$$w = \frac{K_3}{G}\sqrt{\frac{2r}{\pi}} \sin\theta$$

3.18

Subsequent discussion will be limited to mode1 deformation.

## 3.2 Small scale yielding

In ductile metals, the stress levels close to the crack tip are limited by yielding. Linear elastic fracture mechanics is limited by the requirement that the plasticity around a crack tip is small compared to the surrounding elastic region. This is called contained yielding or small scale yielding (henceforth s.s.y.). The size of the crack tip plastic zone may be estimated by applying the Tresca or Von Mises yield criterion to the elastic field ahead of the crack (Irwin 1957). This can be done by writing the Westergaard equations in terms of principal stresses $\sigma_1$, $\sigma_2$ and $\sigma_3$ which are given by :

$$\sigma_1 = \frac{K}{\sqrt{2\pi r}} \cos\frac{\theta}{2}\left(1 + \sin\frac{\theta}{2}\right)$$

$$\sigma_2 = \frac{K}{\sqrt{2\pi r}} \cos\frac{\theta}{2}\left(1 - \sin\frac{\theta}{2}\right) \qquad 3.19$$

The out of plane stress $\sigma_3$ depends upon whether plane strain or plane stress conditions are applied. For plane strain conditions :

$$\sigma_1 - \sigma_2 = \sigma_0$$

Here $\sigma_0$ is the yield stress in uniaxial tension and the plastic zone radius $r_y$ is given by :

$$r_y = \frac{1}{2\pi}\left(\frac{K}{\sigma_0}\right)^2 \sin^2\theta \qquad 3.20$$

For plane stress conditions :

$$\sigma_1 - \sigma_3 = \sigma_0 \quad \text{where} \quad \sigma_3 = 0$$

and the corresponding plastic zone radius is given by :

$$r_y = \frac{1}{2\pi}\left(\frac{K}{\sigma_0}\right)^2 \cos^2\frac{\theta}{2}\left(1 + \sin\frac{\theta}{2}\right)^2 \qquad 3.21$$

### 3.2.1 Validity of LEFM.

The ratio of the plastic zone size to the thickness of a specimen ( $r_y/B$ ), is an important factor in determining the state of stress. The ratio ($r_y/B$) should appreciably be less than unity for plane strain conditions. The plastic zone size $r_y$ is proportional to $( K/\sigma_0)^2$ so that high intensity factor and a low yield stress give rise to large plastic zones. Formally, application of LEFM requires that there is contained yielding and plane strain conditions. This is expressed formally by the codified requirement :

$$B, a \geq 2.5\left(\frac{K}{\sigma_0}\right)^2 \qquad \text{( B.S DD3 ) (1978 )} \qquad 3.22$$

$$B, a, (w-a) \geq 2.5\left(\frac{K}{\sigma_0}\right)^2 \qquad \text{( ASTM-E399-70 ) (1974 )} \qquad 3.23$$

where B, a, ( w-a) are the thickness, the crack length and the ligament respectively.

The aim of plane strain fracture toughness testing is to obtain reproducible values for the lower limiting critical toughness of a material, tested in thick sections (Knott 1973). The critical toughness value in mode 1 opening is denoted $K_c$. The distinction between $K_c$ and K is important, and is comparable to the distinction between strength and stress. To determine a $K_c$ value, a cracked specimen of suitable dimensions, as illustrated in Fig 3.2 is loaded until the crack extends . The K value corresponding to the load at which crack extension is observed is the $K_c$ value determined in the test. Under restricted conditions, the $K_c$ level of a material can be used to estimate the load that a structural member containing a crack of specified dimensions could sustain without fracture. Toughness estimates based on $K_c$ assume a high degree of constraint to plastic flow of the material at the crack tip, corresponding to a state of plane strain. It is necessary to develop specifications for valid $K_c$ testing because real materials do not behave in the ideal elastic-brittle way assumed in linear elastic fracture mechanics. Nevertheless, when a sufficiently large cracked specimen is tested, the analysis is appropriate because the crack tip plastic region remains small relative to the significant specimen dimensions. Fig 3.3 shows a schematic representation of the shape of a crack tip plastic zone in a plate specimen, based on the Mises yield criterion for plane strain and plane stress as given by McClintock and Irwin (1965). In a sufficiently thick specimen, plane strain conditions prevail in the middle part of the thickness, while plane stress conditions prevail

near the faces.

As a concluding argument, it may be reasoned that the region around the crack tip in which the elastic stresses are adequately described by a K field, will increase with crack size and other pertinent specimen dimensions ( crack length, thickness, and uncracked ligament length ). Thus, the usefulness of K as a descriptive parameter regarding the fracture process increases as the region of plastic strain at the crack front decreases in size compared with these dimensions.

An alternative way of expressing the codified requirement for the validity of linear elastic fracture mechanics is to represent the size requirements as a function of the elastic energy release rate J (the discussion of J as an elastic-plastic parameter is delayed until section 5, but here it is sufficient to note that G=J in s.s.y). As an example, consider a mild steel designated 50D under B.S 4360 whose yield stress $\sigma_0$ = 360 MN/m$^2$ and Young's modulus E=210 GN/m$^2$. Rearranging Eqs 3.6 and 3.23 would give :

$$B\ ,\ a,\ (\ W\text{-}a\ ) \geq 1500\ (\ \frac{J}{\sigma_0}\ ) \qquad 3.24$$

3.3 The elastic T-Stress

The state of the elastic stress field close to the tip of a sharp crack can be written as an asymptotic series about the crack tip in a form provided by Williams (1957) :

$$\sigma_{ij} = A_{ij}\ (\theta) r^{-0.5} + B_{ij}\ (\theta) + C_{ij}\ (\theta) r^{0.5} + \text{------} \qquad 3.25$$

where ( r,θ ) are polar coordinates centred at the tip.
Restricting attention to the first two terms of the Williams expansion, the local stresses can be written in the form :

$$\begin{bmatrix} \sigma_{xx} & \sigma_{xy} \\ \sigma_{yx} & \sigma_{yy} \end{bmatrix} = \frac{K}{\sqrt{2\pi r}} \begin{bmatrix} f_{xx}(\theta) & f_{xy}(\theta) \\ f_{yx}(\theta) & f_{yy}(\theta) \end{bmatrix} + \begin{bmatrix} T & 0 \\ 0 & 0 \end{bmatrix} \qquad 3.26$$

From this equation, T can be seen to be a uniaxial stress parallel to the crack flanks.

The effect of the T-stress on the shape of the plastic zones and the crack tip stress field ahead of the crack are delayed until section 5 and discussed in detail.

Leevers and Radon (1983) have represented the T-stress in a non-dimensionalised way introducing a geometric factor called the stress biaxiality ratio, β ( the usual nomenclature is B, but β has been used here to avoid confusion with specimen thickness ) given by :

$$\beta = \frac{T\sqrt{\pi a}}{K} \qquad 3.27$$

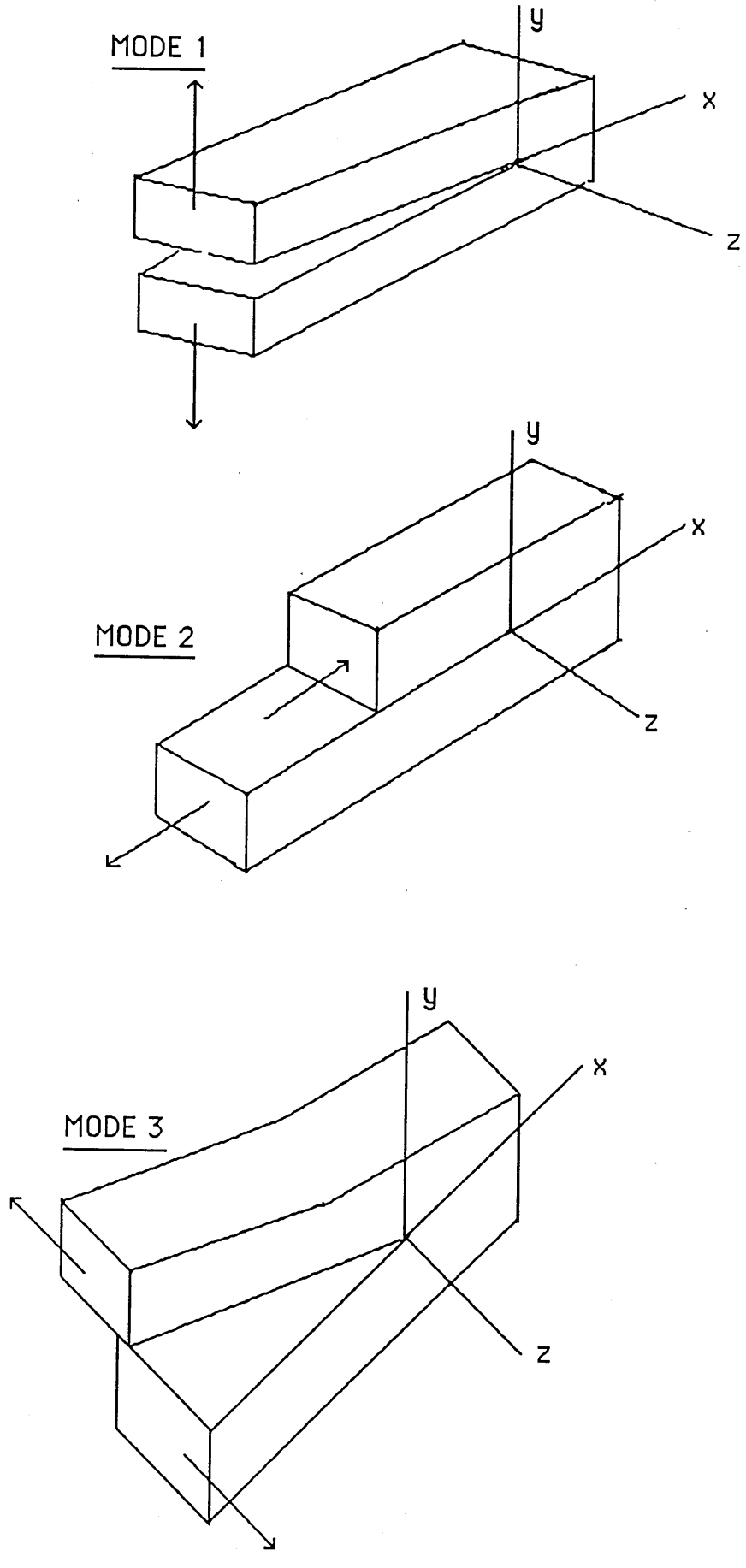


Fig 3.1

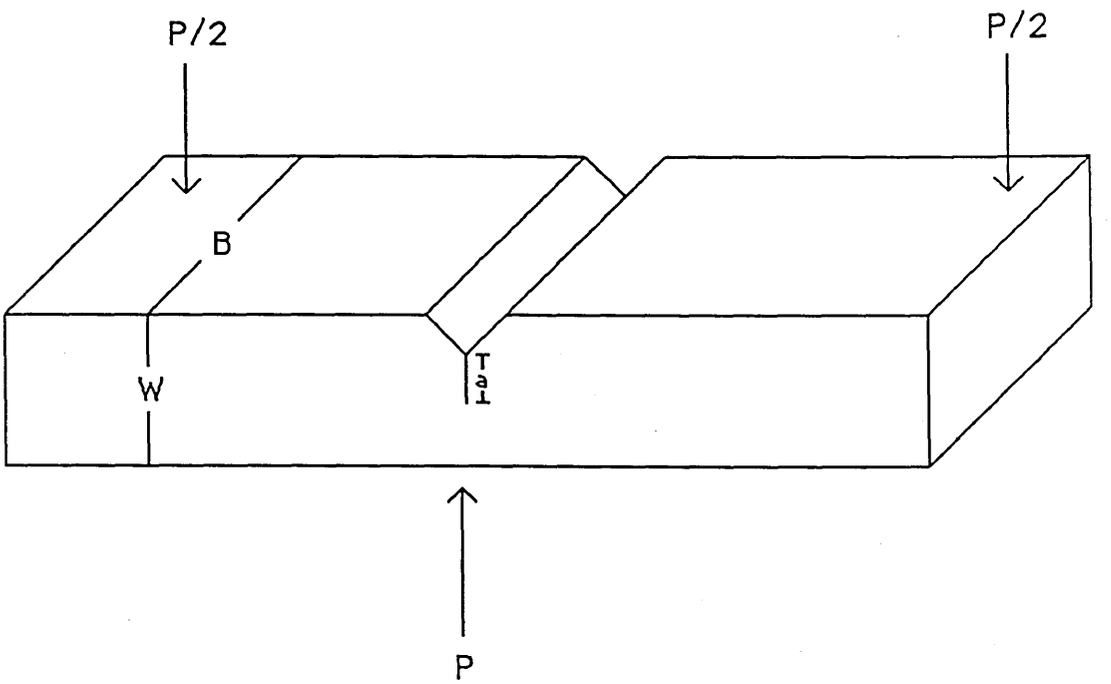


A Cracked Specimen Subject To Three-Point Bend

Fig 3.2

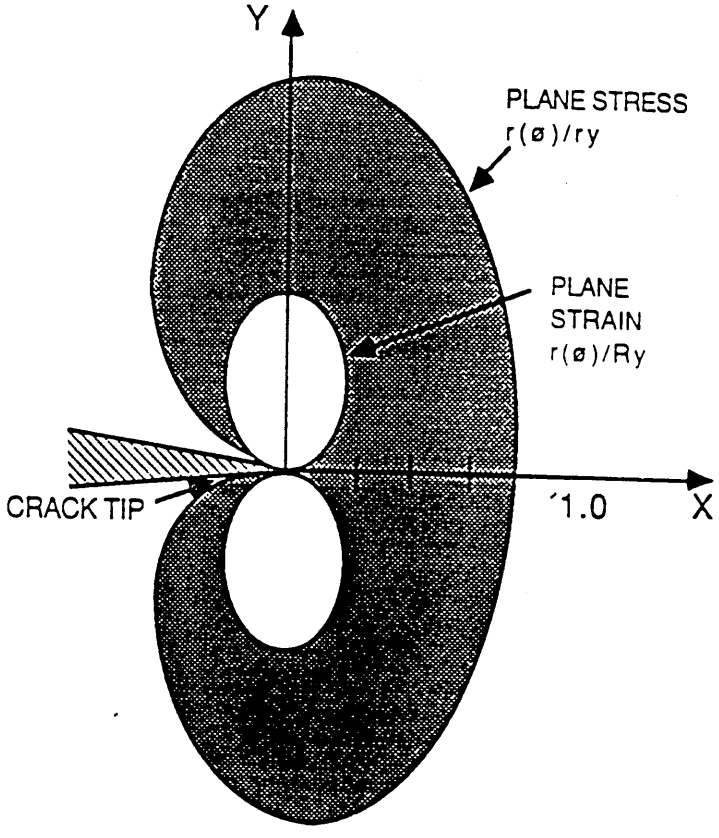


Dimensionaless Plane Strain and Plane Stress Plastic Zone

Fig 3.3

# 4 Linear Elastic Benchmark Calculations

## 4.1 Introduction

The two parameters that characterise linear elastic crack tip fields are the stress intensity factor K and the biaxiality parameter $\beta$ (alternatively T). In this section, these parameters were determined quantitatively for a double edge crack specimen whose dimensions are given in Figure 4.1. The finite element package used to carry out the analysis is called Abaqus (1982). Various methods for the determination of the stress intensity factor K and the biaxiality parameter $\beta$ are presented. The aim of these analyses was to determine the best methods for evaluating K and $\beta$ and compare the results with published solutions. This is intended to verify the present numerical techniques for later use in other problems.

## 4.2 Numerical Methods

Stress intensity factors for a wide range of engineering geometries are available in many standard reference books (Rooke and Cartwright 1976, Tada et al 1973 and Sih 1973). When a geometry is relatively simple, analytical methods are often used. On the other hand, when analysing complex engineering components, analytical methods become complicated and modelling depends upon the use of numerical methods to provide accurate results. In the present analysis, the mesh illustrated in Fig 4.2 was generated with the aid of a commercial program called Patran (1988). In the present calculations, only a quarter of the double edge cracked bar was used

with appropriate boundary conditions applied. The mesh used eight noded quadratic isoparametric elements with focussed elements concentric with the crack tip. The mesh comprised 184 eight-noded plane strain elements consisting of 621 nodes and 1241 degrees of freedom. The nodes at the crack tip were initially independent but coincident. Poisson's ratio was taken to be 0.3 and the dimensionless Young's modulus $10^{11}$. The model was force loaded uniformly on the remote boundary by a uniform tensile stress.

## 4.3 Stress Intensity Factor

To determine the stress intensity factor, two methods were used; the stress method and the displacement method. These methods are known as direct methods of evaluating K. For higher accuracy, the use of special crack tip elements was relied on. This technique consists of moving the mid-side nodes in the inner ring of elements to quarter point positions. Since the displacements are proportional to the square root of the distance from the crack tip denoted r, changing the nodes to the quarter point position forces the displacements to represent the correct displacement function at the crack tip. The use of special crack tip elements reduces the number of elements required to obtain accuracy (Blackburn1972). This technique is discussed in detail by Barsoum (1976), Henshell and Shaw (1975).

### 4.3.1 The Stress Method

The stress method is a direct method of evaluating the stress intensity factor using the Westergaard equation :

$$\sigma_{ij} = \frac{K}{\sqrt{2\pi r}} f_{ij}(\theta) \qquad 4.1$$

The stress intensity factors K were obtained from finite element calculations by considering the stresses $\sigma_{yy}$ ahead of the crack tip where the angle $\theta=0$ gives $f_{ij}(\theta) = 1$. To obtain the actual stress intensity factor K, $\sigma_{yy}(2\pi r)^{0.5}$ was extrapolated to the crack tip :

$$K = \lim_{r \to 0} \sigma_{yy} \sqrt{2\pi r} \qquad \theta = 0 \qquad 4.2$$

However, in numerical solutions there are significant problems in extrapolating to the crack tip as the stresses close to the crack tip do not adopt the correct form and numerical finite element calculations are unable to obtain singular elastic stresses. Therefore data from the first two elements close to the crack tip were rejected.

Results are expressed non-dimensionally. This allows the present numerical data to be related to published solutions by using different dimensions and loading conditions. In the present analysis, the stress intensity factor obtained was non-dimensionalised by $K_0$ which is defined as :

$$K_0 = \sigma \sqrt{\pi a} \qquad 4.3$$

Here, the stress $\sigma$ was taken to be as the total distributed force on the remote boundaries of the specimen divided by its area A :

$$\sigma = \frac{\Sigma F}{A} \qquad 4.4$$

The extrapolation of the non-dimensionalised function $\sigma_{yy}(2\pi r)^{0.5}$ is shown in Fig 4.3. This extrapolation to the crack tip gives the appropriate value of K and is presented together with previously published solutions in Table1. The graph showing the extrapolation to the crack tip by the use of the quarter point nodes technique is illustrated in Fig 4.4. The corresponding value together with previously published solutions is depicted in Table1.

4.3.2 The Displacement Method

The stress intensity factor K was also obtained using the displacement method. The displacement method is also a direct method for evaluating the stress intensity factor. The plane strain displacement field for mode1 deformation was taken from the Westergaard relation :

$$u = \frac{K}{G}\sqrt{\frac{r}{2\pi}}\cos\frac{\theta}{2}\,(1-2\upsilon + \sin^2\frac{\theta}{2}) \qquad 4.5$$

Here, u is the displacement of the nodes in the x direction ahead of the crack tip at $\theta = 0$. By rearranging this equation , K can be defined as :

$$K = \frac{G\sqrt{2\pi}}{1-2\upsilon}\,\frac{u}{\sqrt{r}} \qquad \text{for } \theta=0 \qquad 4.6$$

Lim r———>0

Here, G is the shear modulus, $\upsilon$ is Poisson's ratio and u is the relative displacement in the x direction ($\theta$=0) given as :

$$u = u_{node} - u_{tip}$$

where $u_{node}$ is the displacement of the nodes at a distance r ahead of the crack tip and $u_{tip}$ is the displacement of the first node in the crack tip. As in the case of the stress method, the function at each node was plotted as a function of the corresponding non-dimensionalised r/a and by extrapolating to the crack tip, the appropriate stress intensity factor for the present geometry was obtained. The non-dimensionalisation was performed in the same manner as in the case of the stress method. An illustration of the extrapolation is presented in Fig 4.5. The result for the quarter point node technique is presented in Fig 4.6. Both the K results for the displacement method together with published solutions are presented in Table1.

4.3.3 The Virtual Crack Extension Method

The virtual crack extension method is based on the energy release rate and is an indirect method for the evaluation of the stress intensity factor K. In linear elastic analyses, the stress intensity factor is related to the energy release rate by the relation :

$$J = \frac{K^2}{E'} \qquad 4.7$$

For plane strain conditions, G = J. The J-integral was determined

by the virtual crack extension method of Parks (1974) as implemented in Abaqus (1982). When crack extension occurs, the crack length is increased by an amount da and the energy change is evaluated between contours. Four contours were chosen and values of J were always taken from the second contour. The argument is that values of J have always been taken from the second contour as they exhibit the best results in other problems. The value of K obtained using this method was non-dimensionalised in the same way as for the stress and displacement methods. The results are given in Table1.

4.3.4 Benchmark Solution

Bowie (1964) analysed the problem under consideration using a complex variable approach with the help of a mapping function to describe the geometry. The success of this approach was previously demonstrated by Bowie for complicated geometries. The technique used involved the formulation of this problem in terms of an integral equation. These formulations, although mathematically elegant, required a numerical solution of an integral equation. The mapping approach was therefore reintroduced as an effective means for solving the problem of the double edge crack configuration. For the double edge crack specimen in tension, $0<a/w<0.7$ and $h/w>3$ Bowie's result were expressed in the form of a polynomial :

$$\frac{K}{K_0} = 1.12 + 0.2\left(\frac{a}{w}\right) - 1.2\left(\frac{a}{w}\right)^2 + 1.93\left(\frac{a}{w}\right)^3 \qquad 4.8$$

where :

$$K_0 = \sigma\sqrt{\pi a} \qquad 4.9$$

4.3.5 Discussion And Conclusion.

The present result for the stress intensity factor derived from the stress, displacement and virtual crack extension methods are compared with the benchmark value given by Bowie (1964) in Rooke and Cartwright (1976). The results given in Table1 show that the virtual crack extension method gave the best result (1% accuracy) in comparision with the benchmark value. In the case of the stress method the value of K was correct to within 5%,and by using the quarter point node technique, the result improved slightly to 4.5%. On the other hand, the value of K from the displacement method using the mid-side node approach, was 17% lower than the reference value. Nevertheless, by advancing the mid-side nodes to the quarter point position, the result improved to a 6% accuracy. From the results obtained it may be concluded that the virtual crack extension method is the most accurate method for determining the stress intensity factor K and can be relied on to give results with an accuracy in the order of 1%. In addition, the use of virtual crack extension method does not involve inspection of stresses and displacement ahead of the crack tip and the main advantage in using this method lies in the convenience of achieving a greater accuracy in a short time. For further linear elastic analyses, the stress intensity factor was always evaluated by the use of the virtual crack extension method.

## 4.4 Biaxiality Parameter β

The most direct methods for determining the biaxiality parameter β involve inspection of the stress and displacement fields in the crack flanks. In the present analysis, two methods are presented and the resulting values of the biaxiality parameters β are compared with the benchmark value, before proceding to problems of more interest.

### 4.4.1 The Stress Method

The stress method consists of obtaining the stresses $\sigma_{xx}$ parallel to the crack plane ($\theta=\pi$) and substracting the corresponding stresses $\sigma_{yy}$ normal to the crack plane. These calculations were performed for each node in the crack flanks. The non-dimensionalisation was obtained in terms of the biaxiality parameter β in the following form :

$$\beta = \frac{(\sigma_{xx} - \sigma_{yy})\sqrt{\pi a}}{K} \qquad 4.10$$

On the crack flanks ($\theta=\pi$), the stress $\sigma_{yy}$ is required to be zero as part of the boundary conditions. However in the numerical solutions, small but finite stresses in the vicinity of the crack tip were found due to the inability of the elements to satisfy the equilibrium equations exactly. As a result of this, data at the nodes near to the crack tip with $\sigma_{yy} \geq 0.1\ \sigma_{xx}$ were rejected. The biaxiality parameter values at each node were plotted as a function of the non-dimensionalised distance r/a behind the crack

as illustrated in Fig 4.7. The appropriate value of the biaxiality parameter $\beta$ for the present geometry was obtained by extrapolating to the crack tip as r/a approaches zero. The $\beta$ value obtained is presented together with the benchmark solution in Table 2.

### 4.4.2 The Displacement Method

The biaxiality $\beta$ as a function of the displacement u is given directly by inspection of the second term of the displacements relations :

$$u=\frac{K}{E}\left[2\left(1+\upsilon\right)\sqrt{\frac{r}{2\pi}}\,f_{xx}\left(\theta\right)\right]+\left[\left(1-\upsilon^2\right)\left(\frac{\beta}{E\sqrt{\pi a}}K\,r\cos\theta\right)\right] \qquad 4.11$$

$$v=\frac{K}{E}\left[2\left(1-\upsilon\right)\sqrt{\frac{r}{2\pi}}\,f_{yy}(\theta)\right]-\left[\upsilon\left(1+\upsilon\right)\frac{\beta}{E\sqrt{\pi a}}K\sin\theta\right]$$

On the crack flanks ( $\theta=\pi$ ) the angular functions $f_{xx}$ are zero, allowing the biaxiality parameter to be determined for each node using u. Here, u is the displacement in the x direction ($\theta=\pi$) given in cylindrical co-ordinates centered at the tip :

$$u= u_{node} - u_{tip} \qquad 4.12$$

The displacement of the first node at the crack tip is denoted $u_{tip}$ and $u_{node}$ is the displacement of a node at a distance r from the tip. The resulting values of the biaxiality parameters were plotted against r/a for each node behind the crack. By extrapolating to the crack tip, the biaxiality parameter for the present geometry was obtained.

However, there were significant problems in extrapolating to the crack tip as the displacement functions did not adopt the appropriate form close to the tip even though the data at the nodes near to the crack tip with $\sigma_{yy} \geq 0.1\ \sigma_{xx}$ were rejected. This resulted in the graph illustrated in Fig 4.8. In order to obtain a better result from the displacement method, the multi-point constraint facility available in Abaqus through the "*EQUATION" option was used. This technique allows the elements at the crack tip to follow the correct form of the displacement function. The stress in the crack flanks should simply be a uniaxial tensile or compressive field corresponding to a tensile or compressive T stress. Corresponding to this simple stress field, the displacement parallel to the crack flanks should just increase linearly with distance r from the tip and the result is shown in Fig 4.9. The *EQUATION option allows this relation to be established by writing a series of equations relating the displacements in adjacent nodes. As an example, consider the first element close to the crack tip at $\theta = \pi$. Then the equations are formed in the following manner :

$$u_n - u_{tip} = \alpha ( r_n - r_{tip} )$$

$$u_{n1} - u_{tip} = \alpha ( r_{n1} - r_{tip} ) \qquad 4.13$$

Here, $r_{tip}$ is the distance of the first node at the crack tip (in this case zero). $r_n$ is the distance of the first node behind the crack tip and $r_{n1}$ is the distance of the second node behind the crack tip. The displacements u correspond to each of the nodes considered in the equation above. $\alpha$ is a constant. By rearranging the equation to eliminate the constant $\alpha$, the reduced form is given as :

$$A_{tip}\, u_{tip} + A_n\, u_n + A_{n1}\, u_{n1} = 0 \qquad 4.14$$

where $A_{tip}$ , $A_n$ and $A_{n1}$ are constants obtained by substituting the values of the distances r corresponding to each node.
This procedure ensured the correct form of displacement function for the biaxiality $\beta$ in the crack flanks in the same way that the well known quarter point node technique does for the displacement associated with the K field. The results obtained are given in Table 2 and compared with the benchmark data of Kfouri (1986).

### 4.4.3 Discussion and Conclusions

The values of the biaxiality parameters obtained from the stress and the displacement methods were compared with the published solutions of Kfouri (1986). To evaluate T, Kfouri (1986) used a theorem attributed to Eshelby (1968). In the present analysis, the biaxiality parameter numerical value derived with the use of the stress method was accurate to within 2% compared to the published solution if the nodes close to the crack tip are neglected. However, when using the displacement method, the $\beta$ value obtained differed from the reference value by 50%. In order to improve the result, the technique of using *Equation was adopted. This technique improved the value of the biaxiality parameter $\beta$ to an accuracy of 2%. Finally, by considering all the methods used throughout this analysis, the preferred method is the stress method as it offers a straightforward and simple way

of calculating the biaxiality parameter.

## 4.5 Solutions For Double Edge Crack Bars

In section (4.4) a double edge cracked bar with a/w=0.5 was analysed in order to determine the best method for evaluating the biaxiality parameter $\beta$. The preferred method was the stress method in the crack flanks. In this section, a range of different geometries with a/w varying from 0 to 1 are analysed and the values of the biaxiality parameters $\beta$ are calculated.
Figure 4.10 shows the biaxiality parameter $\beta$ as a function of the non-dimensionalised crack length (a/w). For a/w < 0.9, the values of the biaxiality parameters $\beta$ are negative corresponding to compressive stresses parallel to the crack flanks. However, for deeply cracked geometries (a/w = 0.97 and a/w=1), the values of $\beta$ become positive corresponding to tensile stresses parallel to the crack flanks. Kfouri [6] analysed double edge cracked specimens for a range of a/w varying from 0.2 to 0.6 and noted that for H/w >1.5, the derived values of the biaxiality parameters $\beta$ were maintained at $\beta$ = -0.49. In this case the double edge crack specimen analysed has dimensions of H/w=3 as shown in Fig1 and the calculated biaxiality parameters were approximately $\beta$= -0.45. Nevertheless, as the crack becomes deeper, the values of the biaxialities become less negative. At a/w = 0.95, the biaxiality parameter $\beta$ = 0. For very deep cracks, a/w= 0.97 and a/w=1, the biaxialities $\beta$ become positive. Table 3 represents the values of the biaxiality parameters as a function of a/w.

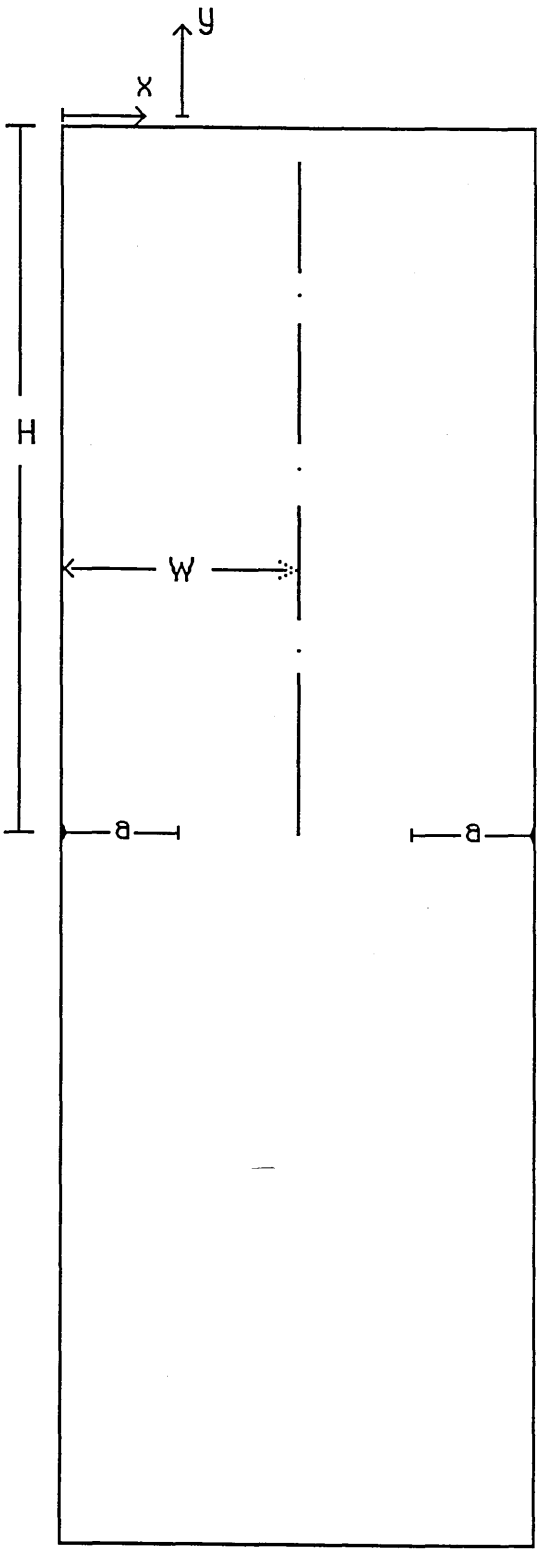


a/w=0.5

H/w=3

Dimensions of a double edge crack bar specimen a/w=0.5

Fig 4.1

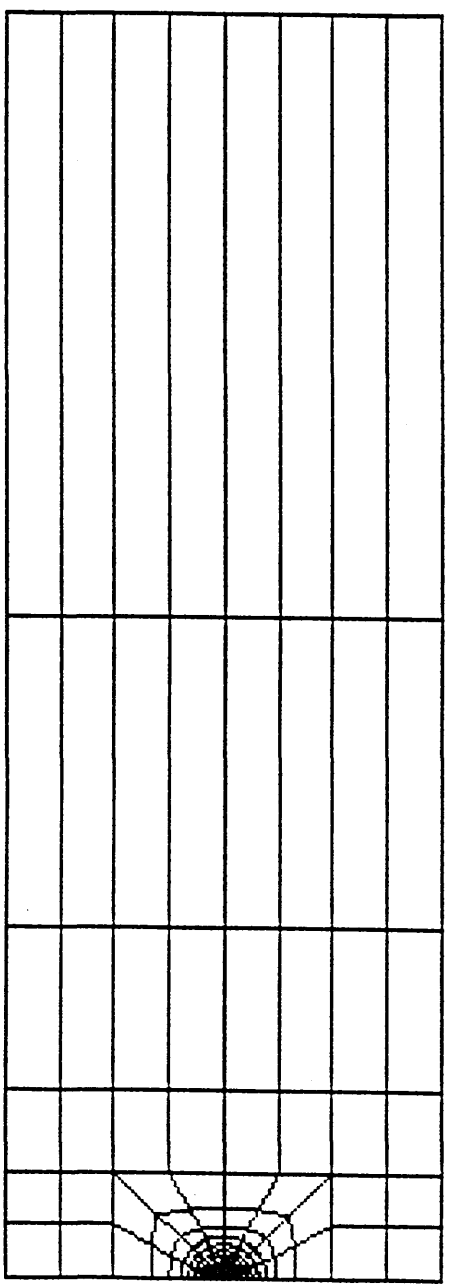

Finite Element Mesh with a/w=0.5

Fig 4.2

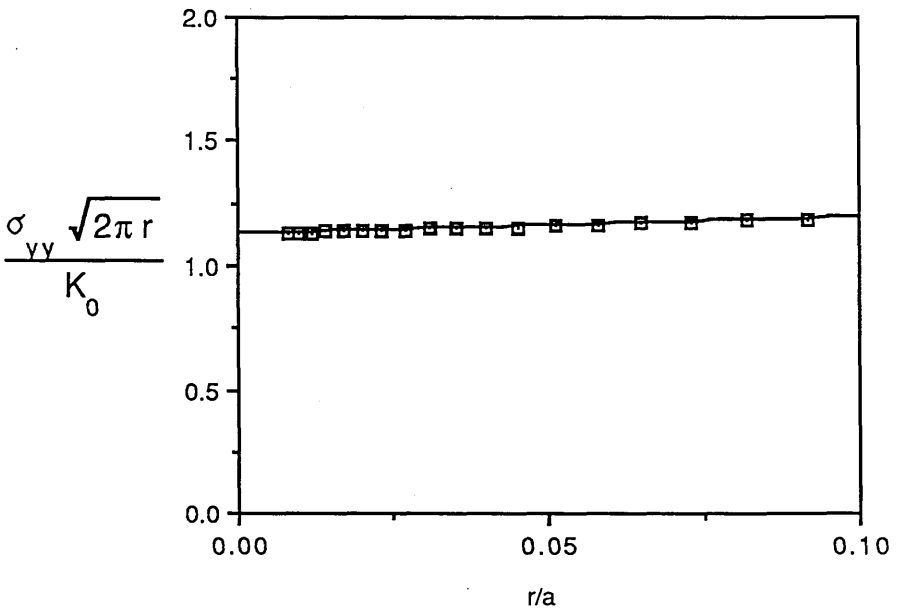


Non-dimensionalised stress intensity factor versus r/a for mid-side nodes using the stress method.

Fig 4.3

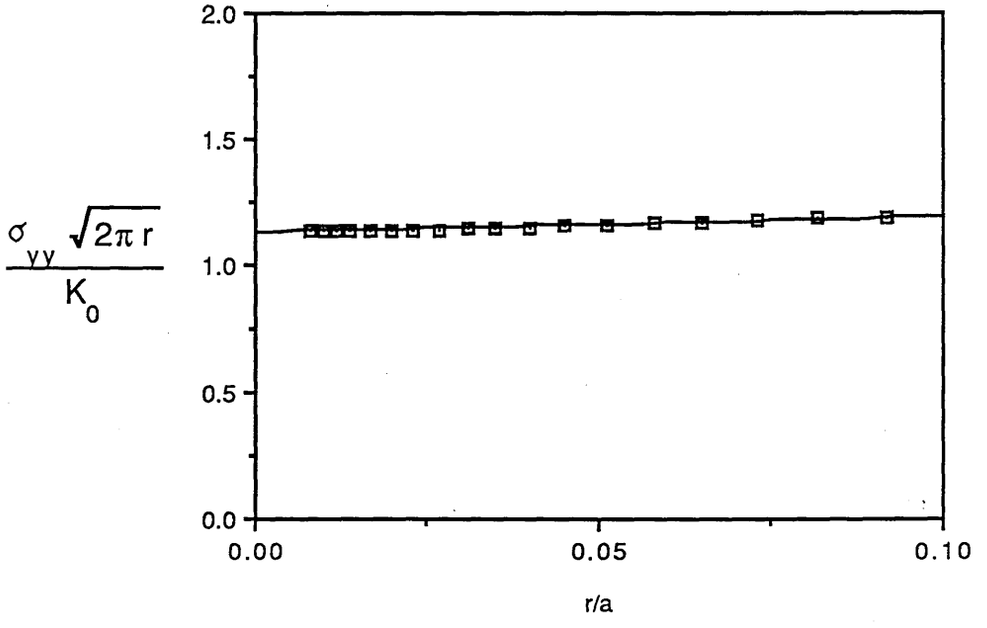


Non-dimensionalised stress intensity factor versus r/a for quarter point nodes using the stress method.

Fig 4.4

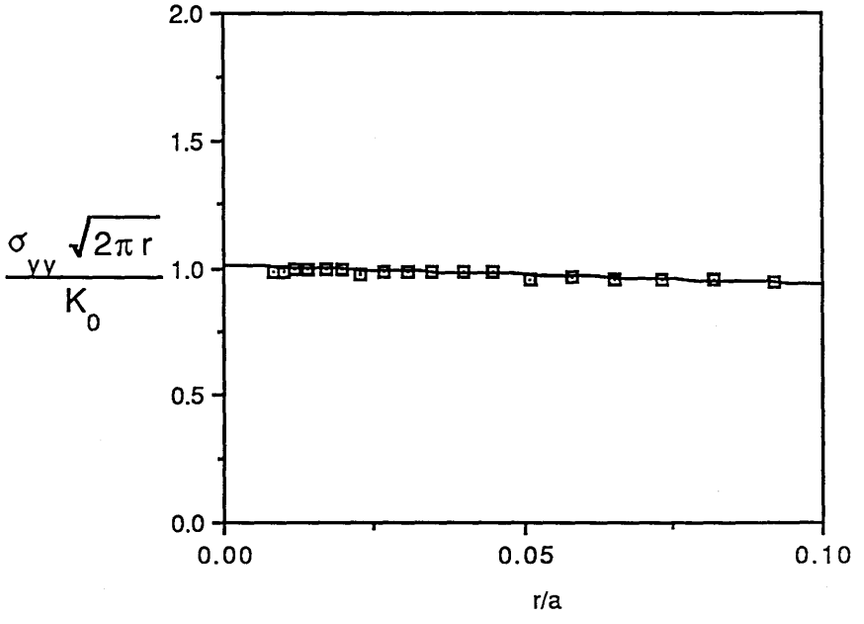


Non-dimensionalised stress intensity factor versus r/a for mid-side nodes using the displacement method.

Fig 4.5

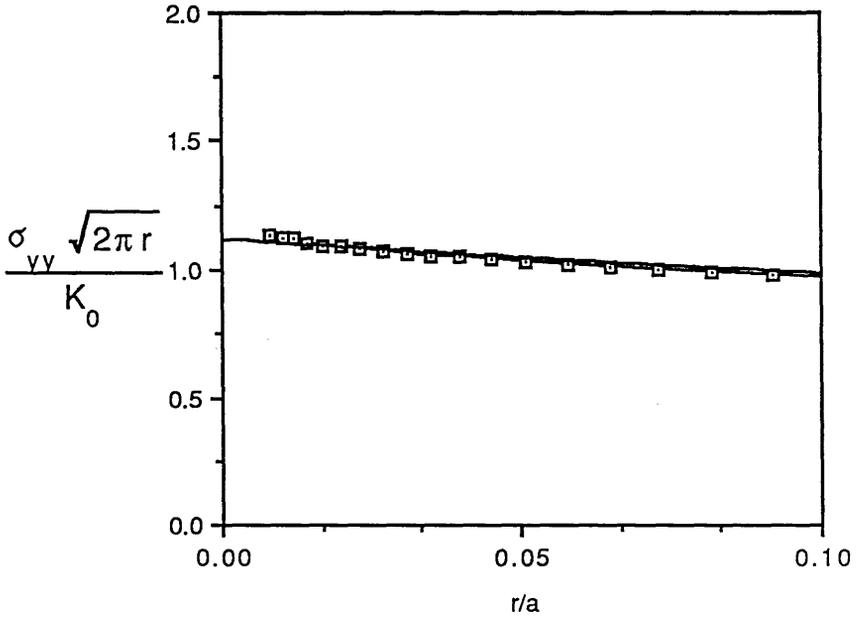


Non-dimensionalised stress intensity factor versus r/a for quarter point nodes using the displacement method.

Fig 4.6

| | Mid-side nodes | Errors | Quarter point nodes | Errors |
|---|---|---|---|---|
| Stress Method | 1.124 | 5% | 1.128 | 4.5% |
| Displacement Method | 1.01 | 17% | 1.13 | 5% |
| Virtual Crack Extension Method | 1.17 | 1% | 1.18 | 1% |

Benchmark Result : $\frac{K_1}{K_0} = 1.18$

Non-dimensionalised stress intensity factors $K/K_0$ for the different method used together with the benchmark value from Bowie [5].

Table 1

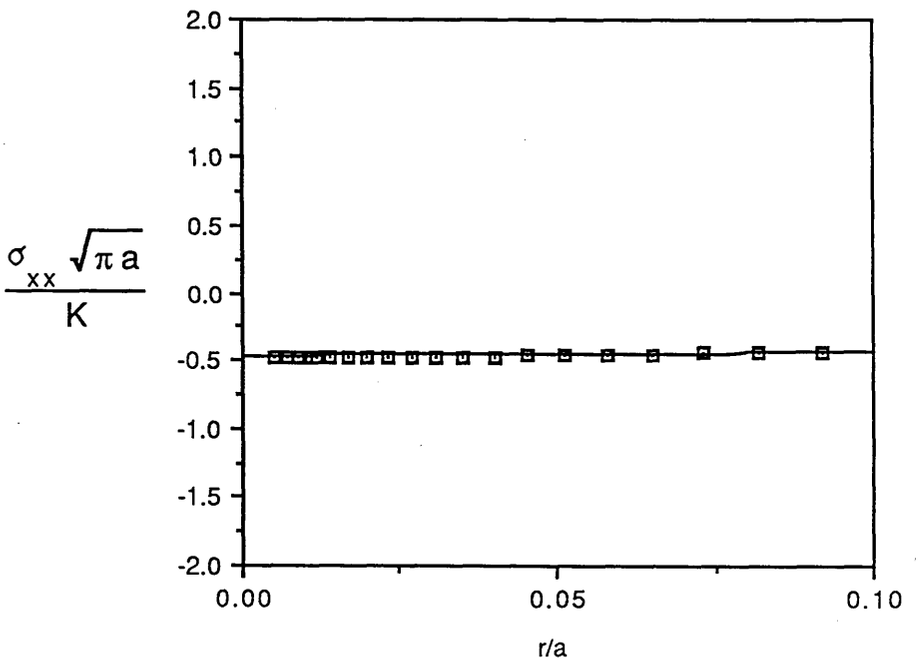


Biaxiality parameter versus r/a using the stress method

Fig 4.7

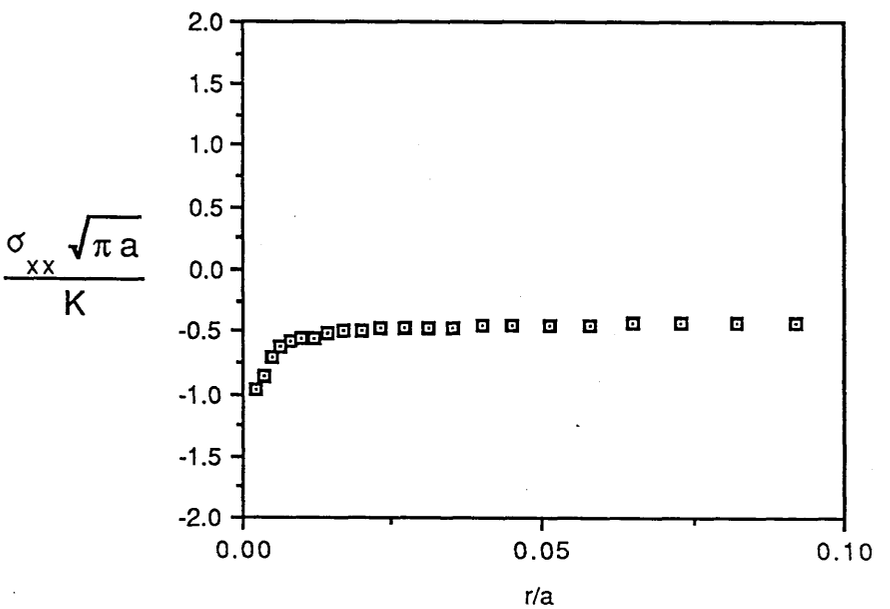


Biaxiality parameter versus r/a using the displacement method.

Fig 4.8

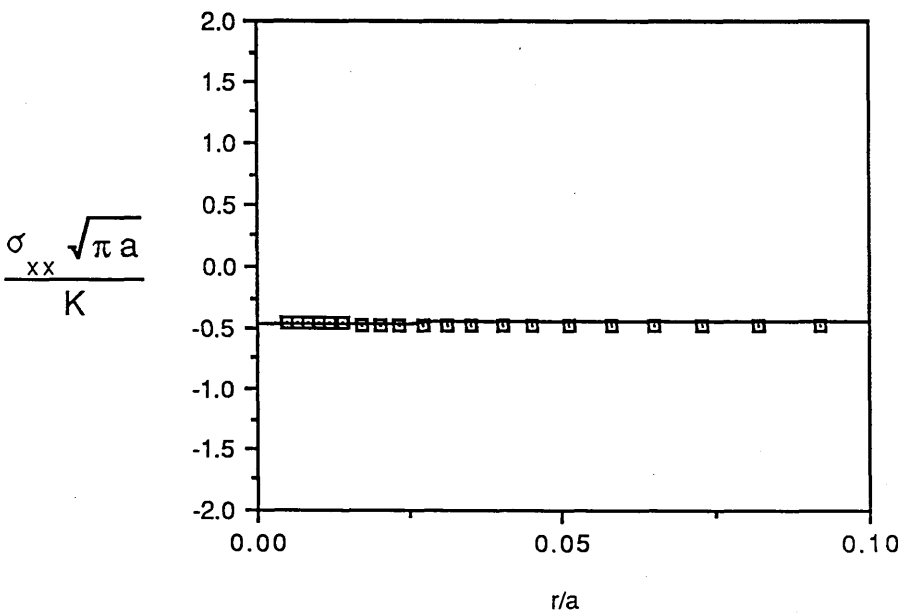


Biaxiality parameter versus r/a using the displacement method with the *Equation option

Fig 4.9

| | B |
|---|---|
| Stress Method | -0.47 |
| Displacement Method Without *EQUATION | - 1.0 |
| Displacement Method Using *EQUATION | -0.47 |
| Benchmark Result From Kfouri (1986) | -0.48 |

Biaxiality parameters $\beta$ for the different methods used together with the benchmark value from Kfouri (1986).

Table 2

| a/w | B |
|---|---|
| 0 | -0.470 |
| 0.03 | -0.464 |
| 0.1 | -0.436 |
| 0.3 | -0.458 |
| 0.5 | -0.471 |
| 0.7 | -0.411 |
| 0.9 | -0.196 |
| 0.97 | +0.077 |
| 1 | +0.13 |

Values of the biaxiality parameters $\beta$ for different crack lengths a/w.

Table 3

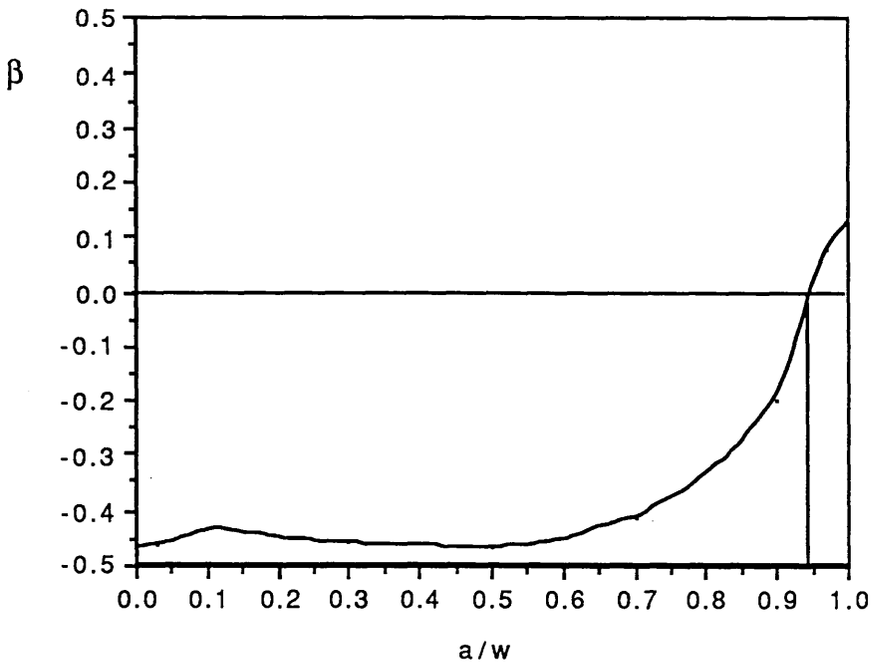


Biaxiality Parameters as a Function of Crack length ratios a/w

Fig 4.10

# 5 Elastic-Plastic Fracture Mechanics

## 5.1 Introduction

Most structural materials, particularly metals, fracture with at least some plasticity at the crack tip. Even fracture of materials, dominated by cleavage separation of lattice planes or interfaces, involves significant plastic flow. Linear elastic fracture mechanics can be usefully applied as long as the plastic zone is small compared to the crack or ligament size (Section 3). This is usually the case in components where fracture occurs at stresses appreciably below the yield stress. In large scale yielding (l.s.y.), it is no longer possible to use linear elastic solutions to crack problems; elastic-plastic solutions must be used instead, (Hutchinson 1979). Fracture behaviour is bounded by the extremes; linear elastic, and fully plastic failure. Interpolation between the two extremes is made possible by the use of either the J-integral failure parameter or the crack tip opening displacement (C.T.O.D.). In the following section, the J-integral is introduced and used to extend fracture mechanics into large scale yielding. A detailed definition of the crack tip opening displacement and its relation to the J-integral is also described. Limitations of single parameter characterisation are discussed with recent developments in two parameter characterisation.

## 5.2 Crack tip opening displacement

The crack tip opening displacement (C.T.O.D) was proposed, as an elastic-plastic failure parameter by Wells (1961), as a measure of the plastic strain close to the crack tip. Wells (1963) focussed attention on the amount of crack opening prior to crack extension as a parameter characteristic of the crack tip deformation. In general, depending upon the choice of plastic zone correction, the crack tip opening displacement for small scale yielding in mode 1 deformation is given by :

$$\delta = \frac{K^2}{m \sigma_0 E'} \qquad 5.1$$

This is consistent with the linear elastic fracture mechanics failure criterion $K = K_c$ . Hence :

$$\delta_c = \frac{K_c^2}{m \sigma_0 E'} \qquad 5.2$$

Here, m is a factor determined by Robinson (1976), and usually taken between 1 and 2. The relation between the crack tip opening displacement (C.T.O.D) and the energy release rate J is based on the strip yielding model of Dugdale (1960) and Bilby et al (1963) and is given by :

$$J = m \sigma_0 \delta \qquad 5.3$$

Alternatively, the crack tip opening displacement can be related to the applied load by the relation :

$$\delta = \frac{8\, a\, \sigma_0}{\pi\, E'} \ln \sec \left( \frac{\pi\, \sigma}{2\, \sigma_0} \right) \qquad 5.4$$

## 5.3 The J-Integral

The J-integral is a powerful technique for analysing elastic-plastic failure. J can be regarded in three ways. Firstly it can be derived as a path independent integral around the crack tip. On this basis, J was independently proposed by Cherepanov (1967), Eshelby (1968) and Rice (1968). However, its application to fracture mechanics is attributable to Rice (1968). For non-linear elastic materials J is introduced through a contour integral. The two dimensional form of the integral can be written as :

$$J = \int_{\tau} \left[ w\,dy - F \left( \frac{\partial u}{\partial x} \right) ds \right] \qquad 5.5$$

where $\tau$ is a closed contour or path that goes from the lower crack surface to the top in an anti-clockwise direction, as illustrated in Fig 5.1, and u is the displacement in the $\underline{n}$ direction ( $\underline{n}$ is a unit vector) and ds is an increment of arc length with a normal in direction $\underline{n}$.

The strain energy per unit volume W, also known as the strain energy density, is given by :

$$W = \int \sigma_{ij}\, de_{ij} \qquad 5.6$$

Here, $\sigma_{ij}$, $e_{ij}$ are the stress and strain tensors. The traction vector F is given as :

$$F = \sigma_{ij} n_j \qquad 5.7$$

where $n_j$ are the coefficients of a unit vector normal to $\tau$ .
Extending this definition, J has a role as a characterising parameter in crack tip fields, Hutchinson (1968), Rice and Rosengren (1968). It also has an energetic significance, in which role it makes contact with the strain energy release rate of linear elastic fracture mechanics. It can be regarded as a generalisation of the strain energy release rate concept introduced by Irwin (1957) for linear elastic solids to the problem of non-linear elastic behaviour. For linear elastic behaviour :

$$G = -\frac{1}{B}\left(\frac{\partial U}{\partial a}\right) \qquad 5.8$$

The above definition can be extended to non-linear elastic behaviour as :

$$J = -\frac{1}{B}\left(\frac{\partial U}{\partial a}\right) \qquad 5.9$$

Here, U is the potential energy. Fig 5.2 illustrates the energy release rate as the area between the load-displacement curves for crack lengths a and a+da. The area is given by JBda, which is equal to the energy release rate. J has been proposed as a more universal fracture criterion than G for it is claimed to be applicable to cases where crack growth and fracture are associated with appreciable plastic deformation.
There are a range of methods available for the determination of J in a standard fracture mechanics specimens such as a deeply edge

cracked bar under pure bending. The moment-rotation relation for a non-hardening material is shown in Fig 5.3. For a deeply edge cracked bar, the moment is only a function of the thickness of the specimen and the ligament.

A dimensional argument then leads to the relation:

$$M_{(a)} = \alpha \sigma_0 B (w-a)^2 \qquad 5.10$$

where $\alpha$ is a dimensionless constant.

For an incrementally longer crack :

$$M_{(a+da)} = \alpha \sigma_0 B [w-(a+da)]^2 \qquad 5.11$$

By substracting $M_{(a)}$ from $M_{(a+da)}$ , it follows that :

$$dM = M_{(a+da)} - M_{(a)} = -2 \alpha \sigma_0 B (w-a) da \qquad 5.12$$

Now the work done is simply defined as the area of the moment-rotation curve comprising incrementally different crack length. The incremental change in the work done U is :

$$dU = \theta dM \qquad 5.13$$

Rearranging Eqs 5.8 and 5.9 and replacing in Eq 5.5 gives :

$$J^p = 2 \frac{U^p}{B (w-a)} \qquad 5.14$$

A similar argument can be used for the determination of J for deeply edge cracked bars under pure tension. In this case a dimensional argument leads to the limit load adopting the relation :

$$P = \alpha \sigma_0 B (w-a) \qquad 5.15$$

which leads to :

$$J^p = \frac{U^p}{B\ (w-a)} \qquad 5.16$$

A general relation of the plastic component of J was introduced by Turner (1973) in the form :

$$J^p = \eta_p \frac{U^p}{B\ (w-a)} \qquad 5.17$$

where the eta factor $\eta_p$ is a non-dimensional constant which depends on the ratio of bending to tension. Further investigations were carried out by Shih and Hutchinson (1986) who analysed edge cracked bars subject to point loads to determine the effect of the loading conditions on $\eta_p$ in plane strain conditions. They gave their results in terms of the parameter $\gamma$ obtained from the moment-load curve shown in Fig 5.4 as :

$$\gamma = \arctan \left[ \frac{M/[\sigma_0\ (w-a)]^2}{P/[\sigma_0\ (w-a)]} \right] \qquad 5.18$$

The angle $\gamma$ is related to the loading application point by the relation :

$$\frac{x}{w} = 1 - \frac{1}{2} \tan \gamma \qquad 5.19$$

Here, w is the width of the specimen and x is the location of the applied load. Their result is described in Fig 5.5 as a relation between the eta factor and x/w for a number of hardening rates n. It is relevant to note that the hardening rate has a weak effect on the non-dimensionalised constant $\eta$. The significance of the eta factor is seen in the direct determination of J from the work done on a specimen by the applied loads.

Sumpter (1973) extended the definition of J by introducing the elastic component $J^{el}$ in a similar form :

$$J = \eta_e \frac{U^e}{B(w-a)} + \eta_p \frac{U^p}{B(w-a)} \qquad 5.20$$

Here, $\eta_{el}$ is obtained from linear elastic fracture mechanics calculations as exemplified by Turner (1973).

The plastic component of the strain energy release rate J can also be related to the load applied by using an approach adopted by Ilyushin (1946) which establishes the basis of the EPRI method (Electric Power Research Institute 1981) for the determination of J for a non-linear material response with a power law $(e/e_0) = \alpha (\sigma/\sigma_0)^n$. It follows that the strains are proportional to the stresses raised to the power n :

$$e \alpha \sigma^n \qquad 5.21$$

Here $\alpha$ denotes proportionality. The loads are also proportional to the stresses and consequently the strains to the power 1/n :

$$P \alpha \sigma \alpha e^{\frac{1}{n}} \qquad 5.22$$

In addition, the displacements are proportional to the strain and therefore:

$$u \alpha e \alpha \sigma^n \alpha P^n \qquad 5.23$$

The plastic component of the J integral obtained in Eq 5.17 could be written in the form :

$$J^p \alpha U^p \qquad 5.24$$

Here U is the work done and defined as a product of the load and displacement. Rearranging Eq 5.22 and 5.23 :

$$J^p \alpha P^{n+1} \qquad 5.25$$

From dimensional considerations, Eq 5.25 can then be written as :

$$J^p = \alpha e_0 \sigma_0 a \left(\frac{P}{P_0}\right)^{n+1} f\left(\frac{a}{w}, n\right) \qquad 5.26$$

where $\alpha$ is a constant, $P_0$ is a reference load, f (a/w, n) is a function which depends upon the geometry and strain hardening rate.

A more general relation involving both the elastic and plastic components of J may be described in the form :

$$J = J^e(a_e) + J^p(a,n) \qquad 5.27$$

Expanding the relation gives :

$$J = \frac{P^2}{E'} g\,(a_e) + \alpha\, e_0\, \sigma_0\, a\, (\frac{P}{P_0})^{n+1}\, f\,(\frac{a}{w}, n) \qquad 5.28$$

Here, g $(a_e)$ is a function of the crack length, $E'$ is the Young's modulus and $a_e$ is the effective crack length to provide smooth interpolation between elastic and plastic solutions.

## 5.4 H.R.R Equations

In a power-law hardening material the stresses and strains for non-linear materials under uniaxial deformation may simply be related by the equation :

$$\frac{e}{e_0} = \alpha\, (\frac{\sigma}{\sigma_0})^n \qquad 5.29$$

Here, $\alpha$ is a material constant, n is the strain hardening exponent and $\sigma_0$ is the yield stress or a material reference stress. By using the deformation theory of plasticity, the expression above may be extended to multiaxial stress states to give :

$$e_{ij} = \frac{3}{2} \alpha\, (\frac{\sigma_e}{\sigma_0})^n \frac{S_{ij}}{E} \qquad 5.30$$

where the effective stress $\sigma_e$ is related to the stress deviators $S_{ij}$

by :

$$\sigma_e^2 = \frac{3}{2} S_{ij} S_{ij} \qquad 5.31$$

Hutchinson (1983) used the minimum complimentary energy thoerem to define the stress distributions which satisfy equilibrium and the stress boundary conditions around a crack tip. The method of solution employed consisted of identifying stress distributions which minimise the complimentary energy over a given volume of material following the relation :

$$U_c = \iint_V e_{ij} \, d\sigma_{ij} \, dv \qquad 5.32$$

Using these relations in terms of the stresses and introducing the conditions for equilibrium and stress free local boundary conditions on the crack flanks, the crack tip stress and strain field for power law hardening materials was obtained in terms of J. The resulting fields are attributed to Hutchinson (1968), Rice and Rosengren (1968) and referred to jointly as the H.R.R fields :

$$\sigma_{ij} = \sigma_0 \left[ \frac{J}{e_0 \, \sigma_0 \, r \, I_n} \right]^{\frac{1}{1+n}} f_{ij} \, ( \theta, n ) \qquad 5.33$$

$$e_{ij} = \frac{\alpha \, \sigma_0}{E} \left[ \frac{J}{e_0 \, \sigma_0 \, r \, I_n} \right]^{\frac{n}{n+1}} g_{ij} \, (\theta, n) \qquad 5.34$$

Here, r and $\theta$ are polar coordinates centered at the crack tip, In is an integration constant and $f_{ij}(\theta, n)$, $g_{ij}(\theta, n)$ are dimensionless functions of $\theta$ and the material hardening exponent n obtained numerically by Hutchinson (1968). As an example, consider a

material under plane strain conditions with a hardening rate n=13 corresponding to In=4.5 at $\theta$=0 giving $f_{ij}$ ($\theta$, n)= 2.6. The stress $\sigma_{yy}/\sigma_0$ at a distance r $\sigma_0$/J=2 is evaluated as $\sigma_{yy}/\sigma_0$=3.69. The H.R.R analyses are asymptotic expansions of the crack tip field in the region where small strain deformation theory prevails, and under conditions in which the solution is restricted to a single dominant term. In the solutions, the only variable is the parameter J which is the dominant term that establishes the basis of elastic-plastic fracture mechanics. The H.R.R field is to be regarded as an asymptotic small geometry change solution in which the crack tip is regarded as remaining sharp. For single parameter characterisation of the crack tip fields to be valid, the region over which the H.R.R singularity dominates must engulf the fracture process zone. The J integral introduced by Rice (1968) is then considered as the amplitude of the H.R.R singularity.

## 5.5 J-Dominance ( One Parameter Characterisation )

J-dominance is defined as the conditions for which the crack tip deformation maintains the character of the small scale yielding field. Therefore under J-dominance, the initiation of crack growth can be expected to be governed by a critical value of J denoted $J_c$ which is a material property. Begley and Landes (1976) were the first to recognize the potential of J in plastic fracture mechanics. In 1971, Begley and Landes (1971) proposed that the J integral could be used as a ductile fracture criterion by providing experimental results in which they argued that specimen geometry could be a possible influence on the suitability of a one parameter

characterisation. These authors (1976) analysed a compact tension specimen and a centre crack panel in tension and formulated their results in terms of a J-resistance curve from which they argued that J was in fact a viable fracture criterion since its magnitude was the same for both geometries at the inception of crack growth even though the trend of the R curves for the centre crack panel and the compact toughness specimen became different after a small amount of crack extension occurred. They justified this difference as an inadequacy in choosing the proper dimensions concerning the centre crack panel. The fact that the crack extension for this geometry follows a 45 degree slip line may indicate that the specimen used in their test was too small to preserve the crack tip field after only a small amount of crack extension. They concluded that the degree to which J could successfully correlate small amounts of crack extension could only be made after care is taken to ensure that the specimens being tested were large enough that crack extension took place in a co-planar manner. In addition they also assumed that since virtually all materials exhibit some strain hardening, the near tip fields up to the initiation of crack extension should be characterised by J. However Rice (1967) showed that for power law hardening materials, the size over which J is dominant in the crack tip region is a decreasing function of strain hardening exponent.

Quantitatively the stress field ahead of the crack tip is considered to be J-dominated if it takes the form of the H.R.R singularity expressed in Eqs 5.33 and 5.34. It is necessary to note that for low hardening rates the H.R.R field dominates at distances less than $2J/\sigma_0$ which is within the region that must be analysed by

a large geometry change solution. Consequently, a one parameter characterisation requires the presence of strain hardening and depends upon the test configuration. This can be illustrated by reference to the slip line field of a range of test configurations. McClintock (1971) pointed out that the perfectly plastic slip line fields for the cracked bend bar (CBB) in pure bending, the centre crack panel (CCP) and the double edge cracked bar (DECB) in tension as depicted in Fig 5.6 are dramatically different. This imposes limitations on the existence of a J-dominated flow field. These limitations have been studied in detail by McMeeking and Parks (1979) who used finite element analysis to compare the local blunting fields in full plasticity with the small scale yielding solution. An alternative technique leading to similar conclusions was developed by Shih and German (1981) who compared the asymptotic plastic field of cracks in tension and bending with the H.R.R field. Both the computations of McMeeking and Parks (1979) and Shih and German (1981) suggest that in bending J-dominance for deeply cracked bars is preserved as long as the uncracked ligament is greater than $25J/\sigma_0$ while in tension J-dominance is maintained if the uncracked ligament is greater than $200J/\sigma_0$.

Recently Al-Ani and Hancock (1989) have performed analyses for short cracks in edge cracked bars in bending and tension. They noted that short cracks exhibit plasticity which extends initially to the cracked face and that J-dominance was lost before the crack length $J=a\sigma_0/200$. They gave their result in terms of the crack length a because for short cracks, the relevant dimension is the crack length unlike deeply edge cracked bars where the controlling dimension is the ligament.

Particular attention is focussed on the size requirement for a J-dominated flow field of the centre crack panel in tension. Its behaviour shows that a one-parameter characterisation is a function of the specimen dimensions chosen. This can be seen by comparing size requirements proposed by McMeeking and Parks (1979) for a deeply cracked specimen with a/w=0.9 and Bilby et al's (1986) requirement for deeply cracked specimen with a/w=0.5 for non hardening materials. The former proposed that J is dominant as long as the uncracked ligament (w-a) $\geq$ 200 $J/\sigma_0$, while Bilby et al's proposed that J dominance is maintained if the ligament (w-a) $\geq$ 1266 $J/\sigma_0$. A further interesting result was obtained by Betegón and Hancock (1989) who analysed the centre crack panel for a wide range of ratios a/w. Based on their results, they indicated that J-dominance criterion was preserved, if the crack length for a given a/w (say 0.5) was of the order of $a \geq 4000\ J/\sigma_0$. These requirements are very severe and led Betegón and Hancock (1989) to conclude that centre crack panels loose J-dominance within the requirements of linear elastic fracture mechanics as codified in both British and American Standards (A.S.T.M. 1970). However, the J-dominance criterion was established with reference to the H.R.R field. Comparasion with the unmodified boundary layer formulations corresponding to the T-stress=0 field, made the requirements less severe but close to the linear elastic fracture mechanics size limitations.

## 5.6 Two Parameter Characterisation Of Elastic-Plastic Crack Tip Fields.

Larsson and Carlsson (1973) performed plane strain elastic-plastic analyses, using the finite element method, for a wide range of specimen geometries. They found significant differences in the plastic zone shapes and sizes for different specimens at the same K level. Nevertheless, they were able to explain their results in terms of a suggestion by Rice (1974) that differences from specimen to specimen in the non-singular terms of Eq 3.21 (section 3) could be responsible for the discrepancies.

The significance of the T-stress is however more profound than just its effect on the shape of the plastic zone. For non-hardening materials, crack tip plasticity has been the focus of discussion in terms of plane strain slip line fields. The slip line field proposed by Prandtl (1920), was identified by Rice (1968) as a representation of the limiting state of stress at the crack tip in small scale yielding. Its significance to small scale yielding was quantitatively studied by Levy et al (1971) and Rice and Tracey (1973) whose numerical data exhibited the necessary features of the Prandtl field. The Prandtl field is based on the assumption that plasticity completely surrounds the crack tip as illustrated in Fig 5.7. Du and Hancock (1990) examined plane strain crack tip deformation by modelling a boundary layer formulation using a focussed mesh, as shown in Fig 5.8. The boundary conditions

consisted of applying remote displacements associated with an elastic K field in addition to the displacements due to the T stress following the relation :

$$u=\frac{K}{E}\left[2(1+\upsilon)\sqrt{\frac{r}{2\pi}}\,f_{xx}(\theta)\right]+\left[(1-\upsilon^2)\left(\frac{\beta}{E\sqrt{\pi a}}K\,r\cos\theta\right)\right] \quad 5.35$$

$$v=\frac{K}{E}\left[2(1-\upsilon)\sqrt{\frac{r}{2\pi}}\,f_{yy}(\theta)\right]-\left[\upsilon(1+\upsilon)\frac{\beta}{E\sqrt{\pi a}}K\sin\theta\right] \quad 5.36$$

The biaxiality parameter $\beta$ was related to the elastic stress intensity factor K by the relation presented in Eq 3.23 (section3).

Du and Hancock (1990) used their numerical data to establish the effect of the T-stress both on the shape of the plastic zone and the crack tip stresses using plane strain slip line fields. The effect of the T-stress on the plastic zone shapes is illustrated in Fig 5.9. It was observed that negative (or compressive) T-stresses caused the radius of the plastic zone to become larger and force the plastic lobes to rotate in a clockwise direction while positive (or tensile) T-stresses caused the plastic radius to decrease in size and rotate in an anti-clockwise direction.

Betegón and Hancock (1990) analysed plane strain crack tip deformation for a strain hardening material using the boundary layer formulation model illustrated in Fig 5.8. They gave their results in terms of the non-dimensionalised tangential stresses $\sigma_{\theta\theta}$ ahead of the crack tip as a function of the non-dimensionalised radial distances $r\sigma_0/J$ for a range of T-stresses. These results are illustrated with the H.R.R solutions

in Fig 5.10. Here it is observed that the effect of either zero T-stresses, corresponding to one term boundary layer formulation, or positive T-stresses causes the stress levels to approach the H.R.R field. Negative T-stresses cause the stress levels to fall significantly below the H.R.R field by a magnitude that depends only on T and is independent of $r\sigma_0/J$.

To evaluate further the development of the stresses ahead of the crack tip for a hardening rate of n=13, distances within the range of validity of small geometry change solution ($2J/\sigma_0$ and $5J/\sigma_0$) as illustrated in Fig 5.11, were considered. It is clear that zero or positive T-stresses cause the crack tip stress fields ahead of the crack to approach the H.R.R, while negative T-stresses cause the stress fields to depart from the H.R.R field.

Attention is now turned on the stress distribution ahead of the crack tip at $r = 2J/\sigma_0$. The result reproduced from Betegón and Hancock (1990), and shown in Fig 5.12, confirms that positive T-stresses raise the stress levels towards the H.R.R field. In contrast, negative T-stresses cause the stress levels ahead of the crack tip to fall below the H.R.R field.

Betegón and Hancock (1990) were able to correlate two term boundary layer formulations with full field solutions for a range of geometries representative of negative, zero and positive biaxiality parameters ß. They concluded that full field solutions for geometries with zero or positive T-stresses (SENB a/w=0.3 and SENB a/w=0.9) matched closely those corresponding to one term boundary layer formulation in which only the K term was applied. In addition, full field solutions for geometries representative of negative T-stresses (CCP a/w=0.5) matched

those corresponding to two term boundary layer formulation in which the K and T terms were applied for n=13 and at $2J/\sigma_0$ and $5J/\sigma_0$.

To describe plane strain crack tip fields, Li and Wang (1986) sought two term asymptotic expansion of the form :

$$\sigma_{ij} = K_{s1}\, r^{s1} f_{ij}(\theta,n) + K_{s2}\, r^{s2} g_{ij}(\theta,n) \qquad 5.37$$

The first term in the right hand side of this equation was associated with the H.R.R field and is dependent upon the singularity r and the exponent s1. The $r^{s2}$ singularity in the second term (which arises directly from T) is much weaker than that of the first term which justifies the independence of the second term on r as indicated by Betegón and Hancock (1990). The results were summerised in terms of the following equation :

$$\frac{\sigma}{\sigma_0} = \left(\frac{\sigma}{\sigma_0}\right)_{(T=0,\ r)} + f(T) \qquad 5.38$$

This equation indicates that the first term on the right hand side is dependent upon r, and that the second term is a function of T and indepenedent of r. This implies that crack tip stress fields are characterised by the first term, if the magnitude of the second term is negligible ($T \geq 0$). If the second term however, is significant ($T \leq 0$), then both terms are necessary to characterise the stress distribution.

To extend the effect of T-stresses on the crack tip stress fields, large geometery change solution were analysed and the effect of T by Bilby et al (1986) was noted . The analysis consisted of analysing a modified boundary layer formulation

solution whose crack was modelled as a notch having a width "δ"and semi-circular tip of radius δ/2. An example of the mesh is illustrated in Fig 5.13. The boundary conditions consisted in applying displacements on the remote boundaries associated with the K field in addition to the displacement due to the T-stress. These authors performed further finite element analyses of specimen representative of negative, zero and positive T-stresses and were able to correlate their results with full field solutions. They proposed their numerical data in terms of the non-dimensional stresses $\sigma_{22}$ ahead of the crack tip as a function of the non-dimensional distances r/δ as shown in Fig 5.14 which is reproduced from Bilby et al's (1986). Here again, positive T-stresses are seen to raise the level of stresses ahead of the crack tip while negative T stresses decrease the level of these stresses at distances greater than 2 crack tip opening displacements ($r \geq 2\,\delta$).

From both small and large geometry change solutions, it may be concluded that the crack tip stress fields can be described by the H.R.R field and characterised by J alone when T is zero or positive ($T \geq 0$). In the presence of negative T-stresses, stress fields are characterised by J and T.

To apply this argument in practice and in order to observe the effect of the T-stress on the fracture toughness $J_c$, experimental investigations were carried out by Betegón (1990) and Sumpter and Hancock (1990). Betegón (1990) tested three-point bend specimens with a range of crack length representative of negative, zero and positive T-stresses. The results depicted in Fig 5.15 show that the fracture toughness is

higher for geometries exhibiting negative T-stresses. However when the T-stress is zero or positive, the difference in fracture toughness magnitudes is not significant. To reinforce Betegón's results, Sumpter and Hancock (1990) also performed experimental analyses. These authors tested single edge cracked bars in tension and three-point bend specimens. They concluded from their data illustrated in Fig 5.16 that negative T-stress were associated with high fracture toughnesses $J_c$. This is well in accord with the results obtained using finite element techniques.

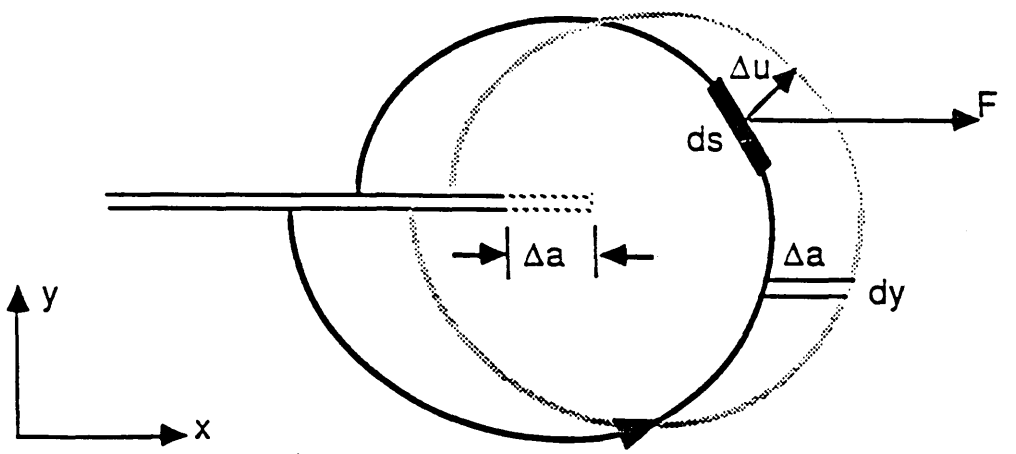


Crack tip coordinate system with arbitrary line integral.

Fig 5.1

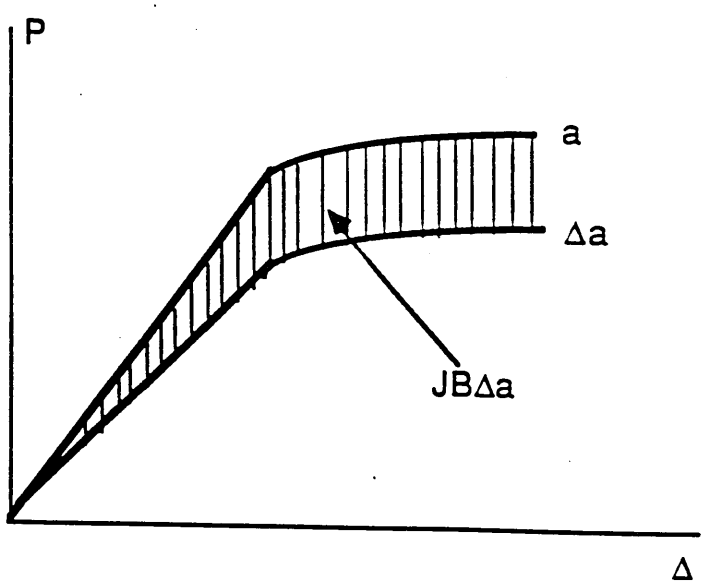


Interpretation of the J integral.

Fig 5.2

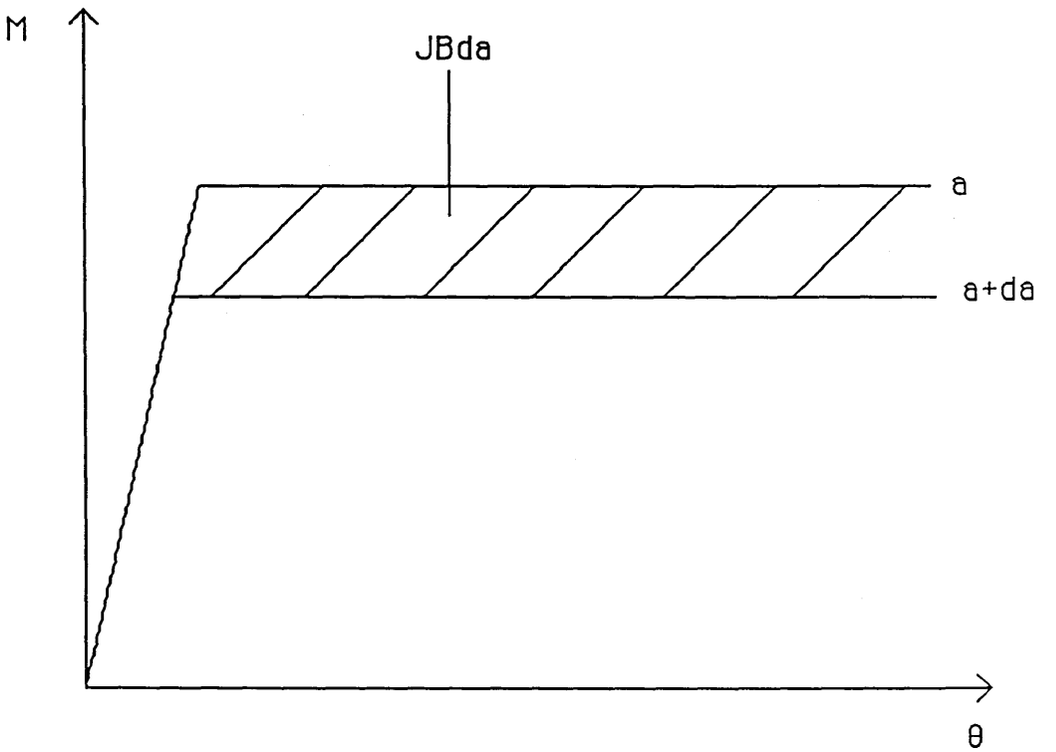


Moment as a function of the rotation θ for non-hardening materials.

Fig 5.3

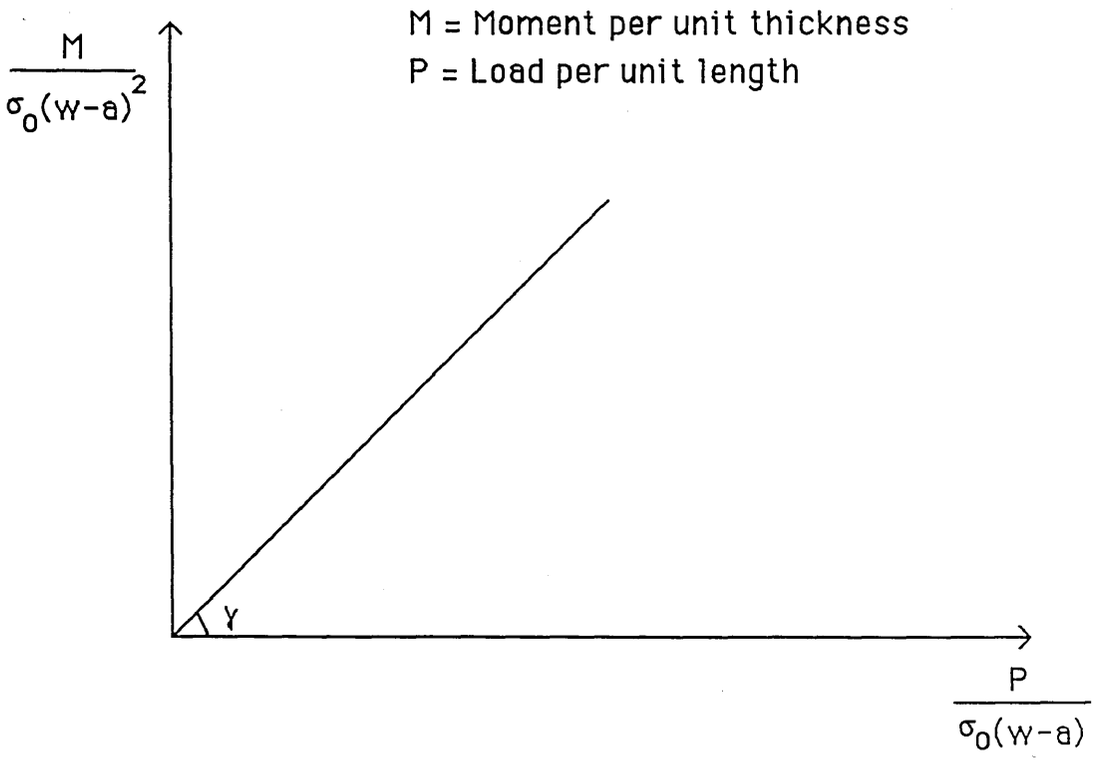


Non-dimensional Moment versus non-dimensional load.

Fig 5.4

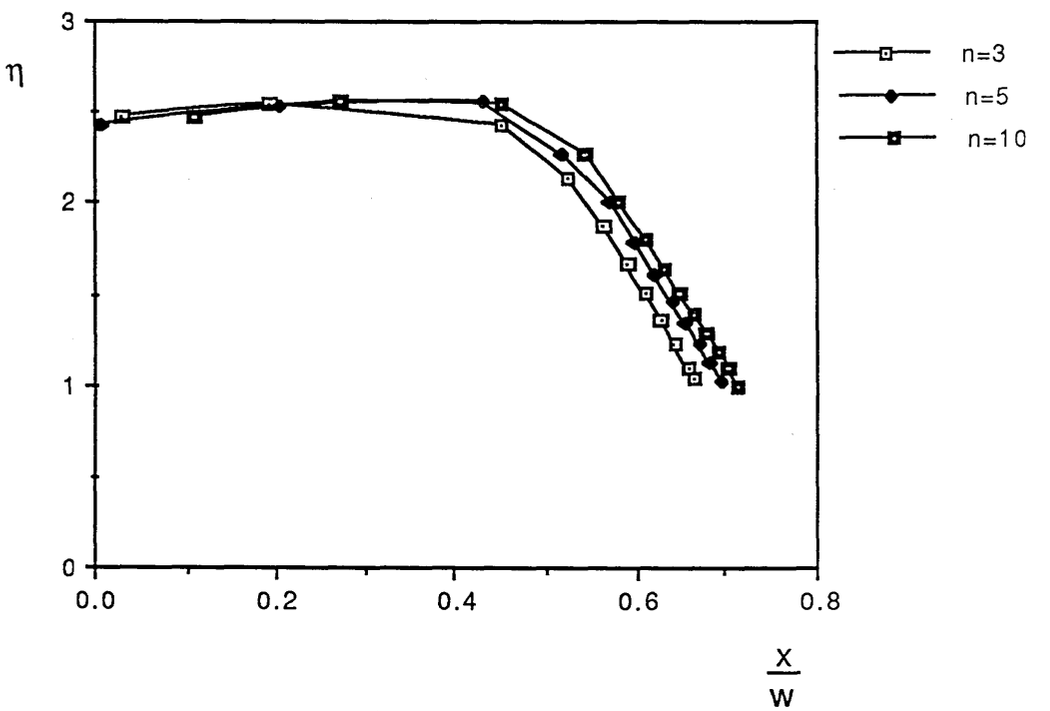


eta factor $\eta$ as a function of the loading point x/w for a range of hardening rates n

(After Shih and Hutchinson)

Fig 5.5

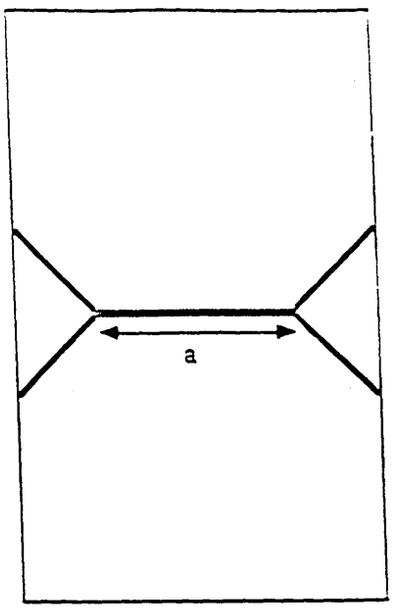


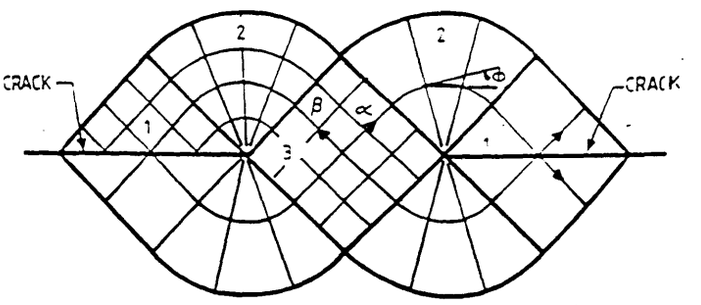


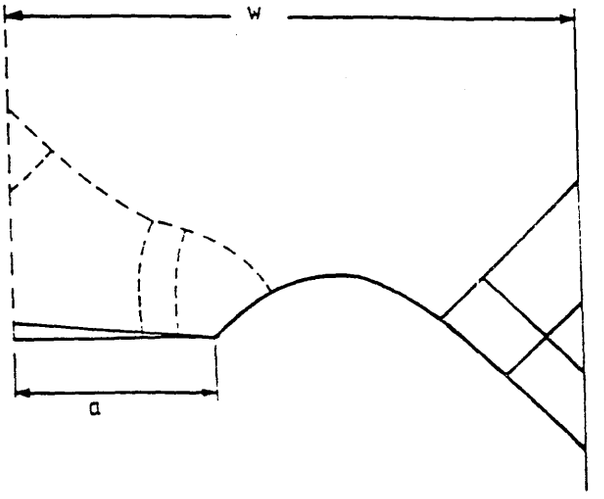


Slip line field for a C.C.P and D.E.C.B in tension and SECB In bending.

Fig 5.6

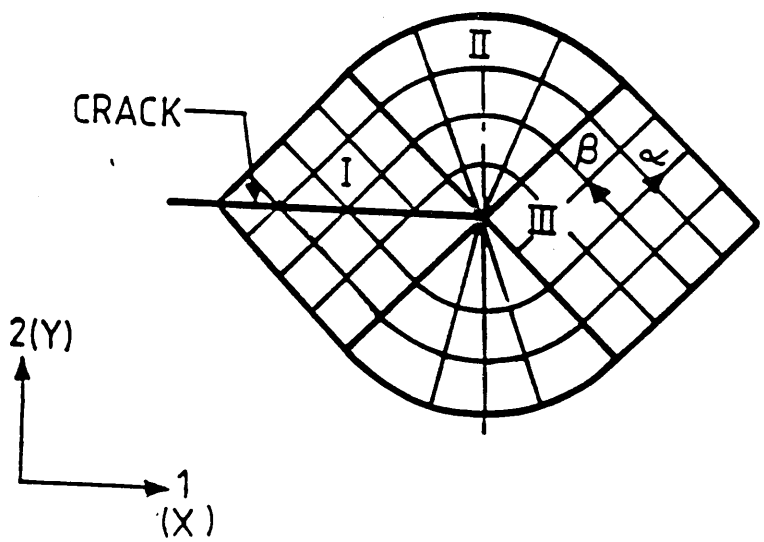


The Prandtl slip line field.

Fig 5.7

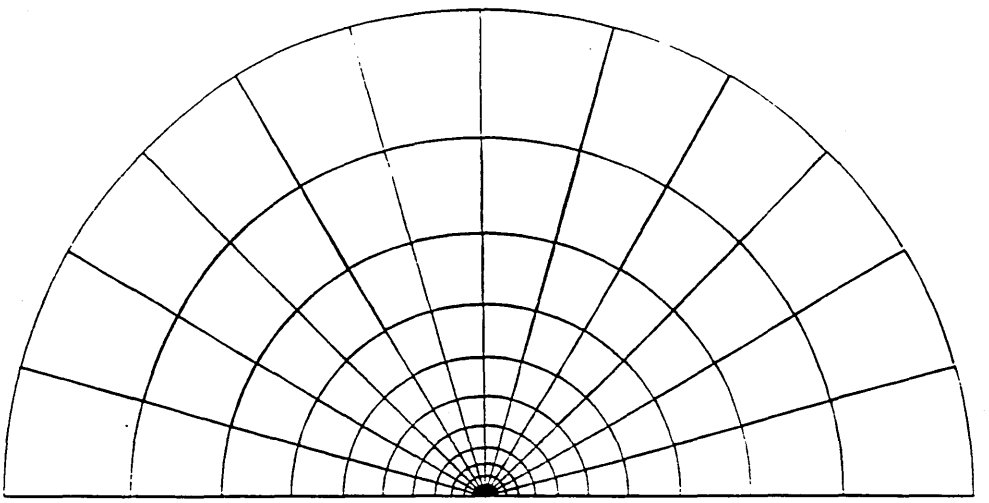

The focussed mesh of a boundary layer formulation.

Fig 5.8

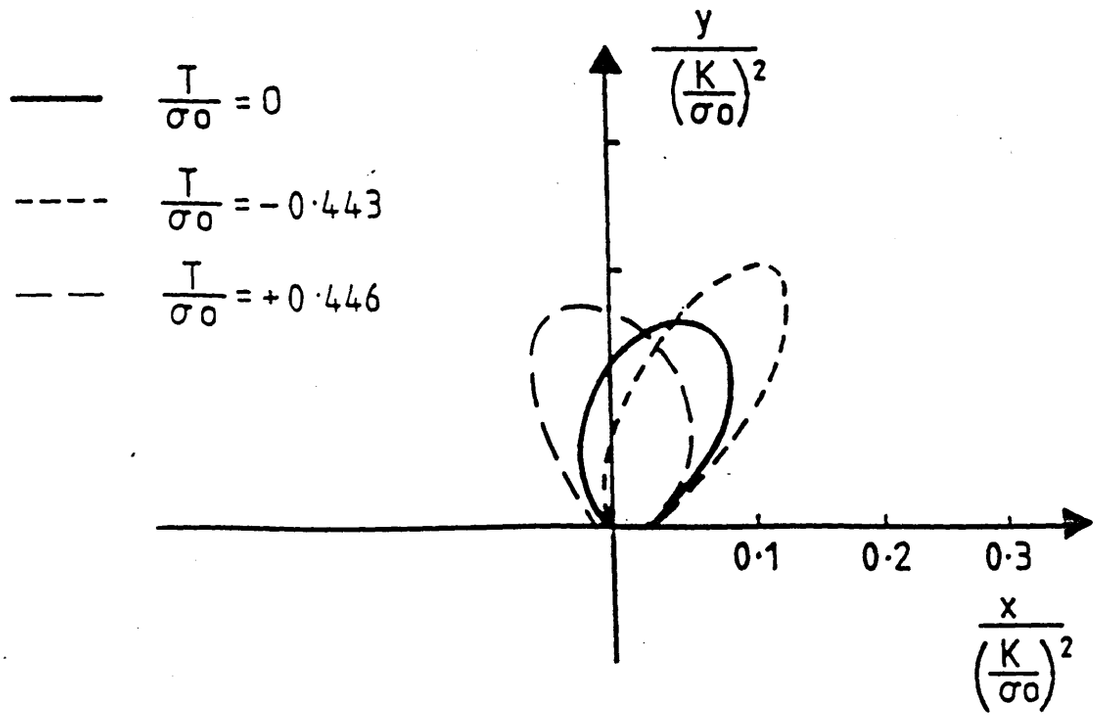


The effect of the T stress on the non-dimensionalised plastic zone shapes.

(After Du and Hancock)

Fig 5.9

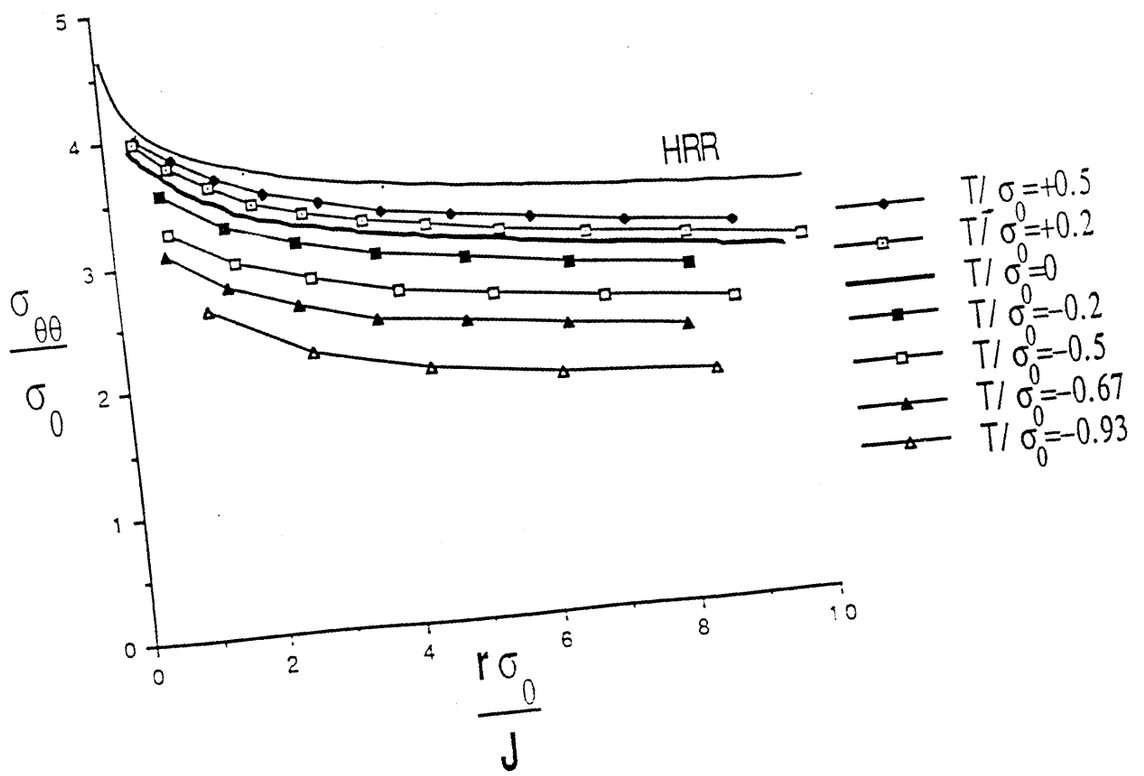


The tangential stress field ahead of a crack in a boundary layer formulation for a range of T stresses at n=13.

(After Betegón and Hancock)

Fig 5.10

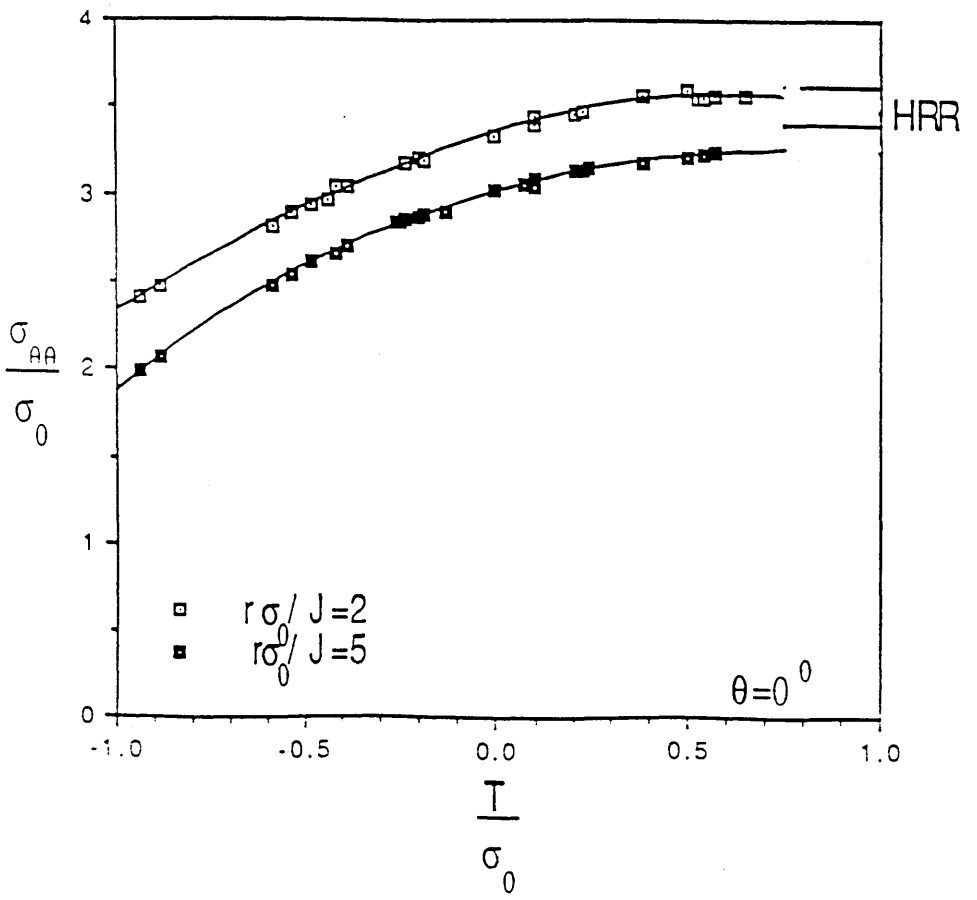


The tangential stress field ahead of a crack in a boundary layer formulation at distances $2J/\sigma_0$ and $5J/\sigma_0$ for n=13.

(After Betegón and Hancock)

Fig 5.11

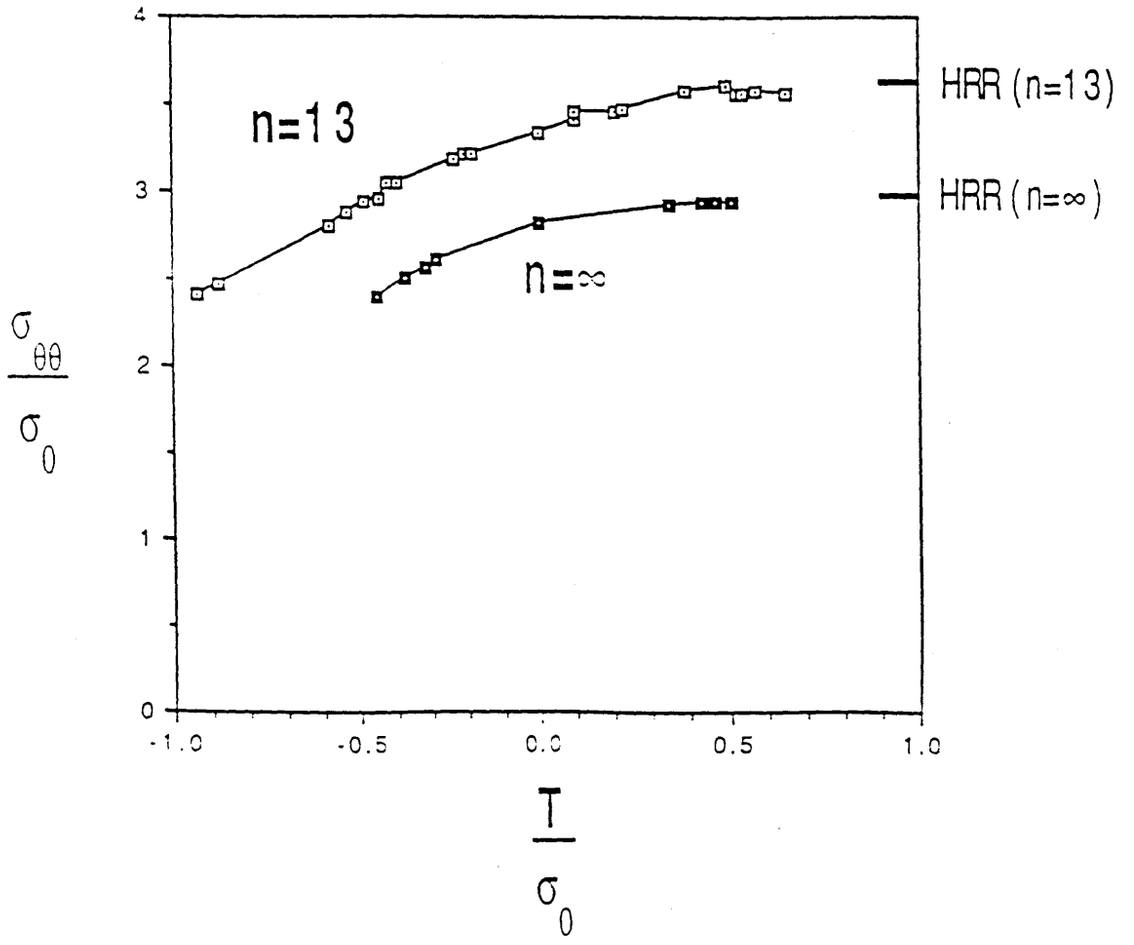


The tangential stress field ahead of a crack for strain hardening rates n=13 and n=∞.

(After Betegón and Hancock)

Fig 5.12

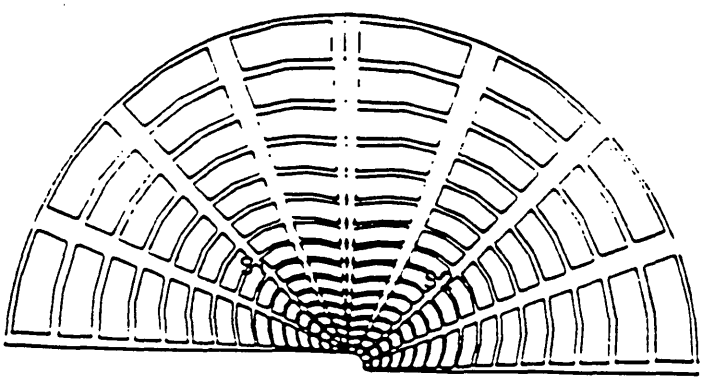

The mesh of a boundary layer formulation having a bulnt crack with a small initial radius.

(After Al-Ani and Hancock)

Fig 5.13

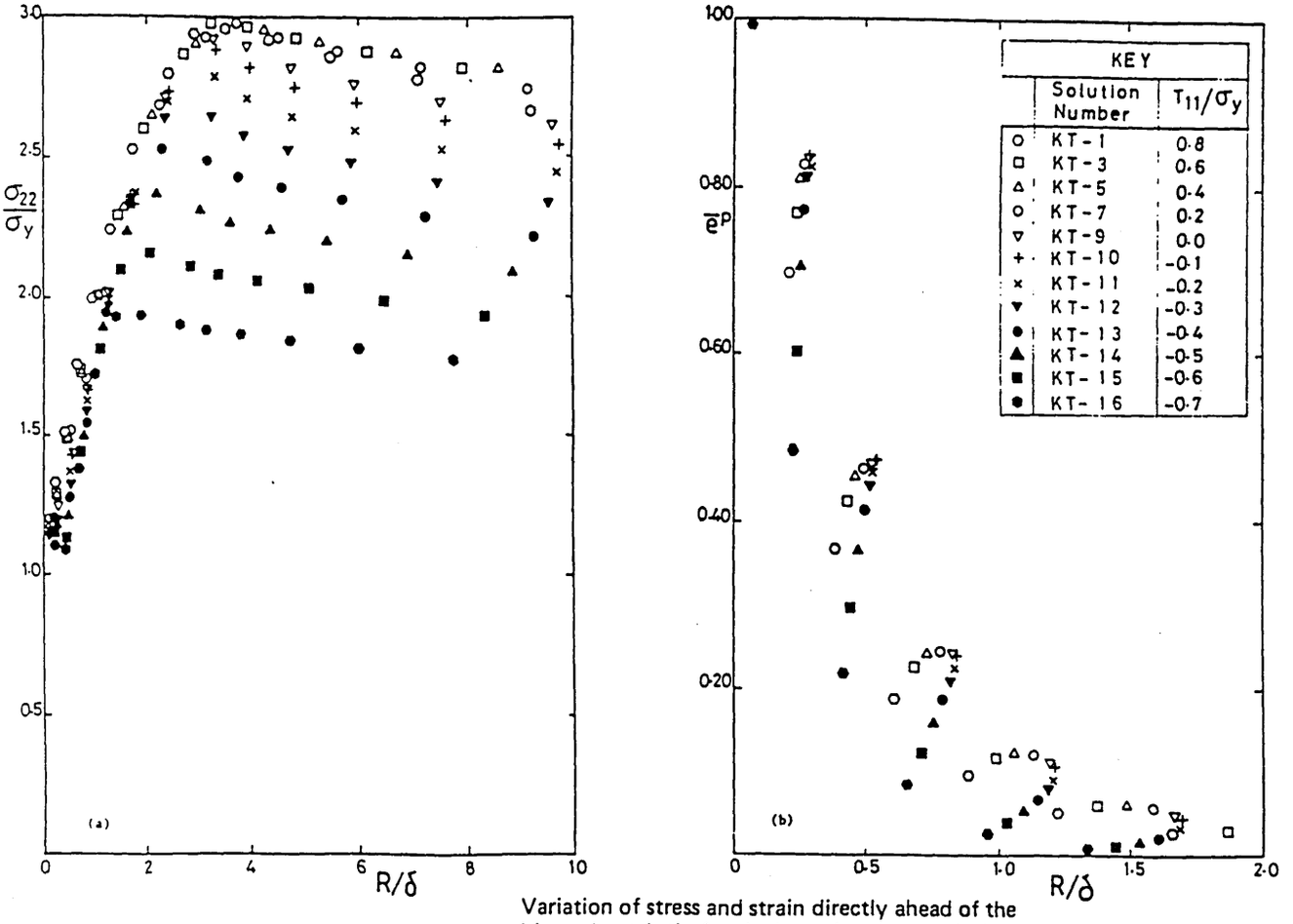


Variation of stress and strain directly ahead of the blunted notch tip for the boundary layer solutions: (a) direct stress, (b) equivalent plastic strain

(After Bilby et al)

Fig 5.14

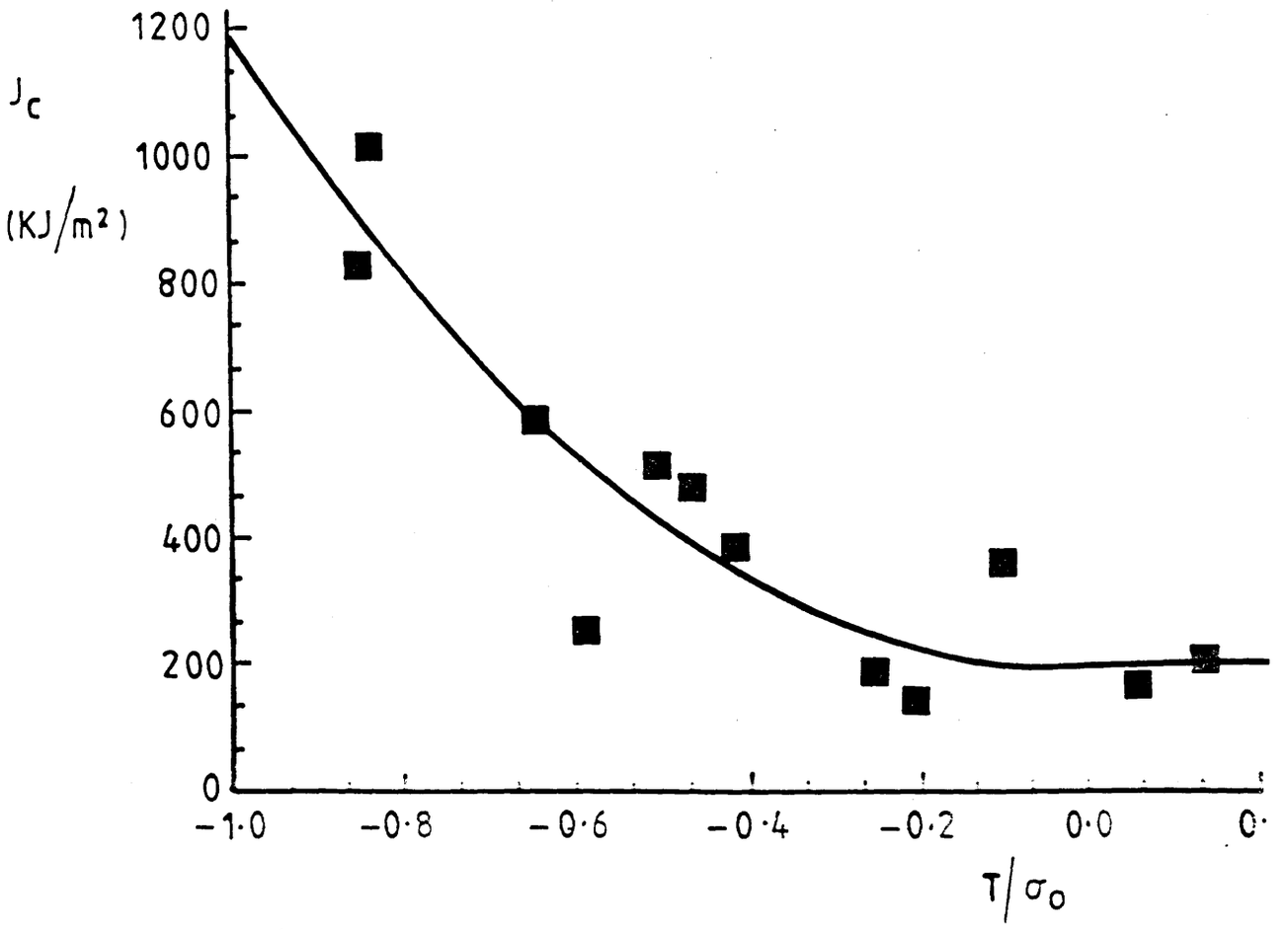


Fracture Toughness $J_c$ as a Function of The T-stress.

(After Betegón)

Fig 5.15

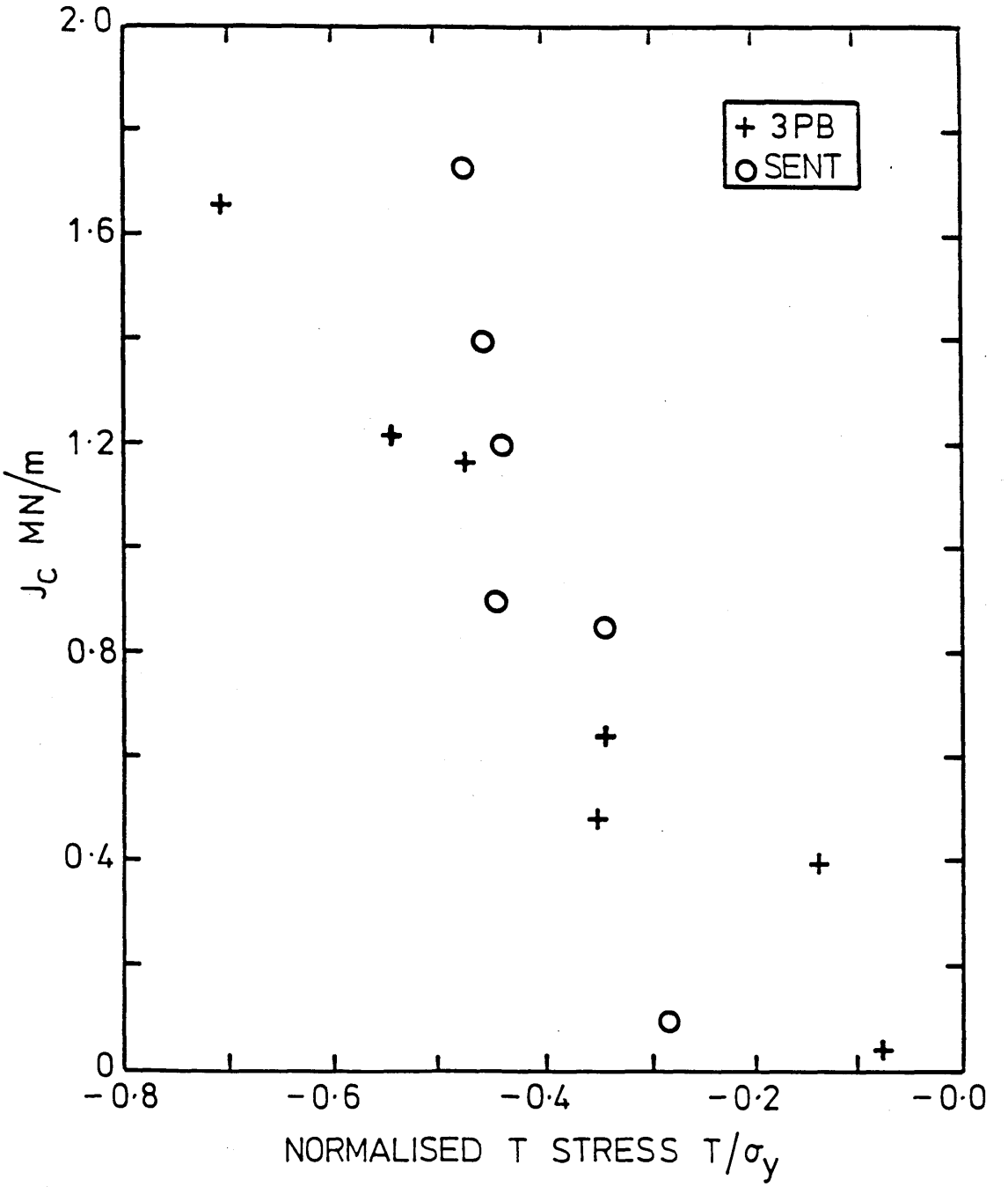


Fracture Toughness $J_c$ as a Function of The T-stress.
(After Sumpter and Hancock)

Fig 5.16

# 6 Design and Analysis of Specimens To Produce a Range of Biaxialities β

## 6.1 Introduction

In order to use the two parameter characterisation of elastic-plastic crack tip fields as a practical fracture criterion, it is necessary to design and analyse simple specimens capable of producing a wide range of biaxialities β. To achieve this, the use of an eccentrically loaded edge cracked bar such as that shown in Fig 6.1 is now proposed. The specimen was cracked halfway through its width giving an a/w=0.5. The eccentric loading produced combined tension and bending in the ligament.

The specimens were analysed under elastic conditions using a point force loading ranging from x/w=0 to x/w=0.75, where x is taken as the distance from the edge of the crack to the loading point. The finite element package Abaqus (1982) was used to carry out the analysis. In addition an analysis was performed to verify whether a distributed force loading (with the centre line of the distribution as the actual position in question) had any effect on the stress intensity factors and the biaxiality parameters in comparison with point force loading. The effect of distributed force loadings was considered because laboratory specimens whose loading configuration used rotating grips were subsequently tested. Further analyses involving distributed displacement loading on the remote boundaries were also performed, for similar reasons. It is relevant to note that in this

case, the rotation about the plane of the crack was not allowed. The finite element analyses provided an appropriate basis for performing the experiments.

## 6.2 Numerical Methods

The model shown in Fig 6.2 was generated with the aid of a commercial program called Patran (1988). The mesh used eight noded quadratic isoparametric elements with a focussed mesh concentric with the crack tip. The mesh comprised 184 eight-noded plane strain elements consisting of 621 nodes and 1241 degrees of freedom. The nodes at the crack tip were initially independent but coincident. Young's modulus was taken to be $10^{11}$ and Poisson's ratio 0.3. The model was loaded on the remote boundaries using point force loadings, distributed force loadings and distributed displacement loadings. The forces were distributed in such a way as to give the centre line as the effective loading point. As an example, consider the centre line to be at x/w=0.5. In this case, the loads were distributed over a non-dimensionalised distance of 0.7 from x/w=0.150 to x/w=0.850 over the span of the specimen such that the middle of the distribution would be at x/w=0.5. Such specific dimensions were considered in order to ensure that the results obtained from the present finite element calculations would be appropriate for use in later experimental investigations (Section 8). At this stage, it is necessary to justify the choice of these specific dimensions. For practical purposes, the laboratory model was loaded using grips. The grip was circular with an area

$A_G$ = 283mm$^2$ and the actual specimen area was $A_s$ = 400mm$^2$ as shown in Fig 6.3. In order to obtain the appropriate distribution, the area of the grip was divided by the area of the actual specimen to give a non-dimensionalised distance of 0.7. However, when part of the grip thickness was shifted beyond the edges of the specimen, the loadings were modelled such that the total loads were distributed over the remaining section. The distance from the crack edge surface to the centre of the distributed load is denoted as the effective loading distance and that to the centre of the grip is known as the nominal loading distance.

## 6.3 Stress Intensity Factor Solutions

The stress intensity factor K was derived using virtual crack extension method as discussed in section 4. Here, the non-dimensionalisation of K was obtained using the form :

$$Y_2 = \frac{KB\sqrt{W}}{P} \qquad 6.1$$

where B is the thickness, W the width and P the load applied. $Y_2$ is known as the stress intensity coefficient or constant of calibration. Fig 6.4 illustrates the variation of the non-dimensionalised stress intensity factor K with respect to point force locations x/w along the width of the specimen. In the case of distributed force loading, the load P in Eq 6.1 was taken as the total force applied on the remote boundaries. Fig 6.5 describes the way in which the constant of calibration $Y_2$ was affected

when the centre line of the distributed force loading was displaced along the width of the specimen. For distributed displacement loadings, similar non-dimensionalised distributions were adopted in order to observe whether both distributed force and displacement loadings gave identical results. For displacement loadings, the load P in Eq 6.1 was obtained in terms of the total reaction forces on the remote boundaries.
Fig 6.6 illustrates the effect of the resulting distributed displacements on the constant of calibration $Y_2$. For practical purposes, Fig 6.4 and Fig 6.5 were grouped together and the resulting point and distributed force loading graph is illustrated in Fig 6.7.

## 6.4 Biaxiality β Solutions

The specimens were also analysed to obtain the corresponding biaxiality parameters β. Here, the biaxiality parameter was calculated using the stress method as discussed in section 4. The resulting biaxiality parameter β for point force loading condition is graphically represented as a function of x/w in Fig 6.8. As for the point force loading, the biaxiality parameters were also obtained for distributed force loading. The resulting graph is illustrated in Fig 6.9. The biaxiality parameters for the distributed displacement loading condition are represented in Fig 6.10. It is appropriate to compare biaxiality parameters for point and distributed force loading. Hence, combining Fig 6.8 and Fig 6.9 together resulted in the graph shown in Fig 6.11.

For simplicity, rather than display the biaxiality parameters $\beta$ and the stress intensity factors K separately, these parameters can be combined by rearranging equations 6.1 and 3.27 (from section 3) to give the simple form :

$$\frac{T}{\sigma_{nominal}} = \frac{B Y_2}{\sqrt{\pi / 2}} \qquad 6.2$$

where the nominal stress $\sigma_{nominal}$ is defined as :

$$\sigma_{nominal} = \frac{P}{BW} \qquad 6.3$$

Here, P is load applied for point force loading or the total force applied for the distributed force loading. The results for point and distributed force loading, illustrated in Fig 6.12, are closely similar and can be expressed in a single polynomial of the form :

$$\frac{T}{\sigma_{nominal}} = 0.72\text{-}2.31 \left(\frac{x}{w}\right) \qquad 6.4$$

Equation 6.4 provides an alternative way of determining the T stress and is directly related to the load applied and the loading position x/w. The convenience of using this relation is seen in the ease of evaluating the T stress for any single edge crack specimen providing the load applied and the non-dimensional point of application x/w are known. There is thus no need required to determine the stress intensity factor K.

## 6.5 Discussion and Conclusions

From elastic analyses of a single edge crack bar in tension, the two characterising parameters, K and $\beta$, were derived for different loadings on the remote boundaries. As the loading point was moved from x/w = 0 to x/w = 0.6875, the K fields decreased corresponding to a decreasing moment on the ligament for both point and distributed force loadings. The constant of calibration $Y_2$ is geometry dependent and changes with the loading position. For both point and distributed force loading, the $\beta$ values changed from positive to negative corresponding to a decrease in the ratio of bending to tension. Fig 6.11 indicates that single edge cracked specimens experience tensile T stresses or compressive T stresses depending on the ratio x/w. Figure 6.12 suggests that whether a point force loading or a distributed force loading is applied, the results of $Y_2$ and $\beta$ are identical. However, when the distributed displacement loading was applied,the values of K and $\beta$ differed from those derived from force loading even though the trend of a decreasing K field and a more negative B field with respect to loading applications were similar. The reason for the difference arises from the fact that the distributed displacement loading inhibits rotation and thus changes the ratio of force to moment on the ligament.

It is relevant to note that irrespective of the nature of the force loading applications, as the loading point moved from x/w=0 to x/w=0.75, the ratio of bending to tension is reduced. This argument is clarified further by taking into account the displaced meshes for point force loading illustrated in figures 6.13 through 6.18 . Firstly, it is observed from Fig 6.13 and 6.14

(x/w=0 and x/w=0.25 corresponding to positive T stresses) that an opening mode of the crack occurred with a positive opening moment. Then, when the loading point was shifted to x/w=0.5, x/w=0.625 and x/w=0.6875 (corresponding to negative T stresses), an opening mode of the crack occurred but with negative closing moment. This is clearly seen by the form of the right hand edge of meshes 6.15, 6.16 and 6.17 respectively. The opening of the crack is related to the magnitude of the opening moment and hence the point of application x/w. When the loading point was applied between x/w=0 and x/w=0.5, the crack opened with a positive opening moment and with negative closing moment between x/w=0.5 and x/w=0.6875. A further analysis was carried out at x/w=0.75 and the biaxiality parameter $\beta$ derived had a very negative value ($\beta$=-1.75). Figure 6.18 illustrates the displaced mesh for this analysis. It is observed that the crack closes which suggests that pure stretch is reached at a point in the vicinity of x/w$\approx$0.7. Ernst (1983) performed analyses on compact tension specimens, whose behaviour is closely related to the present analysis. Care was taken in the set up of the dimensions involved in the present analysis to match Ernst's geometry. Ernst assumed that the stress across the ligament was uniform and predicted that pure tension was reached when a point force was applied over the middle of the ligament, which corresponds in the present investigation to x/w=0.75. In confirmation of the present results, Shih and Hutchinson (1986), Kaiser (1985) and McMeeking (1984) performed similar analyses and concluded that pure stretch was reached at a loading location approximating to x/w=0.7.

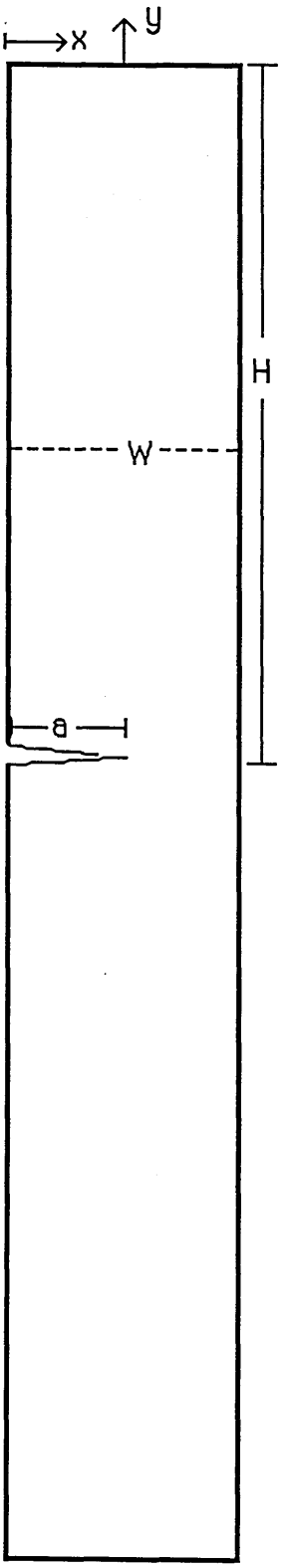


a/W=0.5

H/W=3

Dimensions of a single edge crack bar specimen a/W=0.5

Fig 6.1

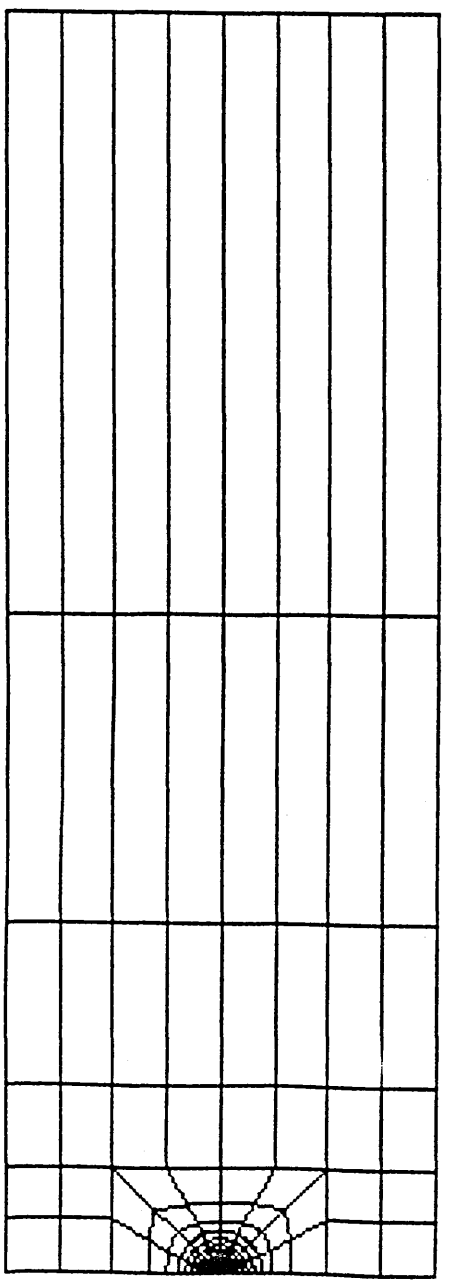

Finite Element Mesh with a/w=0.5

Fig 6.2

P=Load Applied
a=crack length
w=width
$x_{nom}$ = nominal loading distance
$x_{eff}$ = effective loading distance

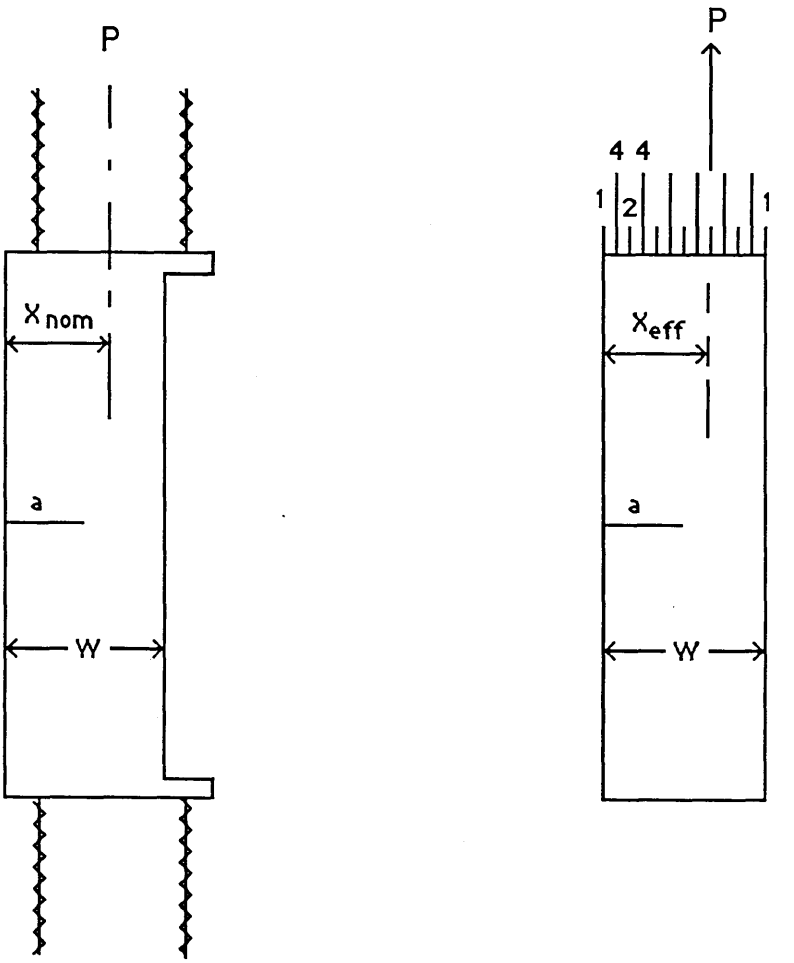


Nominal and Effective Loading Distances

Fig 6.3

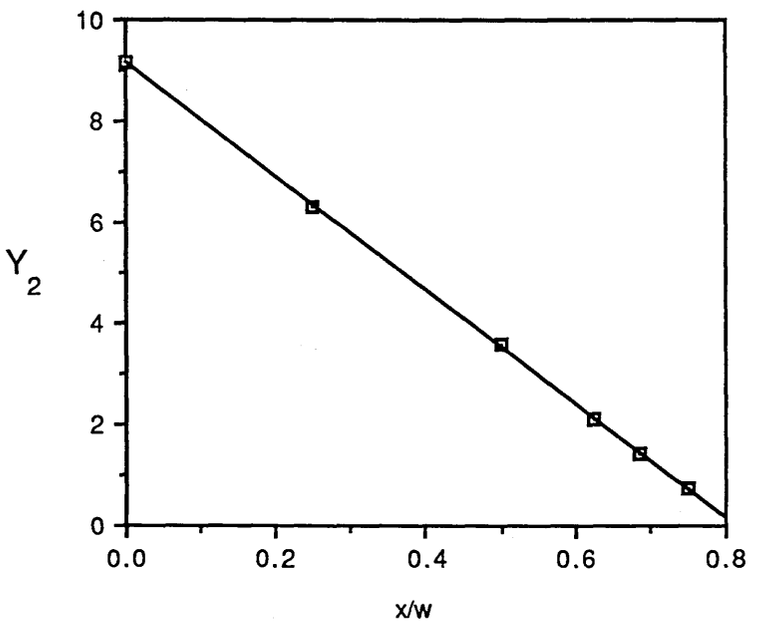


$Y_2$ calibration as a function of x/w for point force loading.

Fig 6.4

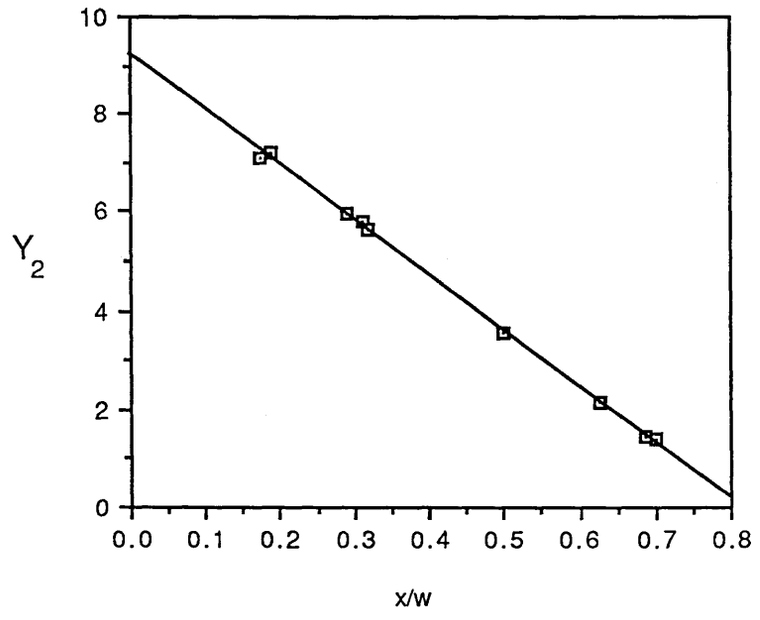


$Y_2$ calibration as a function of x/w for distributed force loading.

Fig 6.5

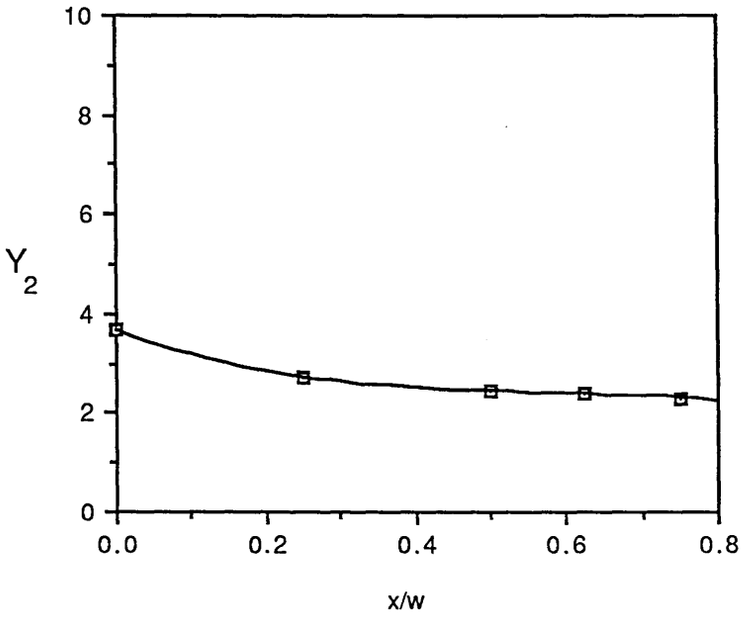


$Y_2$ Calibration As A Function Of x/w For Distributed Displacement Loading

Fig 6.6

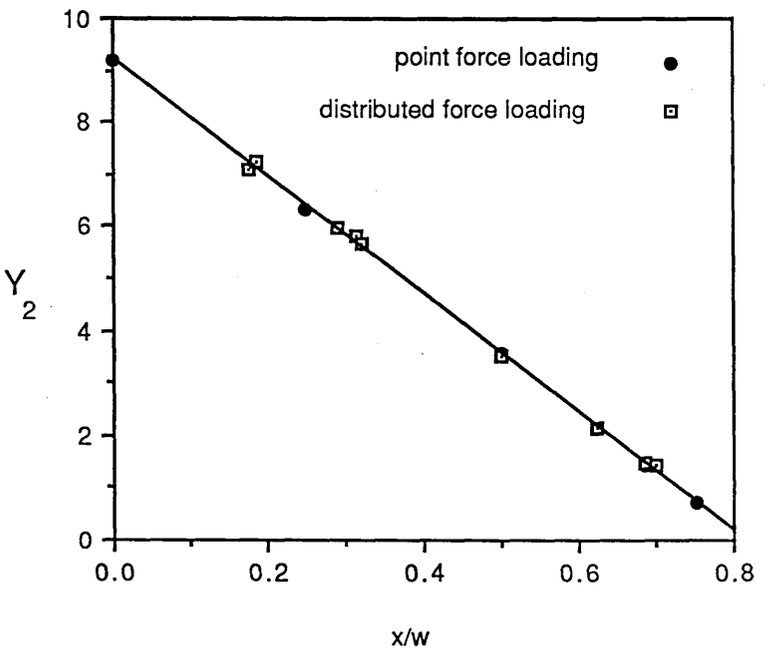


$Y_2$ Calibration As A Function Of x/w For Point And Distributed Force Loading

Fig 6.7

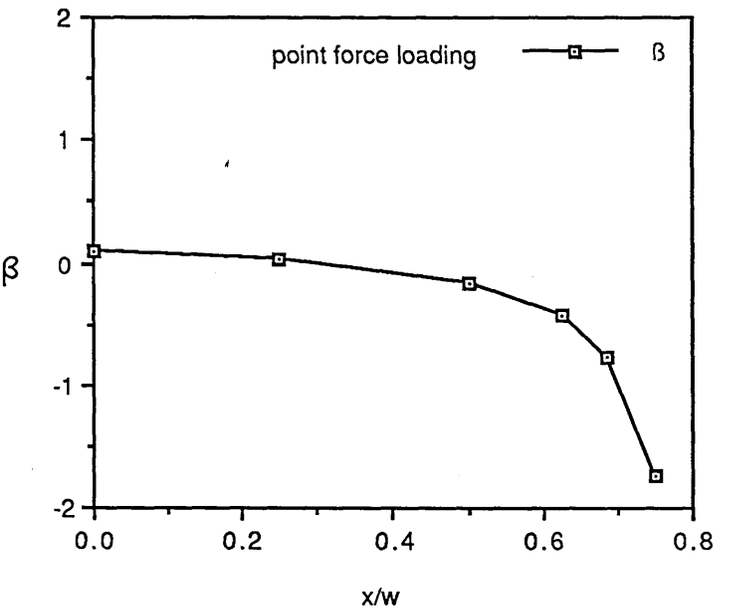


Biaxiality β as a function of x/w for point force loading.

Fig 6.8

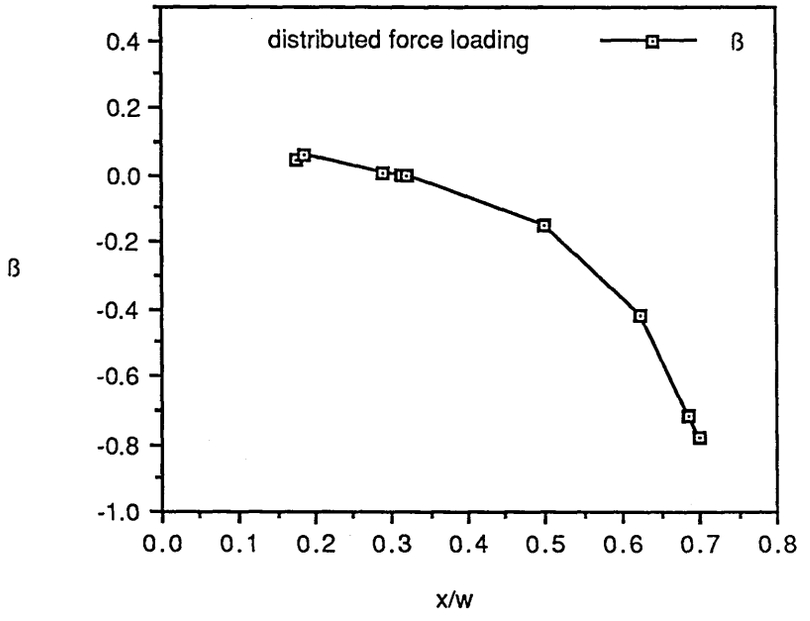


Biaxiality β as a function of x/w for distributed force loading.

Fig 6.9

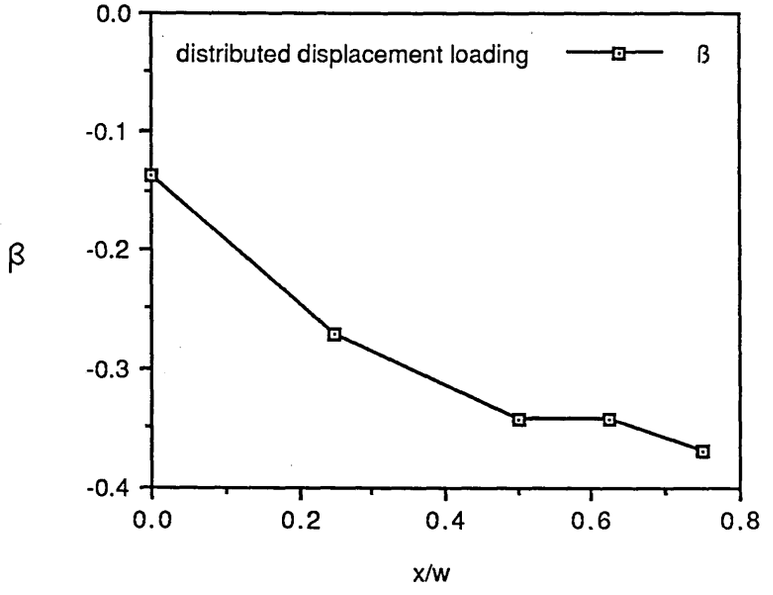


Biaxiality β As A Function Of x/w For Distributed Displacement Loading

Fig 6.10

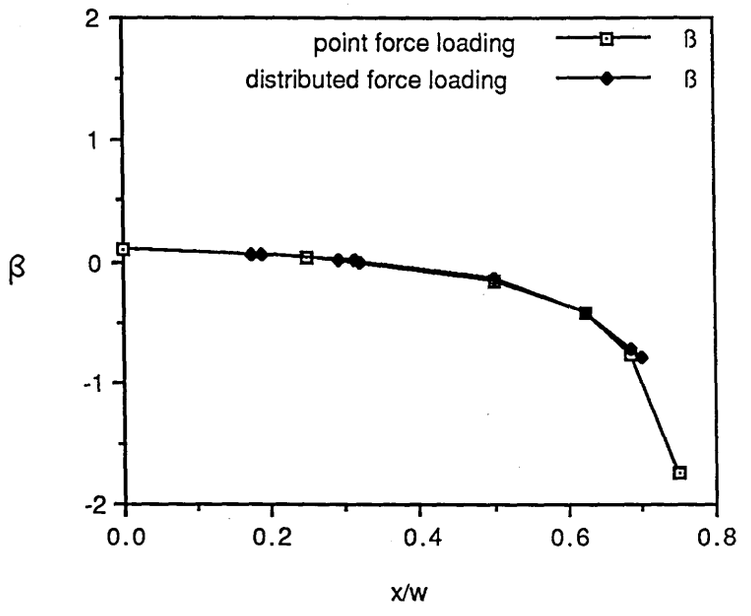


Biaxiality β As a Function Of x/w For Point And Distributed Force Loading

Fig 6.11

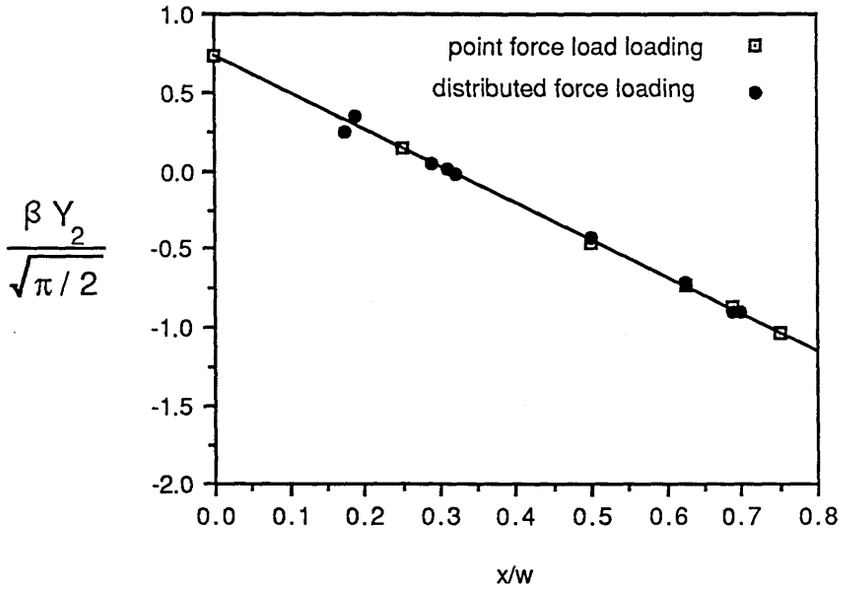


$\beta Y_2 / \sqrt{\pi/2}$ As A Function Of x/w For Point And Distributed Force Loading

Fig 6.12

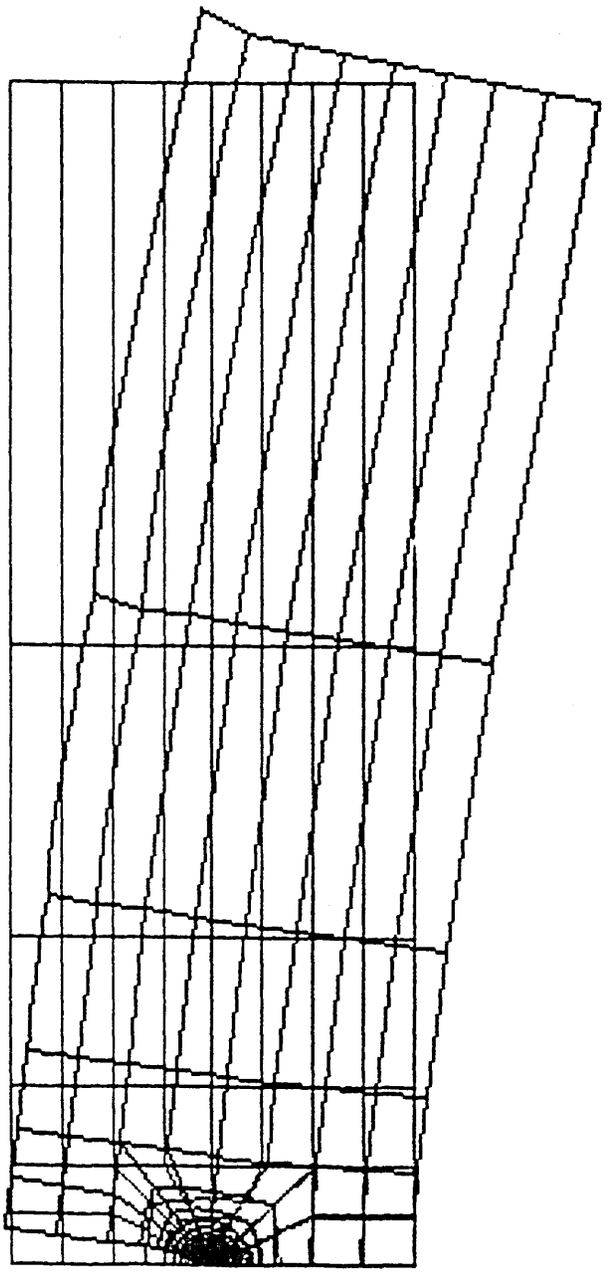

Displaced Mesh for x/w=0

Fig 6.13

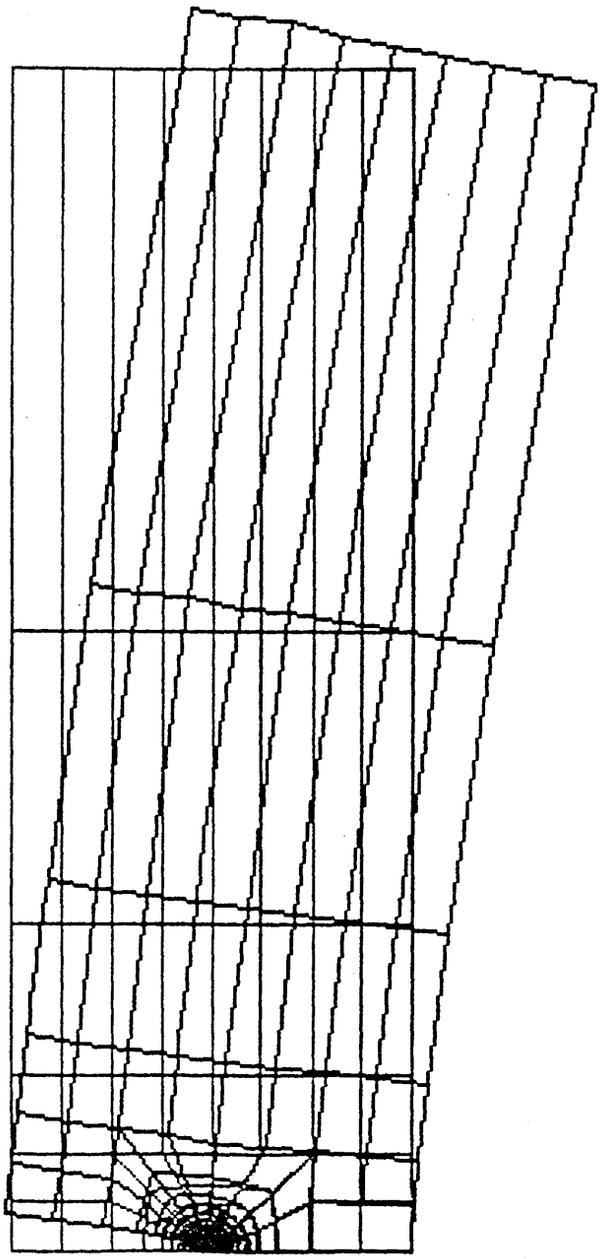

Displaced Mesh for x/w=0.25

Fig 6.14

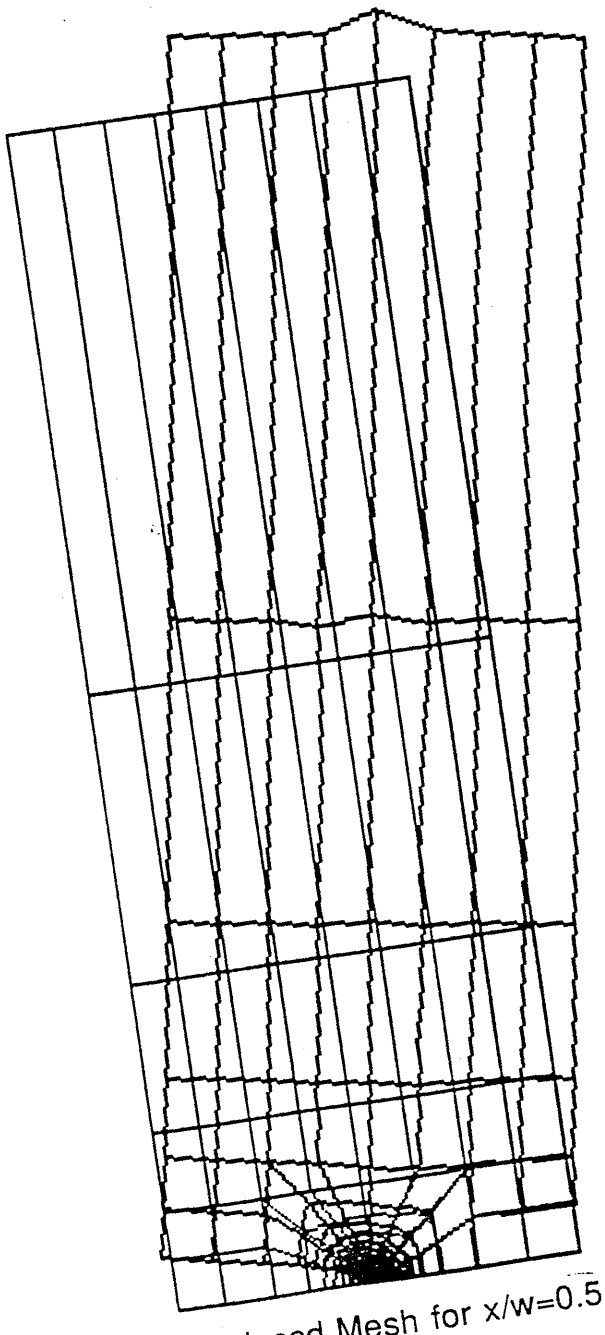

Displaced Mesh for x/w=0.5

Fig 6.15

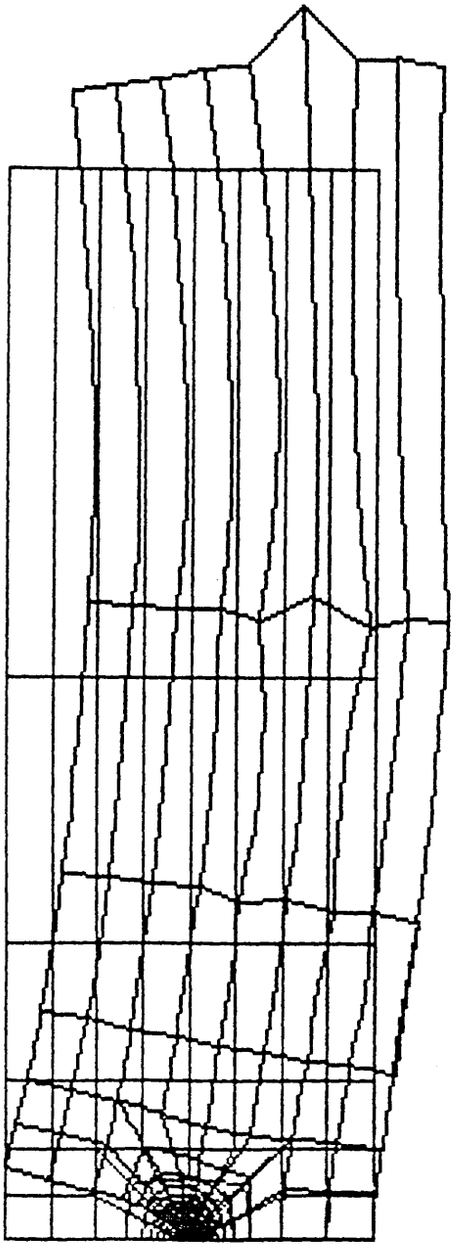

Displaced Mesh for x/w=0.625

Fig 6.16

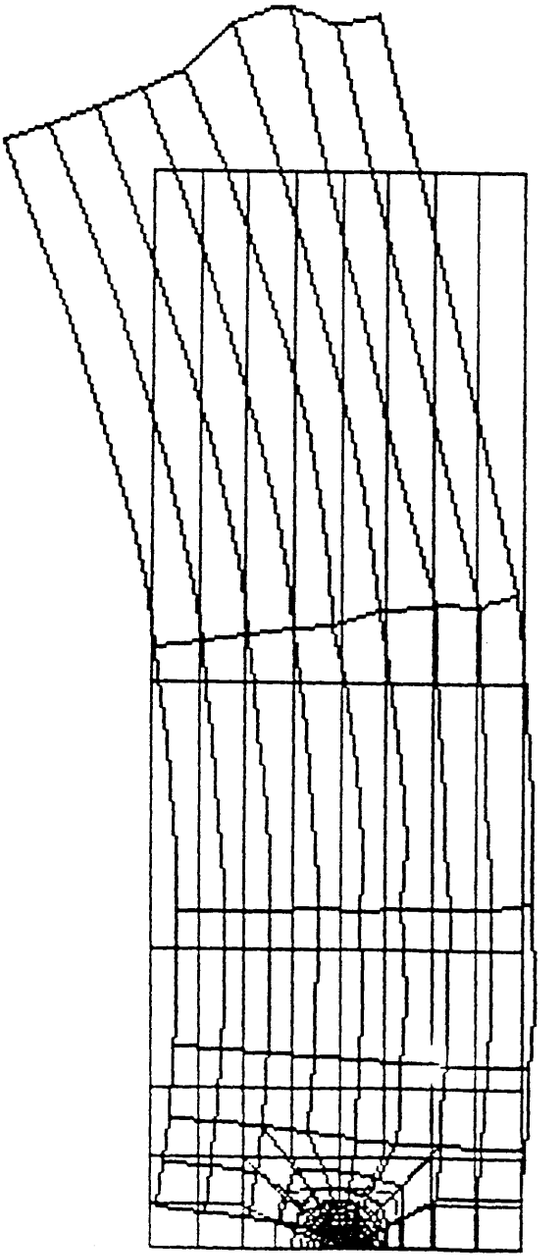

Displaced Mesh for x/w=0.6875

Fig 6.17

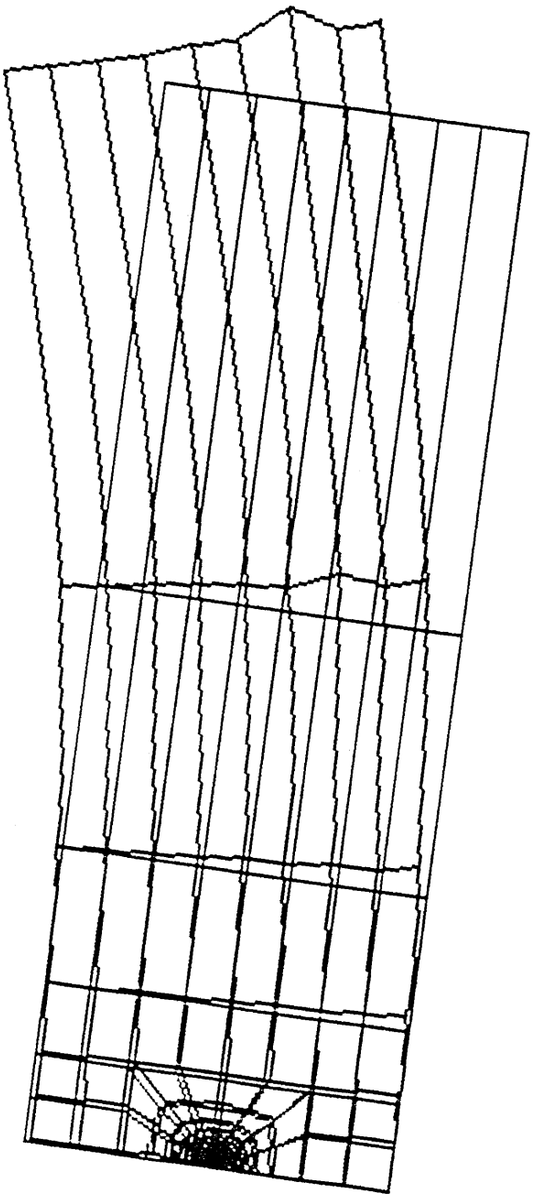

Displaced Mesh for x/w=0.75

Fig 6.18

# 7 Elastic-Plastic Analysis of Single Edge Cracked Bars Subject to Point Displacement Loading

## 7.1 Introduction

In order to use the two parameter characterisation of elastic-plastic crack tip stress fields as a practical fracture criterion, it is necessary to be able to determine both J and T for standard specimens such as eccentrically loaded edge cracked bars. The aim of the present finite element analysis was to establish a method for determining J from applied loadings. To evaluate J, limit loads were calculated for applied point loadings on the remote boundaries of the specimen at various locations (x/w) along the width. The resulting non-dimensionalised J were then plotted as a function of the non-dimensionalised displacement U/H and related to their elastic and plastic components $J^e$ and $J^p$ respectively. The results obtained were then compared with available published solutions.

## 7.2 Numerical methods

In order to limit the c.p.u time, the mesh used for the present elastic-plastic analyses had to be simpler than the mesh used for the elastic analyses. The model shown in Fig 7.1 was generated with the aid of the commercial program Patran (1988). The mesh used eight noded quadratic plane strain hybrid isoparametric elements with reduced integrations to prevent mesh locking. The mesh comprised 44 elements consisting of 163 nodes and 325

degrees of freedom. The nodes at the crack tip were independent but initially coincident. Young's modulus was taken to be $10^{11}$, Poisson's ratio 0.3 and the yield stress $2*10^{8}$. The model was loaded on the remote boundaries using point displacement loading. The point load distances (x/w) involved in this analysis varied from x/w=0 to x/w=0.625.

## 7.3 Limit loads

Limit loads P, were obtained from finite element calculations in terms of reaction forces. Deformation was maintained until the load reached a steady state at limit load. The limit load was non-dimensionalised in the form :

$$\alpha = \frac{P}{\sigma_0 \, B \, (w-a)} \qquad 7.1$$

Here $\sigma_0$ is the yield stress, B the thickness and (w-a) the ligament. The constant $\alpha$ is defined as the constant of calibration. For each point load distance x/w, a corresponding $\alpha$ was derived. In order to illustrate the effect of a varying x/w on $\alpha$, a graph is given in Fig 7.2

## 7.4 The J-Displacement Relation

J is simply given in terms of its elastic and plastic components in the form :

$$J = J^e + J^p \qquad 7.2$$

The elastic component of J can be written in terms of the stress intensity K in the form :

$$J^e = \frac{K^2}{E'} \qquad 7.3$$

Here, E' is the Young's modulus for plane strain conditions. By combining equations 7.1 and 7.3, and replacing P by its relation to the stress intensity coefficient $Y_2$ described in Eq 6.1, it follows that at limit load :

$$J^e = \frac{\alpha^2}{2} \left( \frac{\sigma_0}{E'} \right) (w\text{-}a)\, \sigma_0\, Y_2^2 \qquad 7.4$$

To determine the form of $J^p$, a graph representing the total J as a function of the non-dimensionalised displacement u/H was required. This is illustrated in Fig 7.3. It is suggested that the curves could be divided into two regions, dominated by either $J^e$ or $J^p$. The elastic component $J^e$ is related to the elastic component of displacement by a relation of the form :

$$J^e = \omega \, ( \Delta^e)^2 \qquad 7.5$$

Here, $\omega$ is a constant and $\Delta^e$ is the elastic displacement.
The plastic region could be described as a linear relationship between the plastic component $J^p$ and plastic displacement $\Delta^p$. To obtain the constant of proportionality, the slope of the plastic region was derived in the following form :

$$\gamma = \frac{J^p}{\sigma_0 \Delta^p} \qquad 7.6$$

A combination of Eqs 7.1 and 7.6 above produced the form for $J^p$ :

$$J^p = \left(\frac{\gamma}{\alpha}\right) \frac{P}{B.(w-a)} \Delta^p \qquad 7.7$$

In this equation, $\gamma/\alpha$ is equivalent to the eta factor given by Turner (1973) as :

$$J^p = \eta \frac{U^p}{B\ (w-a)} \qquad 7.8$$

where $U^p$ is the plastic work done and defined as ($P.\ \Delta^p$).
The effect of x/w on $\gamma$ is shown in Fig 7.4. In addition, the results based on the eta factor were obtained simply by dividing the plastic constant of proportionality $\gamma$ by the constant of load calibration $\alpha$. Finally, the graph representing the eta factor as a function of the load applications x/w is shown in Fig 7.5 together with available published solutions obtained from Shih and Hutchinson (1986).

## 7.5 Discussion and Conclusions

The present analysis was carried out in order to investigate the effect of point displacement loading applications on J, for single edge cracked bars subject to a combined bending and tension loading on the remote boundaries, under elastic-plastic conditions. As the loading point was moved from x/w=0 to x/w=0.625, the limit loads increased, as shown in Fig 7.2. The

increase in the limit load corresponds clearly to a decrease in the ratio of bending to tension on the ligament which has a significant effect on the shape of the plastic zone as depicted in Fig 7.6. The plastic zones were determined with the help of the Abaqus post processor. It is observed from these plastic shapes that when the specimen was loaded at x/w=0, the plasticity was constrained to the ligament. However, when x/w shifted progressively from 0 to 0.625 the shape of of the plastic zone tended to rotate about the ligament. At x/w=0.625, plasticity developed at an approximate angle of $45^0$ to the ligament. In addition to this, the plastic constant of proportionality $\gamma$ increased when the loading application was shifted between x/w=0 and x/w=0.625, as illustrated in Fig 7.4. From this figure, an interesting result was observed when the specimen was loaded at x/w=0.5 and x/w=0.625. At these locations, the plastic constant of proportionality $\gamma$ remained constant at approximately $\gamma$=1.85. This is further confirmed by considering the total J results shown in Fig 7.3. Here, the corresponding curves lie on top of each other.

The issue arises as to which location x/w, pure tension for elastic-plastic conditions was reached. From elastic analyses performed in section 6, the pure tension condition is reached at x/w≈0.7. To clarify this statement further, the graph of the eta factor as a function of x/w illustrated in Fig 7.5, suggests that when x/w was applied in the range x/w=0 to x/w=0.5, the constant $\eta$ had approximately a constant value and was maintained between $\eta$=2.4 and $\eta$=2.5. However when x/w was applied at x/w=0.625, where the state of stress was controlled

by tension, $\eta$=1.83. The argument is that pure tension is reached at $\eta$=1. To reinforce the present results , comparasion was made with published data available from Shih and Hutchinson (1986). These authors performed elastic-plastic analyses on compact tension specimens subjected to mode 1 deformation. They concluded that pure tension, corresponding to $\eta$=1 was reached at x/w≈0.7. Their results were reinforced by McMeeking (1984) and Kaiser (1985). Shih and Hutchinson (1986), also analysed their specimens for various hardening rates ( n=3, n=5, n=10). The specimen analysed in the present investigation was made to have a non-hardening material response (n=∞). The illustration in Fig 7.5 indicates that the eta factor is independent of the hardening rate of the material, which implies that $J^p$ can be determined directly from Eq 7.8.

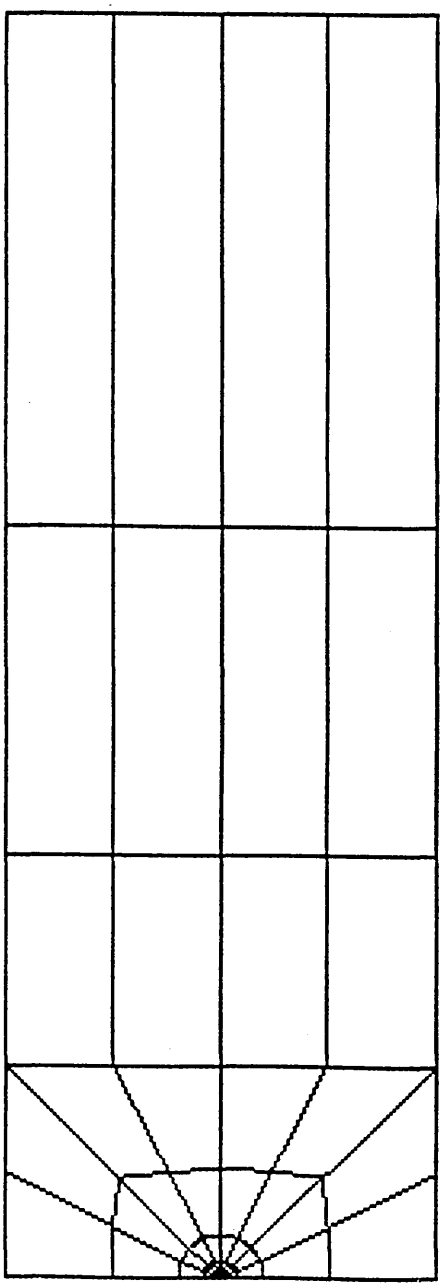

Finite Element Mesh with a/w=0.5

Fig 7.1

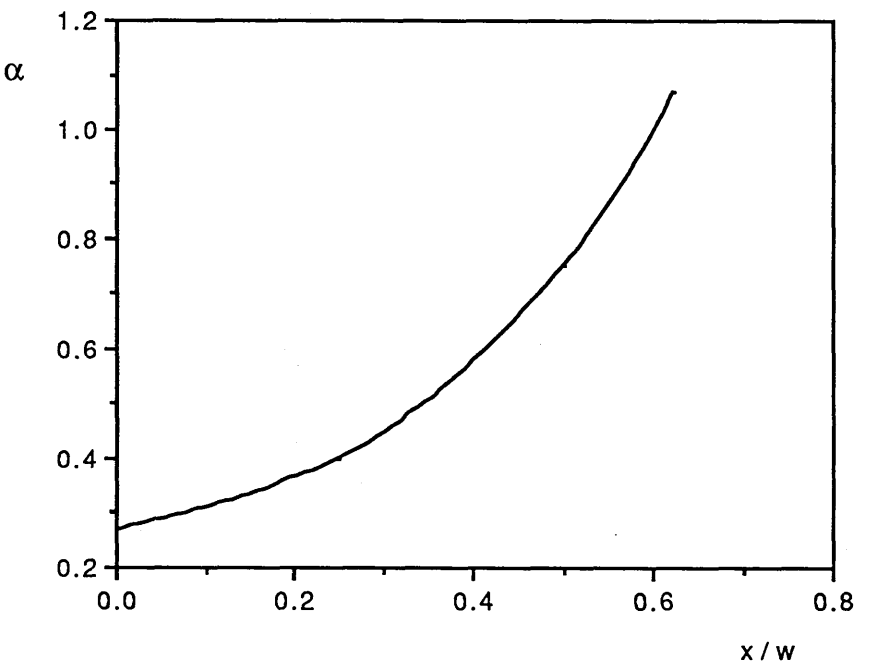


α Calibration as a Function of x/w

Fig 7.2

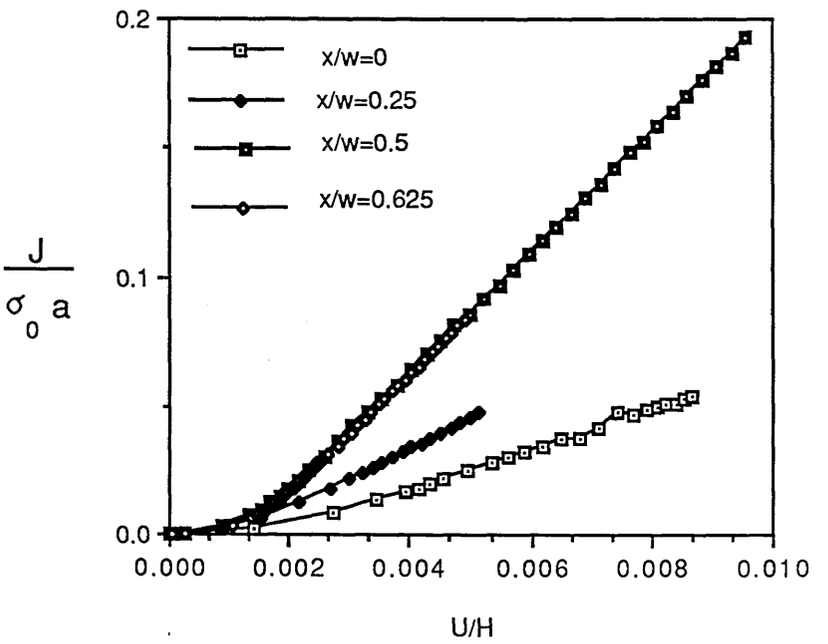


Non-Dimensionalised Total J As A Function Of Non-Dimensionlised Total Displacement U

Fig 7.3

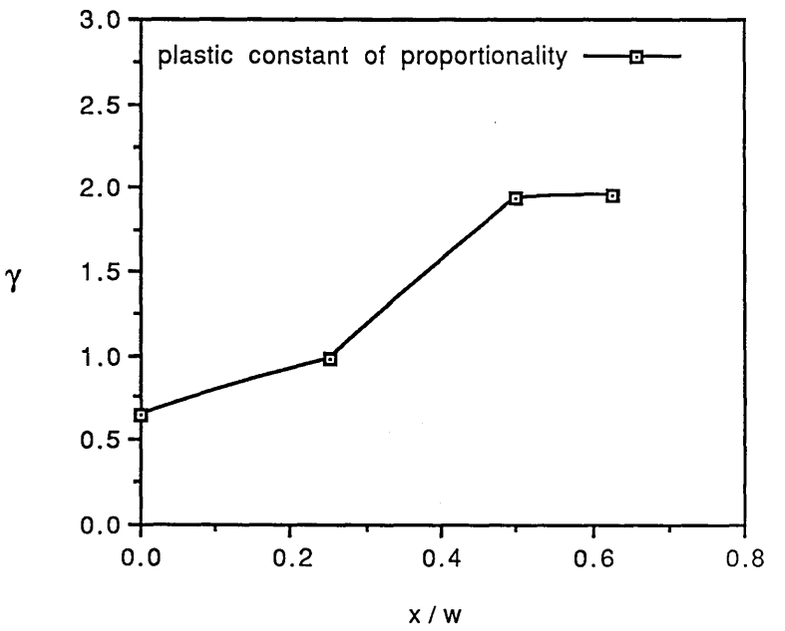


Plastic constant of proportionality $\gamma$ as a function of x/w.

Fig 7.4

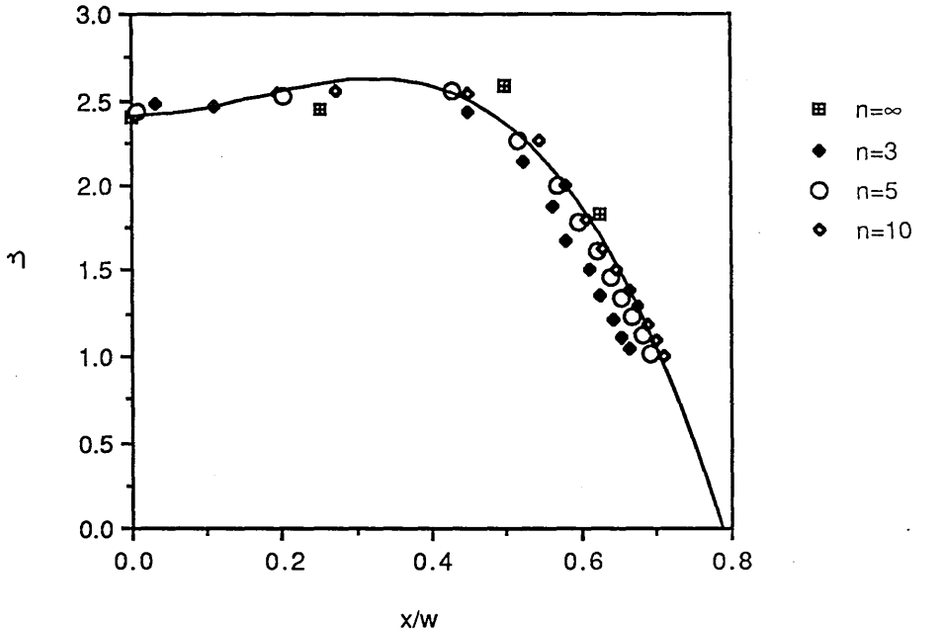


The "eta factor" $\eta$ as a function of x/w for non-hardening materials Together with different rates of hardening from Shih and Hutchinson.

Fig 7.5

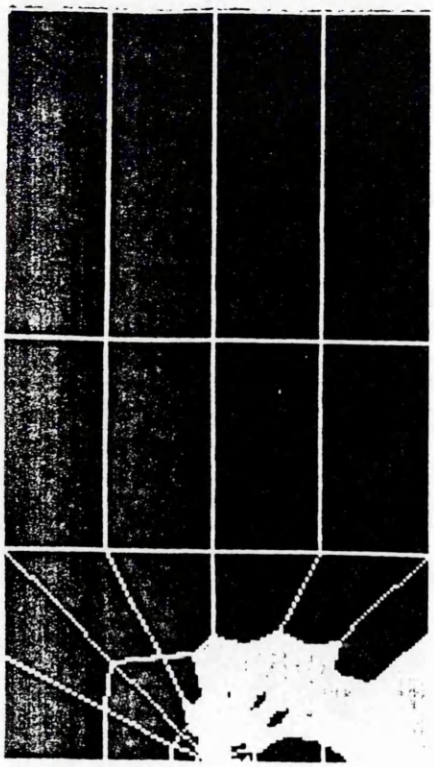

Shape of the Plastic Zone for x/w=0

Fig 7.6(a)

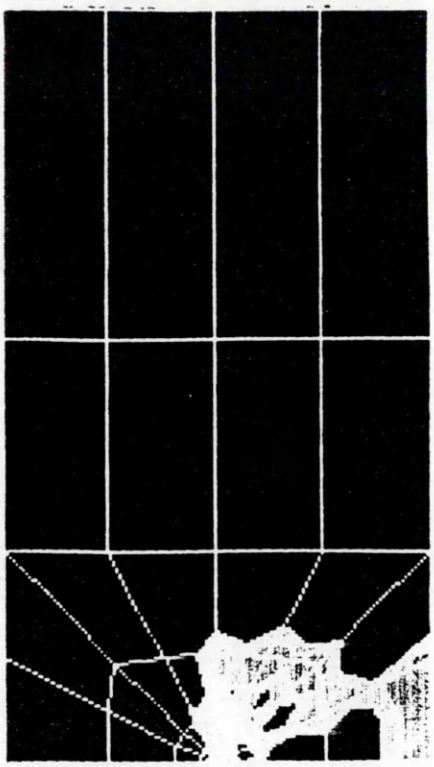

Shape of the Plastic Zone for x/w=

Fig 7.6(b)

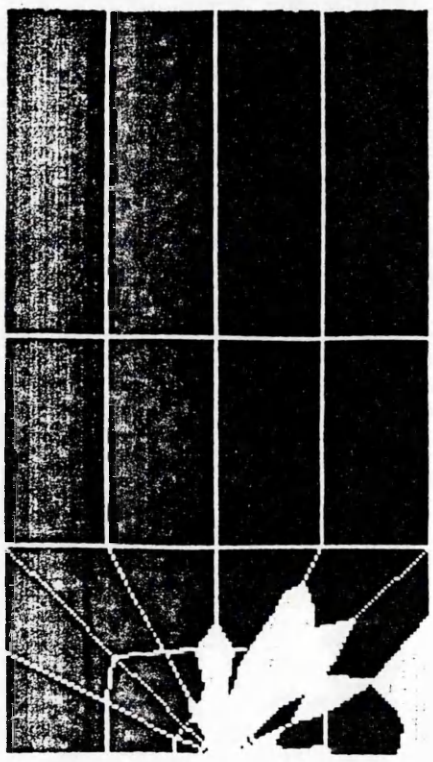

Shape of the Plastic Zone for x/w=0.5

Fig 7.6(c)

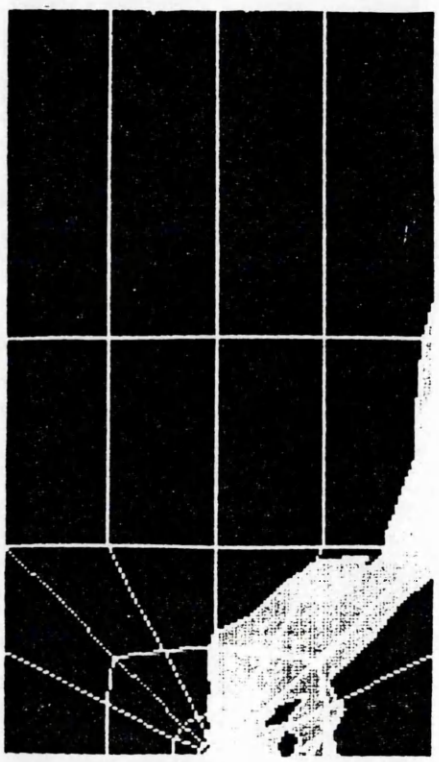

Shape of the Plastic Zone for x/w=0

Fig 7.6(d)

# 8 Experimental Results

## 8.1 Introduction.

Recent theoretical studies (Betegón and Hancock 1990, Du and Hancock 1990) suggest that negative T-stresses are predicted to produce geometry dependent enhanced fracture toughness values. In contrast, positive T-stresses are expected to produce geometry independent lower bound fracture toughness values. Two parameter fracture mechanics is intended to extend the range of application of single parameter fracture mechanics to deal with geometry dependent toughness.

In the present work, tests were performed on single edge cracked steel bars subject to eccentric tensile loads at low temperatures. These tests were carried out for a range of bending to tension loading configurations to verify both the validity of linear elastic fracture mechanics and the extent to which a single parameter fracture criterion could be used. At temperatures where one parameter fracture mechanics was not valid, the newly developed two parameter fracture mechanics was introduced in the form of fracture toughness/T-stress locus (C.T.O.D/T locus) to test its applicability as a failure criterion.

## 8.2 Material Properties and Experimental Methods.

The steel chosen for this experiments was a normalised mild steel designated 50D under B.S 4360 having a room temperature yield stress $\sigma_0$ = 360 MN/m$^2$. To obtain the yield stress as a function of temperature, the data of Bennett and Sinclair (1966)

is presented in Fig 8.1. At -200C, the yield stress (Bennett and Sinclair 1966) would be $\sigma_{(-200C)} = 3\ \sigma_0$. The chemical and mechanical properties of 50D are shown in Fig 8.2.

Specimens were cut from a rolled plate in the orientation shown in Fig 8.3. To introduce a fatigue crack, a 5mm v-notch was machined on the specimen such that the crack plane included the long and short transverse directions.

The bar shown in Fig 8.4 was then fatigue-cracked in three-point bend with a 100KN Dartec machine, at a loading frequency of 10 Hz. The maximum load used at the start of the fatigue-cracking was 55KN and the minimum was 5 KN, giving an average load of 30KN. As the crack proceded, the load was gradually decreased until the desired crack length to width ratio was obtained (in this case a/w=0.5).

The bar was then machined to the geometry shown in Fig 8.5, in which the crack length "a" was 10mm and the width B 20mm giving an a/w ratio of a/w=0.5. In the experiments, the ratio (a/w) was kept constant and the specimen was subjected to a combined bending and tension loadings by moving the loading axis x/w (x is the point of application of the load) from x/w=0 to x/w=0.625. The centre line of the 19mm grip corresponded to the effective loading application x/w. The machine used for the present tensile tests was a 250 KN Instron machine. The resulting displacements were associated with the machine crosshead displacements and together with the loads applied, at a displacement rate of 8.33 μm/s, were recorded graphically.

The experiments were carried out at low temperatures for a range of x/w ratios. These temperatures were -196C, -100C and

-50C. At -196C, the specimen was immersed in liquid nitrogen in a cylindrical container and left for approximately one hour to allow the temperature to equilibrate. At higher temperatures (-100C or -50C), a different technique was used. The specimen was surrounded by a copper coil which in turn was covered with cotton wool to insulate the specimen. The coil was then cooled by pumped liquid nitrogen until the specimen cooled to the required temperature, as recorded by a thermocouple attached to the specimen.

## 8.3 Analyses of Results.

### 8.3.1 Fracture Toughness.

At -196C the specimen cleaved and the load-displacement curve was basically elastic in which case $J_c$ was related to the K applied in the following way :

$$J = \frac{K^2(1-\upsilon^2)}{E} \qquad 8.1$$

Here, the stress intensity factor K is related to the load applied by the relation :

$$K = \frac{Y_2 P}{B\sqrt{w}} \qquad 8.2$$

Rearranging Eq 8.1 and 8.2 results in :

$$J = \frac{Y_2^2 P^2 (1-\upsilon^2)}{B^2 w E} \qquad 8.3$$

Here, $Y_2$ is the stress intensity coefficient determined from linear elastic finite element calculations as discussed in detail in Section 6 and P is the load applied. At this temperature, the fracture surface was reduced to a $1cm^2$ sample and examined in a scanning electron microscope. The cleaved and the fatigue-cracked surfaces are shown in Fig 8.6(a) and 8.6(b) respectively.

At -100C, the specimen also cleaved but with extensive plasticity. In this case, the fracture toughness $J_c$ was determined with the use of the relation :

$$J = \frac{K^2}{E'} + \eta \frac{U^p}{B\ (w-a)} \qquad 8.4$$

Here the elastic component was evaluated using Eq 8.1, and the plastic component $U^p$ was derived from the work done as the area under the curve. $\eta$ is the eta factor derived from finite element calculations (Section 7).

At -50C, the specimen displayed extensive plasticity and failure occured by ductile void growth and coalescence. To obtain the fracture toughness at this temperature, several specimen were tested in order to estimate the condition at which crack extention initiated. This corresponded to the start of crack tearing which was observed under an optical microscope, by sectioning and polishing the specimen to its centreline. A micrograph of the polished section showing the initiation of

tearing is presented in Fig 8.7. The fracture toughness $J_c$ was determined by using a similar approach as that adopted at -100.

The effect of temperature on $J_c$ is shown in Fig 8.8. In order to observe the size restrictions associated with one parameter characterisation, the limit of J-dominance is also drawn on the $J_c$/temperature graph.

### 8.3.2 The Crack Tip Opening Displacement.

The crack tip opening displacement corresponding to the initiation of tearing was measured with the help of an optical microscope fitted with measuring devices, for specimens tested at -50C. However at -100C and -196C, where brittle failure occured the crack tip opening dipsplacement prior to failure was evaluated from its relation to J following :

$$\delta = d_n \frac{J}{\sigma_0} \qquad 8.5$$

Here, $d_n$ is a function of the material response, and was evaluated from its relation to J at -50C. The variation of the crack tip opening displacement with temperature is shown in Fig 8.9.

### 8.3.3 The Elastic T-stress.

The T-stresses were calculated at each temperature following the relation derived from the finite element calculations as :

$$\frac{T}{\sigma_{nom}} = 0.72 - 2.31\left(\frac{x}{w}\right) \qquad 8.6$$

where x is the loading axis at which the load was applied and $\sigma_{nom}$ is the nominal stress. Equation 8.6 above relates the T-stress directly to the applied load. However, an alternative route leading to the determination of the T-stress was also applied. This consisted in relating the T-stress to the biaxiality parameter $\beta$ and the stress intensity factor K (Section 6). The stress intensity factor K was derived using Eq 8.2. Both techniques produced similar results for the T-stress.

Rather than represent $J_c$ as a function of the T-stress, a more convenient approach is the use of the equivalent crack tip opening displacement parameter which is physically more convenient as it can be measured directly from laboratory tests. The crack tip opening displacement as a function of the T-stress is given in Fig 8.10 for a temperature of -50C.

## 8.4 Discussion and Conclusions.

The data obtained from the experiments indicates that at very low temperatures (-196C) the material exhibited a brittle behaviour. At this temperature, the magnitude of $J_c$ was independent of the loading conditions and the T-stress. This was associated with a linear elastic response to failure, and the L.E.F.M size requirement were satisfied. By replacing the appropriate values in the relation :

$$B, a, (w-a) \geq 2.5 \left(\frac{K}{\sigma_0}\right)^2 \qquad 8.8$$

the magnitude of 2.5 $(K/\sigma_0)^2$ was 3.77mm, which was less than the specimen dimensions (B, a, w-a, 20mm, 10mm, 10mm). This confirmed that L.E.F.M was valid at 196C.

When the temperature was increased, the fracture toughness also increased. At -100C, cleavage fracture was proceded by extensive plasticity and the L.E.F.M size requirements were not satisfied. At this temperature 2.5 $(K/\sigma_0)^2$ was 27mm which was greater than the specimen dimensions, implying that L.E.F.M was not valid, but geometry independent results were obtained for $J_c$ and $\delta_c$.

At -50C it was observed that $J_c$ increased as the ratio of bending to tension decreased. At x/w=0, the state of stress was dominated by bending while at x/w=0.625, the state of stress was controlled by tension. Under these conditions, $J_c$ was dependent upon the loading conditions and consequently T.

From Fig 8.8 it is seen that for $J= \sigma_0(w-a)/25$, which defines J-dominance for bending, single parameter characterisation can be used for temperatures below approximately -160C. However the present test results indicate that J-dominance would be valid for temperatures up to -100C suggesting $J= \sigma_0 (w-a)/6$. Above this temperature, the one parameter characterisation is not valid and a two parameter fracture criterion is necessary.

Similarly, the crack tip opening displacement as a function of temperature shown in Fig 8.9 implies that at low temperatures (-196C to -100C), the magnitudes of the C.T.O.D's are similar and independent of the remote state of stress. However at -50C, the

resulting C.T.O.D's vary with the ratio of bending to tension and hence depend on T. Here a two parameter characterisation is necessary to establish a fracture criterion.

The two parameter failure locus is presented in terms of the crack tip opening displacement/ T-stress locus at -50C and shown in Fig 8.10. The data obtained from the present analysis shows that the magnitudes of the C.T.O.D's are geometry dependent for negative T-stresses and increase when T becomes more negative. Physically this implies that geometries that exhibit negative T-stresses develop crack tip stresses that reduce progressively at the same distance ahead of the crack tip as the load increases. It is necessary to increase the load in order to reach critical stress values at the same distance. Therefore negative T-stresses produce higher C.T.O.D's (or equivalently a higher $J_c$) as discussed in detail in Section 5. Geometries that exhibit positive T-stresses however, have a crack tip stress distribution similar to that of the small scale yielding distribution. Any increase in T does not make the crack tip stresses more severe which implies that positive T-stresses produce geometry independent C.T.O.D values, as confirmed by the experimental data in Fig 8.10

To reinforce the present C.T.O.D/T locus result shown in Fig 8.10, test results performed by Al-Ani (1991) on the same steel but different geometry were available. This author tested three-point bend specimens for a range of a/w ratios representative of negative T-stresses (short crack with a/w=0.1) and positive T-stresses (deep crack with a/w=0.5) at -50C. The C.T.O.D was measured by a clip gauge attached to the

specimen, and the T-stress was evaluated with the use of Eq 8.7. It is seen that the data points which resulted from the three-point bend tests fall on the same C.T.O.D/T locus obtained from the present tests.

It is concluded that a C.T.O.D/T locus as a two parameter fracture criterion can be used as a failure criterion and extends the range of application of elastic-plastic fracture mechanics.

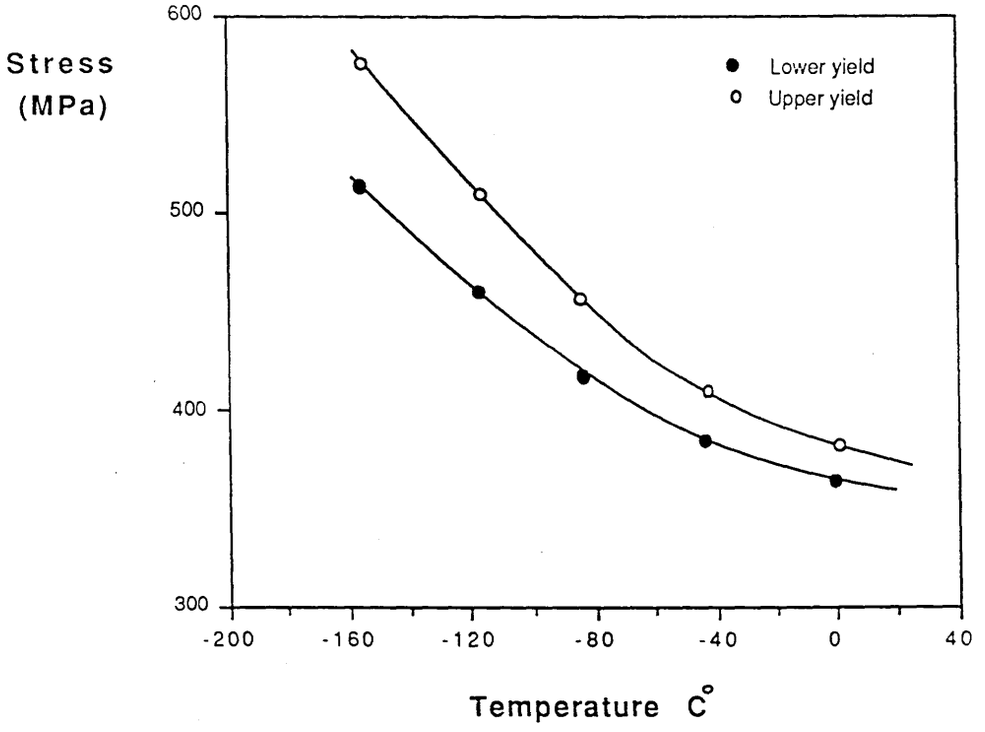


Variation of upper and lower yield stress with temperature

After Bennett, P.E. and Sinclair (1966)

Fig 8.1

Chemical Composition (Wt%)

| C | Si | Mn | P | S | Cr | Mo | Cu | Nb |
|---|---|---|---|---|---|---|---|---|
| 0.17 | 0.29 | 1.30 | 0.010 | 0.008 | 0.09 | 0.01 | 0.11 | 0.045 |

Mechanical Properties

| Yield Stress MPa | Ultimate Stress MPa | Elongation % | Reduction of Area %AV |
|---|---|---|---|
| 360 | 558 | 26 | 56 |

Chemical composition and mechanical properties of BS4360 grade 50D steel

Fig 8.2

R.D = Rolling Direction
L.T = Long transverse
S.T = Short transverse

2L = 230mm
W = 50mm
B = 20mm

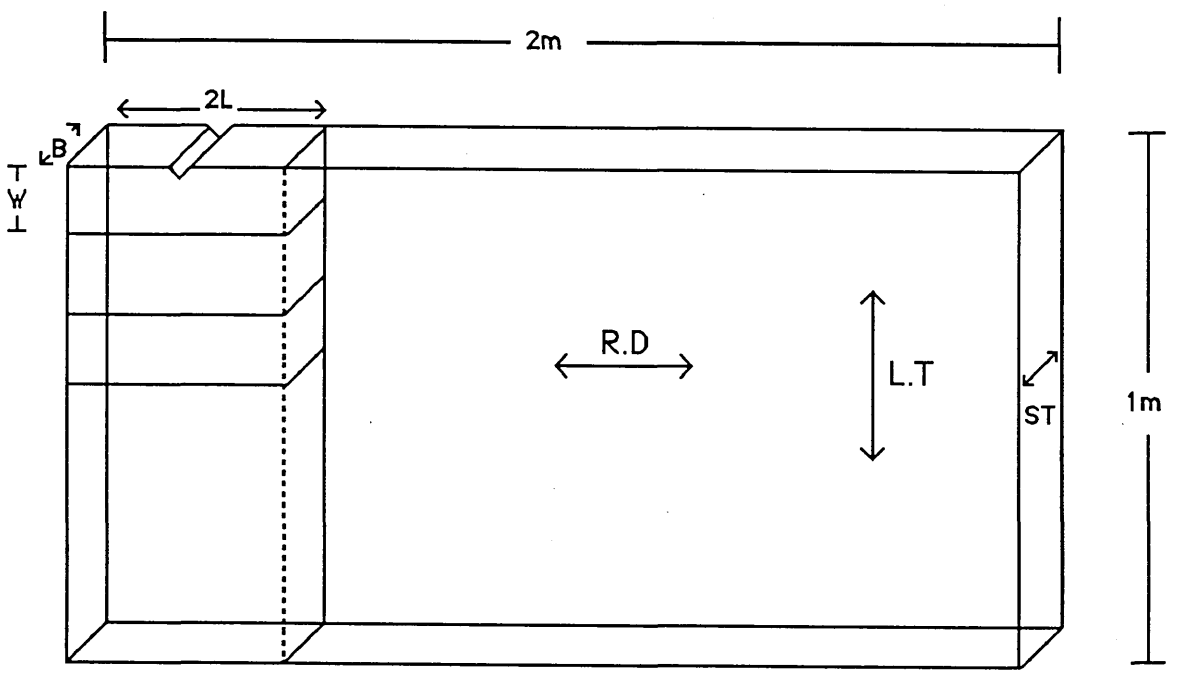


50D Steel Plate

Fig 8.3

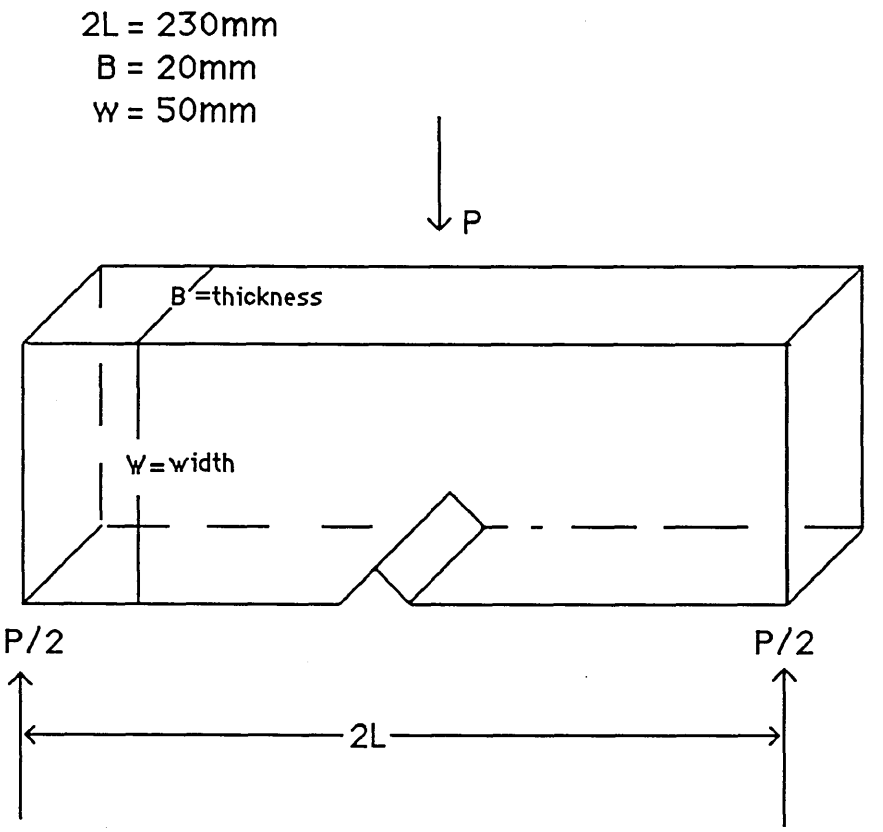


Three-Point Bend Specimen Subject To Fatigue Cracking

Fig 8.4

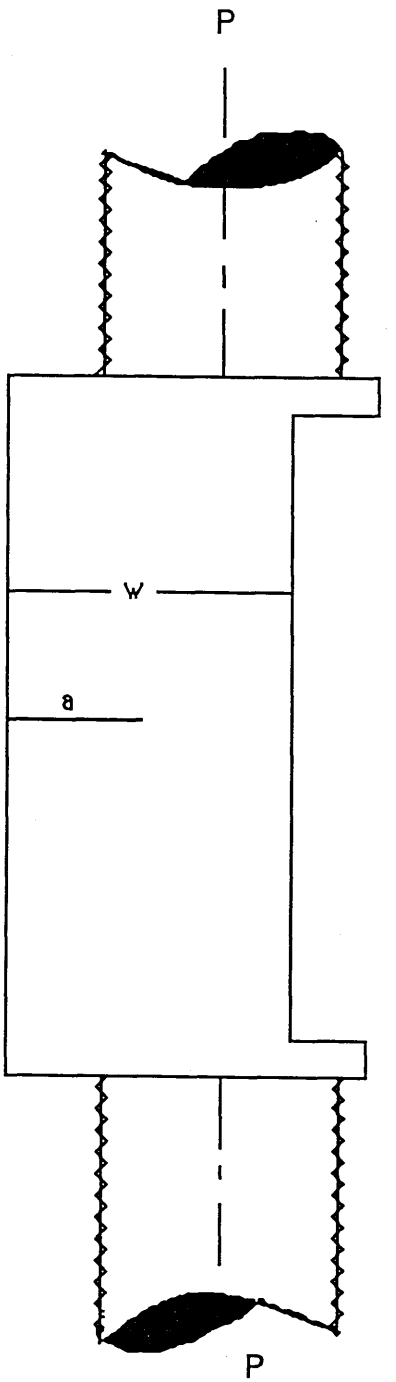


P: Load Applied

w: Width =20mm

a: Crack Length=10mm

Laboratory Specimen Subjected To Tensile Force

Fig 8.5

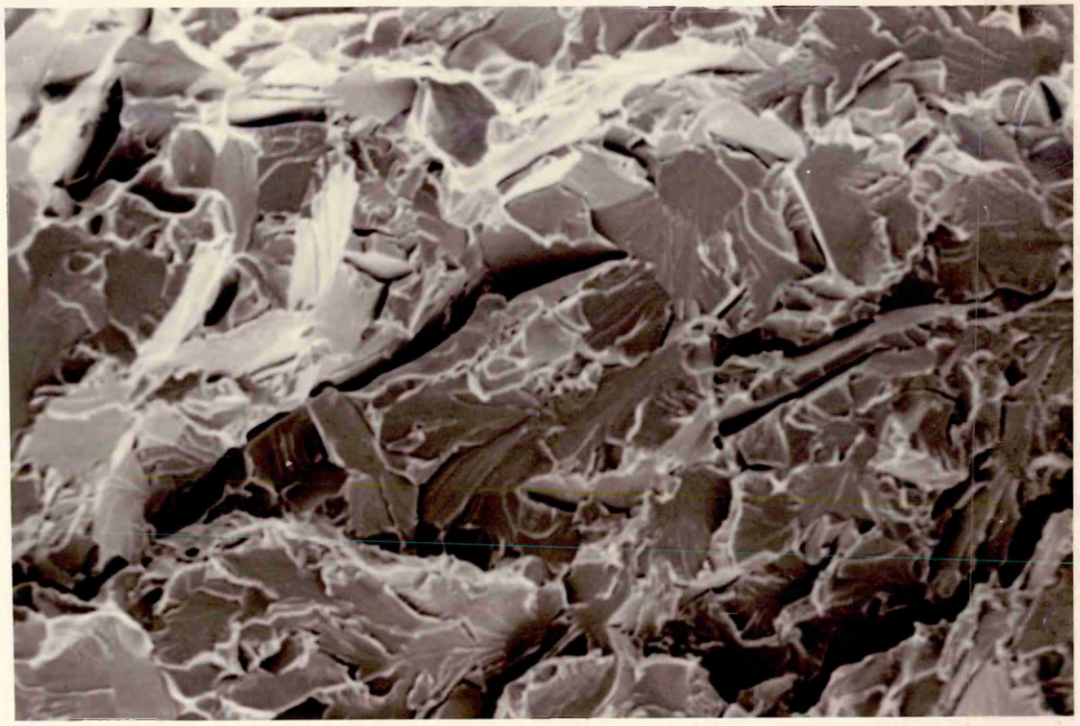

(a) Photographic Representation of The Cleaved Surface.

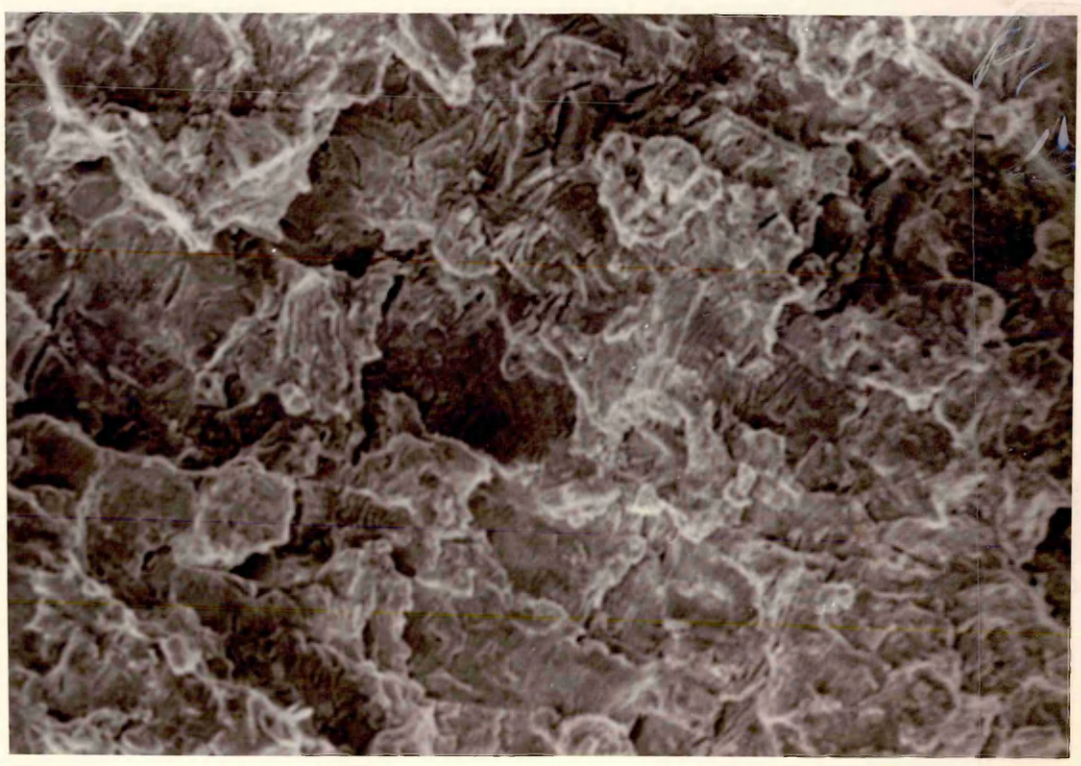


(b) Photographic Representation of the Fatigue Surface

Fig 8.6


Photographic Representation at Inception of Crack Extension

Fig 8.7

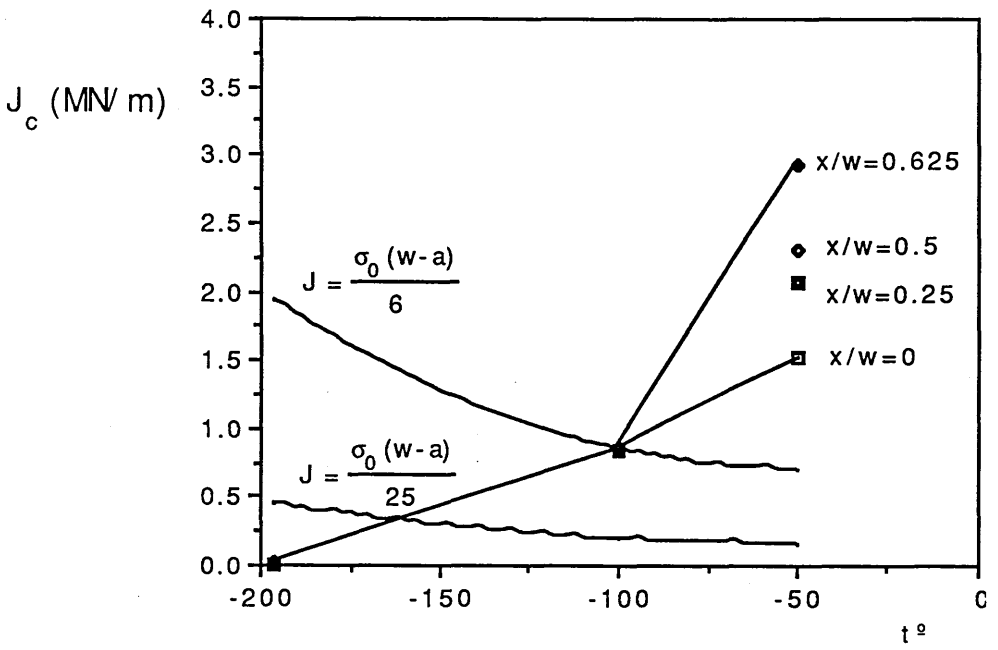


$J_c$ as a Function of Temperature

Fig 8.8

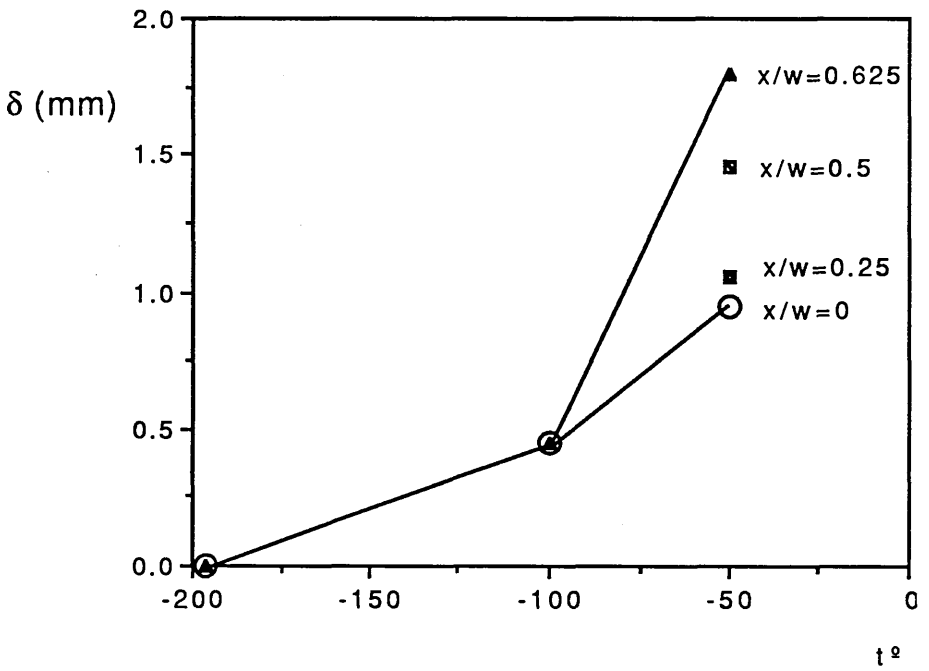


Crack Tip Opening Displacement as a Function of Temperature

Fig 8.9

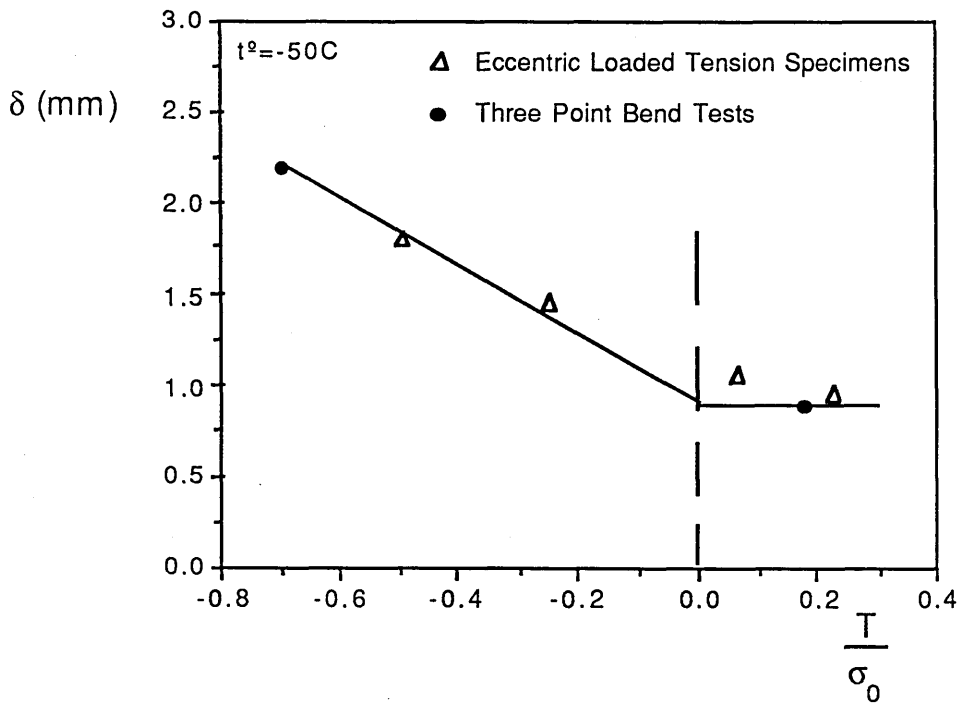


Crack Tip Opening Displacement as a Function of Non-dimensionalised T-Stress

Fig 8.10

# 9 Elastic Analysis of Semi-Elliptical Cracks in Finite Thickness Plates Subject to Pure Bending.

## 9.1 Introduction

Arguably the most common flaws in engineering components are semi-elliptical surface cracks. It is therefore necessary to extend the two parameter characterisation of linear elastic fracture mechanics to deal with such defects. In the present work, a wide plate with dimensions shown in Fig 9.1 was analysed following tests performed by Sumpter (1990). The specimen was a steel plate designated Q1 under B.S. 4360 with a yield stress $\sigma_0$=580 MN/m$^2$. The plate contained semi-elliptical cracks of different geometries.

The elastic analysis to determine K and T, consisted of loading the specimen on the remote boundaries with a uniformly distributed bending moment using the finite element code Abaqus (1982). Stress intensity factors K and biaxiality parameters $\beta$ were obtained, by firstly considering a constant ratio of crack depth a to surface half length c (a/c = 0.2) and a constant ratio of crack depth to plate thickness t (a/t = 0.092) . Subsequent analyses maintained (a/c) constant and varied (a/t) to determine the effect of (a/t) on the stress intensity factors K and the corresponding biaxiality parameters $\beta$ for each section of the crack. In addition, the stress intensity factors K and the biaxiality parameters $\beta$ at the maximum depth were obtained as a function of a/t. The present results obtained from the techniques used to

determine the stress intensity factors are compared with available published solutions.

## 9.2 Numerical Methods

A wide range of methods are available for the determination of stress intensity factors, including three dimensional finite element analysis (Raju and Newman, 1979), the use of boundary integral equations (Hellot and Labbens, 1979), or generalised weight function methods (Oore and Burns 1979). In the present analysis, the crack was modelled by the line spring concept proposed by Rice and Levy (1972) as implemented in Abaqus (1982). Simply stated, the line spring method can be interpreted by considering a plate subjected to general loading on the remote boundaries consisting of a force and a moment as illustrated in Fig 9.2. The remote forces and moments produce local forces $F_x$ and moments $M_x$ which act though each section x of the uncracked ligament. In addition, these local forces and moments will produce displacements $\delta_x$ and rotations $\theta_x$ of the cracked section of the plate. The relationship between $F_x$, $M_x$, $\delta_x$ and $\theta_x$ is of the form :

$$\begin{bmatrix} F(x) \\ M(x) \end{bmatrix} = \begin{bmatrix} S_{11}(x) & S_{12}(x) \\ S_{21}(x) & S_{22}(x) \end{bmatrix} \begin{bmatrix} \delta(x) \\ \theta(x) \end{bmatrix} \qquad 9.1$$

Here, [S] is the local stiffness matrix. The surface crack can be then represented as a number of generalised line springs acting through a discontinuity in a two dimensional plate or shell. The stiffness $S_{ij}(x)$ of each cracked section can be identified with that

of a single edge crack subjected to the appropriate combination of tension and bending.

The mesh of a symmetrical quarter of the model illustrated in Fig 9.3, used 300 eight-noded shell elements consisting of 961 nodes and 1921 degrees of freedom. Young's modulus was taken to be $2.1*10^{11}$ and Poisson's ratio 0.3. The crack shape was taken as that of a semi-ellipse with equation :

$$\frac{x^2}{a^2} + \frac{z^2}{c^2} = 1 \qquad (x \geq 0) \qquad 9.2$$

Here, a is the maximum crack depth, c is the surface crack half length, and x the coordinate of each node in the line spring.

## 9.3 Stress Intensity Factors

The stress intensity factor at any point along the semi-elliptical crack is given in the form :

$$K = \sigma^t \sqrt{\frac{\pi}{Q} a} \quad f\ (\ a/t,\ a/c,\ \phi\ ) \qquad 9.3$$

In this equation, a is taken as the maximum crack depth. Q is the shape factor for an ellipse which is defined as the square of the complete elliptical integral of the second kind as described by Green and Sneddon (1959). Q is geometry dependent and is given by :

$$Q = 1 + 1.464\ (\frac{a}{c})^{1.65} \qquad 9.4$$

The applied stress $\sigma^t$ in the present analysis was taken to be the total reaction force on the remote boundaries, obtained from the finite element calculations over the appropriate area t.w, where t is the thickness and w the width :

$$\sigma = \frac{\Sigma F}{t\ w} \qquad 9.5$$

In equation 9.3, f (a/t, a/c, $\phi$) is defined as the boundary correction factor and is function of the crack depth a, the crack length c, the thickness of the specimen t, and the parametric angle of the ellipse $\phi$. The angle $\phi$ was defined as :

$$\phi = \tan^{-1} \left( \frac{z}{x} \right) \qquad 9.6$$

The results obtained from the finite element calculations provided the magnitude of the stress intensity factor K and the corresponding elastic strain energy rate for each section of the crack. The K values were then non-dimensionalised in terms of the boundary correction factor f(a/t, a/c, $\phi$ ). The parametric angle of the ellipse, $\phi$ was non-dimensionalised by $\pi/2$. For a/c=0.2 and a/t=2, the variation of the stress intensity factor K along the crack as a function of the angle $\phi$ is illustrated in Fig 9.4 together with the published solution of Raju and Newman (1979). By fixing a/c=0.2 and varying a/t from a/t=0.092 to a/t=0.8, further analyses were performed to investigate the effect of the ratio a/t on the stress intensity factors K as the crack became less deep. This is illustrated in Fig 9.5. Interest was centred on the stress intensity factor K at the maximum crack depth ($\phi = \pi/2$) for each ratio a/t. The resulting stress intensity factor K as a function of a/t is illustrated in Fig 9.6. Two available data points from Raju

and Newman (1979) at a/t=0.2 and a/t=0.8 for maximum depth are compared with the present results and tabulated in Table1.

## 9.4 Biaxiality Parameters ß

In order to determine the biaxiality parameters ß corresponding to the stress intensity factors evaluated in the previous section, a single edge cracked bar subject to a combination of uniform distributed tensile loading and moment on the remote boundaries for a range of a/w ratios was considered. For this problem, the non-dimensionalised stress intensity factors K and the corresponding biaxiality parameters ß are given by Sham (1989) using a higher order weight function method. The local forces and moments at each section of the crack were given in the finite element calculations in terms of force per unit crack length and moment per unit crack length respectively.
The results for the tension case are related in the following form :

$$\frac{T_t}{\sigma_{nom}} = \lambda_t \varepsilon_t \qquad 9.7$$

The present notation in which the suffix t refers to tension, $\lambda_t$ is the non-dimensionalised stress intensity obtained for a single edge cracked bar under pure tension :

$$\frac{K}{K_0} = \lambda_t \qquad 9.8$$

The generalised form of $\lambda_t$ is given by :

$$\lambda_t = 1.12-0.23(\frac{a}{w})+10.6(\frac{a}{w})^2-21.7(\frac{a}{w})^3+30.4(\frac{a}{w})^4 \qquad 9.9$$

The above Eq is accurate to within 1% for a/w ≤ 0.6 (Rooke and Cartwright 1976). In Eq 9.8, $K_0$ has the familiar form :

$$K_0 = \sigma\sqrt{\pi a} \qquad 9.10$$

The corresponding $\varepsilon_t$ term from Eq 9.7 (Sham 1990) is related to the $T_t$-stress from the tension case by the relation :

$$\varepsilon_t = \frac{T_t\sqrt{\pi a}}{K} \qquad 9.11$$

From Eq 9.7, $\sigma_{nom}$ is obtained from the finite element calculation in the form :

$$\sigma_{nom} = \frac{S_{11}}{t} \qquad 9.12$$

Here, $S_{11}$ is the derivative of force with respect to the distance along the crack front and is given by :

$$S_{11} = \frac{\partial F}{\partial x} \qquad 9.13$$

Similarly for the bending case :

$$\frac{T_b}{\sigma_{nom}} = \lambda_b\,\varepsilon_b \qquad 9.14$$

The notation above in which the suffix b refers to bending, $\lambda_b$ is the non-dimensionalised stress intensity factor obtained by analysing a single edge crack bar under pure bending (Sham 1989) and derived from :

$$\frac{K}{K_0} = \lambda_b \qquad 9.15$$

The generalised form of $\lambda_b$ is given as :

$$\lambda_b = 1.12-1.39(\frac{a}{w})+7.32(\frac{a}{w})^2-13.1(\frac{a}{w})^3+14.0(\frac{a}{w})^4 \qquad 9.16$$

The Eq above is accurate to within 1% for a/w $\leq$ 0.6. Now from Eq 9.14, $K_0$ has the form :

$$K_0 = \frac{6M\sqrt{\pi a}}{w^2} \qquad 9.17$$

where M is the bending moment per unit thickness. The corresponding $\varepsilon_b$ for the bending case in Eq 9.14 is related to the $T_b$-stress by the relation :

$$\varepsilon_b = \frac{T_b\sqrt{\pi a}}{K} \qquad 9.18$$

From Eq 9.14 $\sigma_{nom}$ was also obtained from the finite element calculations as :

$$\sigma_{nom} = 6\frac{S_{22}}{t.B} \qquad 9.19$$

The term $S_{22}$ is defined as the moment derivative with respect to the distance given in the form :

$$S_{22} = \frac{\partial M_{(x)}}{\partial x} \qquad 9.20$$

To evaluate the T-stress for a semi-elliptical crack in a plate subjected to general loading it is necessary to note that for a given a/c and a/t, each section of the crack experiences a force and a moment and consequently produces a $T_t$-stress term corresponding to tension and a $T_b$-stress term corresponding to bending. The summation of the two terms produces the T- stress for each depth of the crack. In the present work, the T-stress at a given crack depth is evaluated in a non-dimensionalised way as :

$$\beta = \frac{T\sqrt{\pi a}}{K} \qquad 9.21$$

where K is the stress intensity factor at that depth and a is the maximum crack depth. To show the effect of the crack depth on the biaxiality parameter ß, a graphical illustration of ß as a function of $2\phi/\pi$ is given in Fig 9.7.
By fixing a/c=0.2 and varying a/t from a/t=0.092 to a/t=0.8, the resulting graph showing ß as a function of $2\phi/\pi$ is given in Fig 9.8. In addition, the biaxiality parameter ß obtained at the maximum crack depth is given as a function of a/t Fig 9.9.

## 9.5 Discussion and Conclusions.

The technique used in the present analysis to evaluate stress intensity factors K involved the use of line spring elements proposed by Rice and Levy (1972). This computational technique

offered the advantage of computational efficiency by the use of a two-dimensional model with appropriate boundary conditions. The stress intensity factor K obtained as a function of the parametric angle of the ellipse $\phi$ for a/c=0.2 and a/t=0.2 as shown in Fig 9.4 was compared with the results provided by Raju and Newman (1979). These authors used the three dimensional finite element technique which consisted of using nodal forces normal to the crack plane and ahead of the crack front. Their method required that no prior assumption of either plane strain or plane stress was required.

The results shown in Fig 9.4 implied that general agreement was reached and that the present method used, was appropriate.

It is observed from Fig 9.5 that when the crack became deeper, the magnitude of K (corresponding to a/t=0.092 through a/t=0.368) increased until it reached a non-dimensionalised angle of $2\phi/\pi \approx 0.4$ when the magnitudes of K remained relatively constant up to the deepest point. For a/t=0.5, the K values were relatively constant along each section of the crack. However, when a/t was greater than 0.5, the K values of the crack tended to decrease in size as the crack became deeper. The effect of a/t ratio on the stress intensity factors at the maximum crack depth, illustrated in Fig 9.6, indicated that when a/t became deeper, the stress intensity factor decreased in magnitude.

The graph illustrated in Fig 9.7 shows the values of the biaxiality parameters ß as a function of the crack depth. Here again, it was noticed that when the crack depth became deeper, the biaxiality parameters ß tended to become more negative. By maintaining a/c=0.2 and varying a/t between 0.092 and 0.8, as

shown in Fig 9.8, it may be noted that for cracks with a/t $\leq$ 0.5 the resulting biaxialities vary weakly, while for a/t $\geq$ 0.5 the positive biaxiality parameters decreased in magnitude when the crack became deep.

Subsequently, importance was attached to the values of the biaxialities at the maximum crack depth and the influence that a varying a/t could have on these values. This is clearly shown in Fig 9.9. Here, it is seen that when a/t increased from 0.092 to 0.368, the corresponding biaxiality parameters ß became less negative until a/t$\approx$0.368, when ß=0. When the ratio a/t > 0.368, the resulting ß values increased. It is interesting to note that the behaviour of the curve shown in Fig 9.9 is similar to that of single edge cracked bars with the same a/w ratios subject to bending. The numerical data given on this figure were reproduced from Sham (1989). This author analysed single edge cracked bars under pure bending for a range of a/w ratios. Here, the ratios a/t for semi-elliptical cracks analysed in the present work correspond to the a/w ratios in Sham's analyses. The results indicate that when the ratio a/t < 0.368 (a/w < 0.4 for single edge cracked bars), the magnitudes of the biaxiality parameters ß for semi-elliptical cracks are exactly the same as those of single edge cracked bars and are negative (corresponding to compressive T-stresses), and becoming less negative as the ratios a/t varied between 0.1 and 0.368. However when a/t=0.368 (a/w=0.4 for single edge cracked bars), ß=0 for semi-elliptical cracks. Importance was focussed on biaxiality parameter values for a/t $\geq$ 0.368. Here, biaxiality magnitudes for semi-elliptical cracks exhibited greater values than those of single edge cracked bars for the same a/w ratio and

were positive, corresponding to tensile T-stresses. As the ratio a/t increased the biaxiality values tended to become more positive and the difference between the biaxiality magnitudes for semi-elliptical cracks and single edge cracked bars, increased.

As a conclusion it may be noted that the use of simple finite element techniques based on elastic line springs has been developed and allowed direct determination of the biaxiality parameter $\beta$. Confidence can be placed in the method as the K values obtained agreed well with the full three dimensional solutions of Raju and Newman (1979).

W=width
B=thickness
H=height
2c=surface crack length

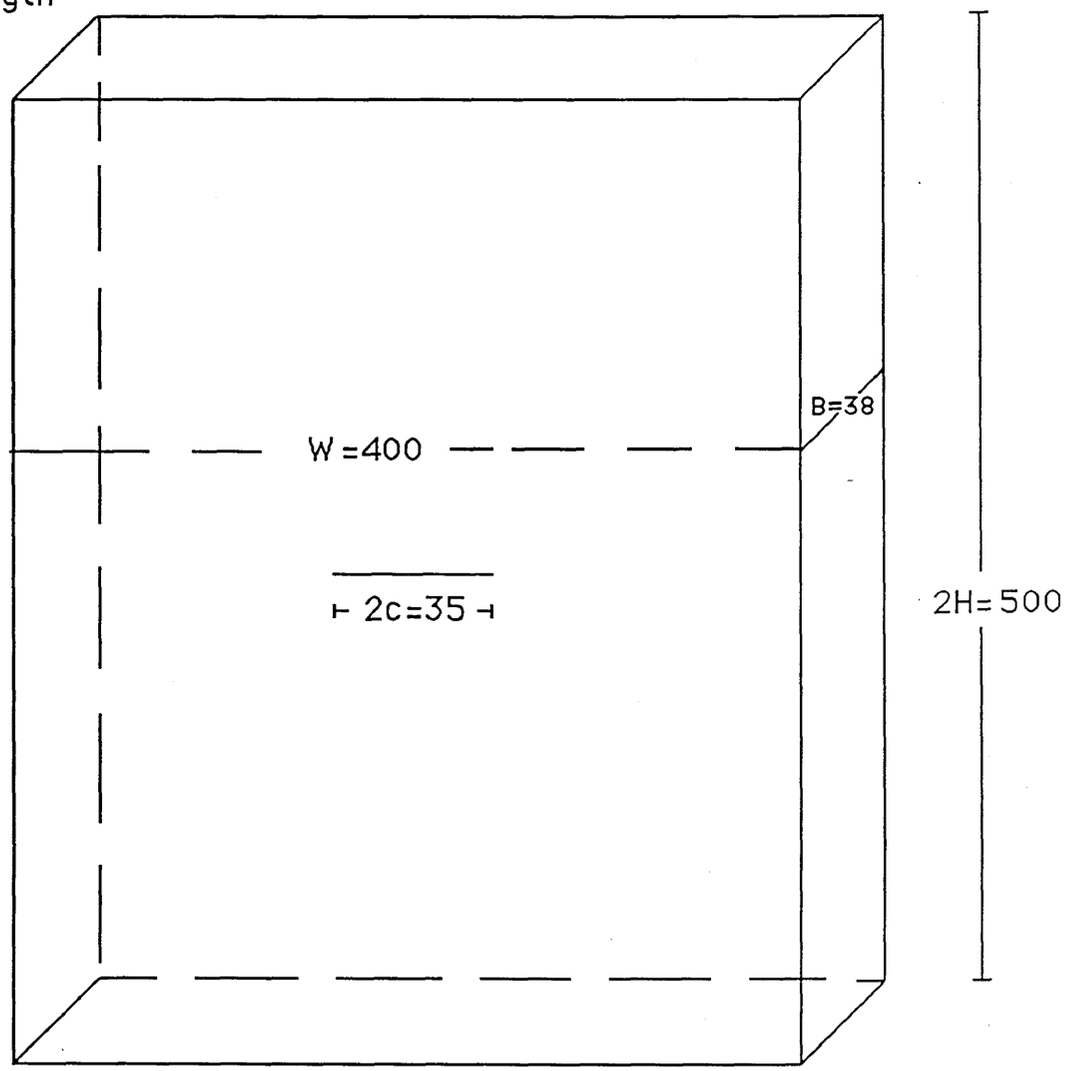


A schematic representation of a plate containing a semi-elliptical surface crack.

Fig 9.1

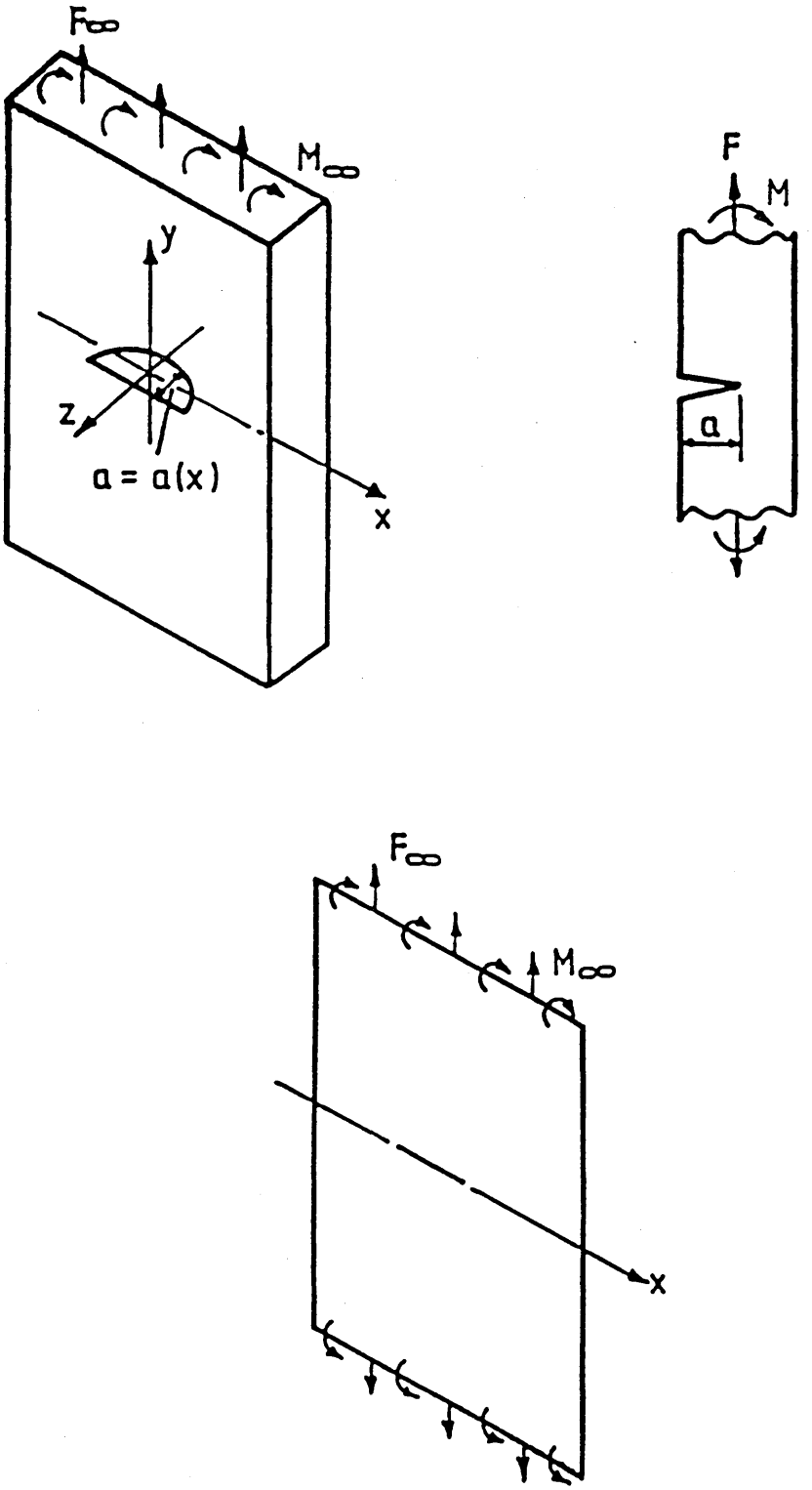


The line spring model of Rice and Levy

Fig 9.2

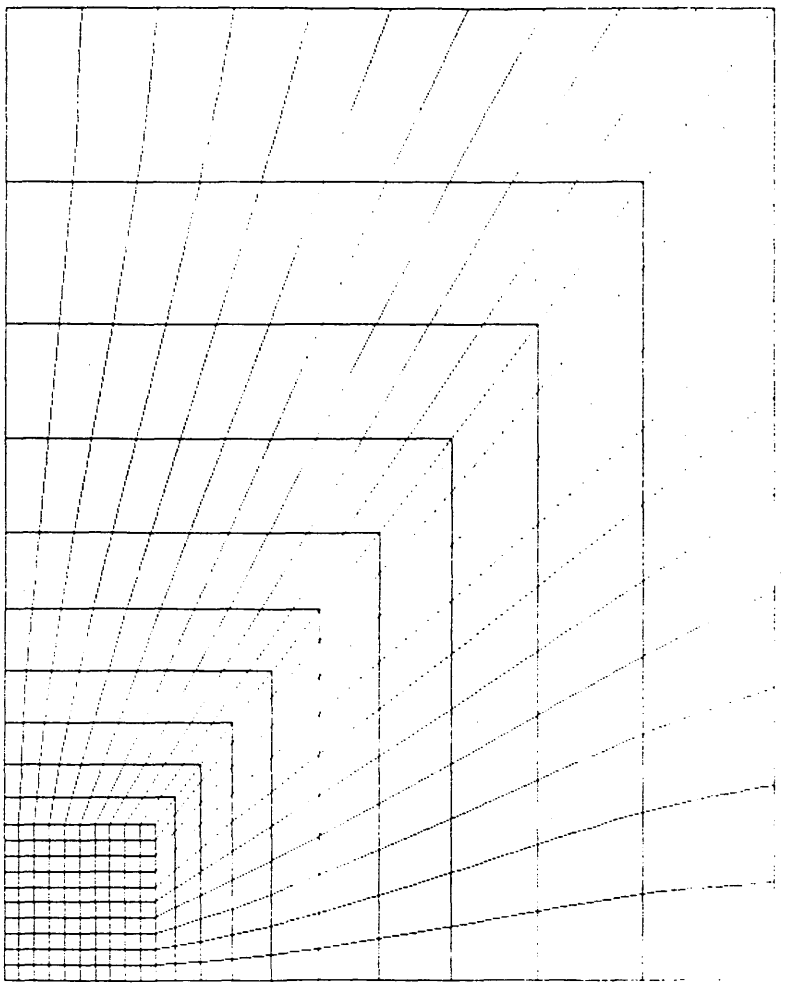

Finite Element Mesh with a/c=0.2

Fig 9.3

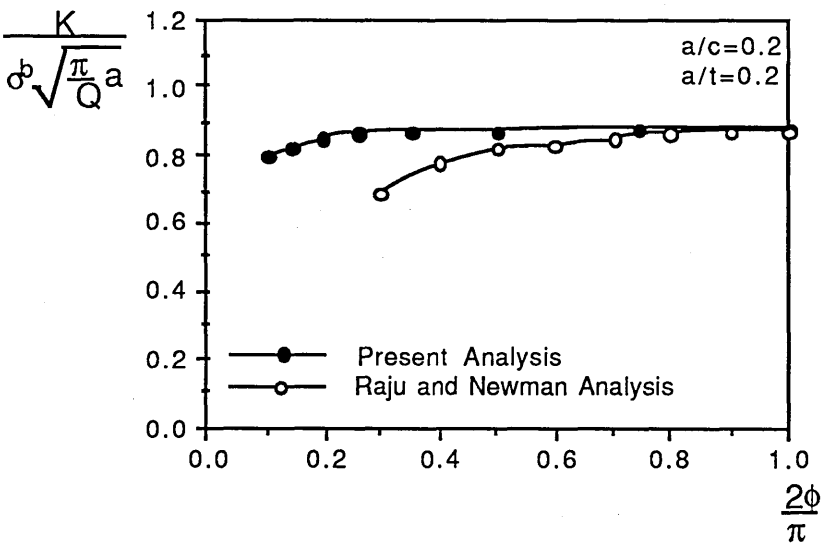


Stress Intensity Factor K as a Function

Of The Crack Depth $\phi$

Fig 9.4

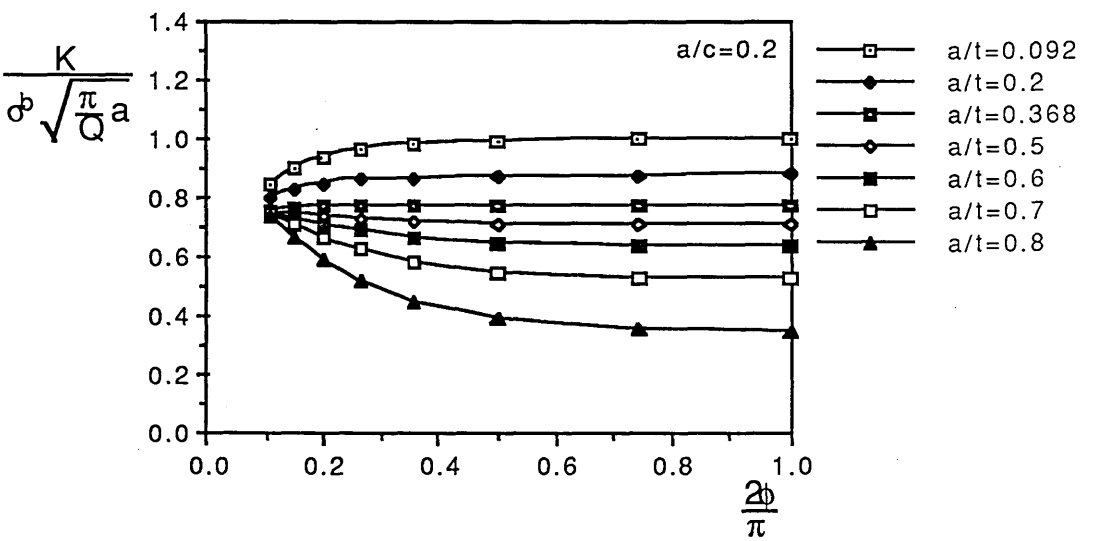


Stress Intensity Factor as a Function of

The Depth For a Wide Range of a/t ratios

Fig 9.5

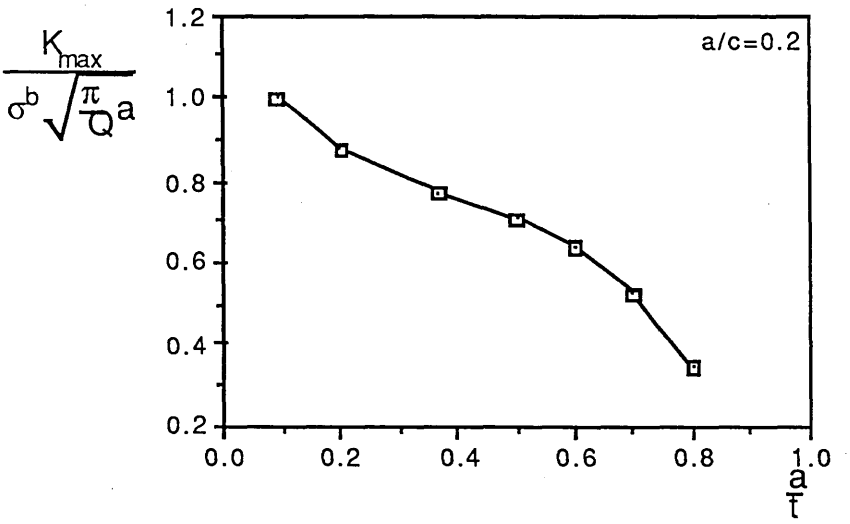


Stress Intensity Factor K At The Maximum Crack Depth For a Range of a/t Ratios

Fig 9.6

| a/t | $K_{max}$ | $K_{max}$ (Raju and Newman) |
|---|---|---|
| 0.098 | 1.001 | |
| 0.2 | 0.878 | 0.870 |
| 0.368 | 0.774 | |
| 0.5 | 0.709 | |
| 0.6 | 0.634 | |
| 0.7 | 0.523 | |
| 0.8 | 0.345 | 0.320 |

Table 1

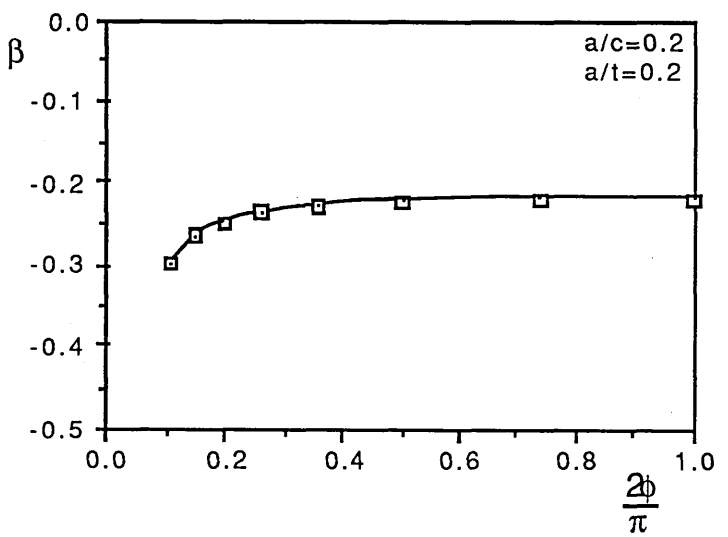


Biaxiality parameter ß as a Function of The Crack Depth

Fig 9.7

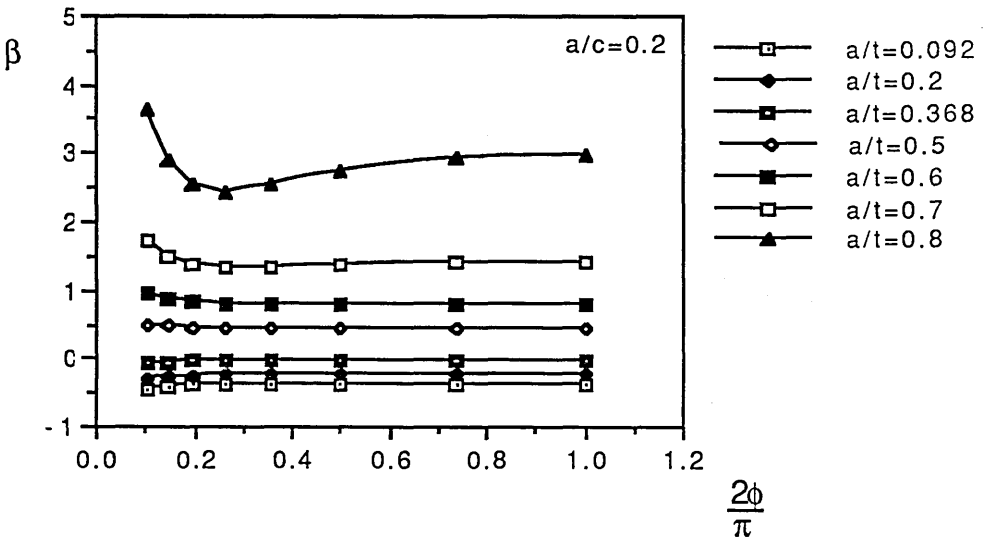


Biaxiality Parameter β as Function of the Crack Depth For a Range of a/t Ratios

Fig 9.8

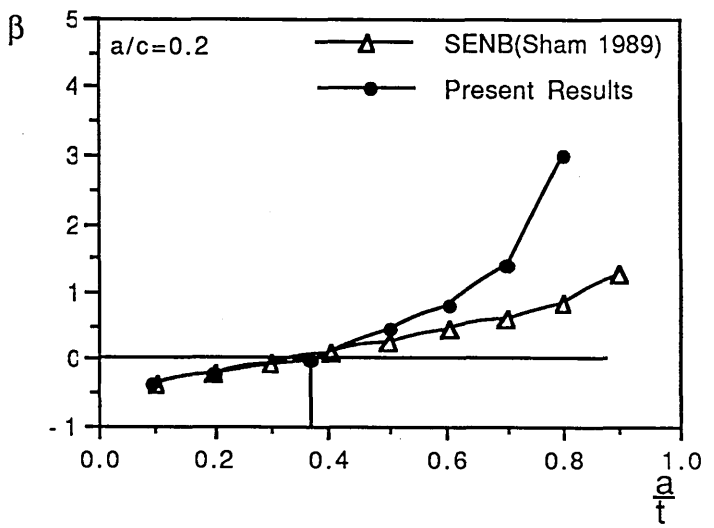


Biaxiality Parameter ß as a Function of ratio a/t

Fig 9.9

## 10 Conclusions

Methods for the determination of the elastic K and T parameters were benchmarked. The vitual crack extension method was found to be the best method in determining the stress intensity factor K. The stress method was found to be most appropriate for the determination of T.

In order to establish failure criteria in the form of a C.T.O.D-T locus, single edge cracked bars subject to eccentric tensile loads and capable of producing combined tension and bending in the ligament, were analysed under elastic conditions with the help of finite element methods. The analyses provided a relationship between the T-stress, the load applied and the geometry of the specimen. Subsequent finite element analyses were performed under elastic-plastic conditions. These analyses allowed a relationship between the fracture toughness J (or equivalently C.T.O.D) and the load applied.

Tests performed on single edge cracked bars, of B.S. 4360 grade 50D steel, subject to eccentric tensile loads showed that L.E.F.M size requirements were satisfied at -196C allowing fracture characterisation by K. Single parameter characterisation of failure by J was possible at -100C when cleavage was proceded by extensive plasticity. For higher temperatures at which failure occured by ductile void growth and coalescence, J-dominance was lost and the newly developed two parameter fracture criterion based on C.T.O.D and T was verified.

The line spring finite element technique used in the determination of K, for realistic engineering defects in simple

geometries, was verified in comparison with benchmark values. This technique was extended further to determine T.

| | | |
|---|---|---|
| Abaqus. | 1982 | User's Manual., Hibbit,Karlsson and Sorensen., Inc. Providence. Rhode Island. |
| Airy, G. B., | 1862 | Brit. Assoc. Advance, Sci. Rept. |
| Al-Ani | 1991 | Private communication. |
| Al-Ani, A. M., and Hancock, J. W., | 1991 | J. of the Mech. and Phys. of Solids. vol 39, pp 23-43. |
| A.S.T.M, | 1970 | American Society for Testing and Materials. Philadelphia, U.S.A. Pt 31, p 911. |
| A.S.T.M, | 1974 | Standard Method for Plane Strain Fracture Toughness Testing., E399-74. |
| Barsoum, S., | 1976 | Int. J. Num. Mech. Eng., vol 110, pp 25-37. |
| Begley, J. A., and Landes, J. D., | 1971 | A.S.T.M. S.T.P 514, American Society For Testing and Materials., pp 1-23 and 24-39. |
| Begley, J. A., and Landes, J. D., | 1976 | Int. J. of Fracture Mech., vol 12, pp 764-766. |
| Bennett, P.E., and Sinclair, G.M., | 1966 | J. Basic Eng., Trans. A.S.M.E Series D vol 88, pp 518-524. |
| Betegón, C., | 1990 | Ph.D Thesis, University of Oviedo, Spain. |
| Betegón, C., and Hancock, J. W., | 1990 | J. App. Mech., In Press. |

| | | |
|---|---|---|
| Bilby, B. A., Cottrell, A. H., and Swinden, K. H., | 1963 | Proc. Roy. Soc., A 272, p 304. |
| Bilby, B. A, Cardew, G. E., Goldthorp, M. R., | 1986 | In Size Effects in Fracture, Int. Mech. Eng., pp 37-46. |
| Blackburn, W.S., | 1972 | Proc. Conf. On " Maths of Finite Elements and Applications." Publisher name will be provided. |
| Bowie, O. L., | 1964 | J. App. Mech., vol 31, pp 208-212. |
| B. S, 5477 | 1978 | The Brtitish Institution. |
| Cherepanov, G. P., | 1967 | J. App. Math. Mech., vol 13, p 503. |
| Du, Z. Z. and Hancock, J. W., | 1990 | J. Mech. Phys. and Solids. In Press |
| Dugdale, D.S, | 1960 | J. Mech. Phys. and Solids vol 8, pp 100-104. |
| Dugdale, D.S., and Ruiz, C., | 1971 | Elasticity for Engineers McGraw Hill, London. |
| Durelli, A. J., | 1967 | Applied Stress Analysis Prentice Hall, International, Inc, London. |
| Ernst, H. A., | 1983 | In A.S.T.M. S.T.P. 701, American Society for Testing and Materials. pp 499-519. |

| | | |
|---|---|---|
| E.P.R.I., | 1981 | Electric Power Research Institute., Fracture Handbook, N.P., 1931, Project 1237-1 Topical Report. |
| Eshelby, J. D | 1968 | I.S.I Publication, vol 121 pp 13-48. |
| Griffith, A.A., | 1921 | Phil. Trans. Roy. Soc., London, A21, p 163. |
| Hellot, J., and Labbens. R. C., | 1979 | Int. J. Frac., vol 15, pp 197-205. |
| Henshell, D and Shaw, K. G., | 1975 | Int. J. Num. Mech. Eng., vol 19 pp 495-509. |
| Hutchinson, J. W., | 1968 | J. of the Mech. and Phys. of Solids., vol 16, pp 13-21. |
| Hutchinson, J. W., | 1979 | A course On Non-Linear Fracture Mechanics. The Technical University Of Denmark. |
| Hutchinson, J. W., | 1983 | J. of. App. Mech., vol 50, pp1042-1051. |
| Ilyushin, A. A., | 1946 | Prikadnaia Matematika i Mekhanika. P.M.M., vol 10, p 347. |
| Inglis, C. E., | 1913 | Trans. Roy. Inst., Naval Architects, vol 60, p 219. |
| Irwin, G. R., and Kies, J. A., | 1952 | Weld Res Suppl., vol 17, and 95s. |
| Irwin, G.R., | 1957 | J. App. Mech., vol 24., p361. |

| | | |
|---|---|---|
| Kaiser, S. | 1985 | Eng. Frac. Mech., vol 22, pp 737-749. |
| Kfouri, A. P., | 1986 | J. of Fracture vol 30, pp 301-315. |
| Knott, J. F., | 1973 | The Butterworth Group, London. |
| Larsson, S. G., and Carlsson, A. J., | 1973 | J. of the Mech. And Physic of Solids, vol 21, pp 263-278. |
| Leevers, P.S., and Radon, J. C., | 1983 | Int. J. of Fracture., vol 19, p 311-325. |
| Levy, N., and Marcal, P. V., | 1971 | Int. J. of Fracture. Mech. vol 7, p143. |
| Li, Y., and Wang, Z., | 1986 | Scientia Sinica (Series A), vol 29, pp 942-955. |
| McClintock, F. A., | 1971 | "Fracture an Advanced Treatise", vol 3, pp 47-55. |
| McClintock, F.A., and Irwin, G. R., | 1965 | A.S.T.M., S.T.P. 381., p 84. |
| McMeeking, R. M., | 1984 | J. of Eng. Materials and Technology, vol 106 pp 278-284. |
| McMeeking, R. M. and Parks., D. m., | 1979 | A.S.T.M. S.T.P.668, Philadelphia, U.S.A., pp 175-194. |
| Oore, M., and Burns, D. J., | 1979 | J. Press. Vess. Tech., vol 102, pp 202-211. |
| Parks, D. M., | 1974 | Int. J. of Fracture., vol 10, pp 487-502. |

| | | |
|---|---|---|
| Patran | 1988 | User Manual, P.D.A. Engineering, California. |
| Prandtl, L. | 1920 | Nachr. Ges. Wiss., Gottingen., p 74. |
| Raju, J. S., and Newman, J. C., | 1979 | Eng. Frac. Mech., vol 11, pp 817-829 |
| Rice, J. R., | 1967 | J. App. Mech., vol 34, pp 287-298. |
| Rice, J. R., | 1968 | Fracture: An Advanced Treatise., vol 2, p 45, Academic Press. N. Y. ed Liebowitz. |
| Rice, J. R., | 1968 | J. App. Mech., vol 35, pp 379-386. |
| Rice, J. R., | 1974 | J. of the Mech. and Physics of Solids., vol 22 pp 17-26 |
| Rice, J. R., and Levy, N., | 1972 | J. App. Mech., vol 39, pp 185-194. |
| Rice, J. R., and Rosengren, G. F., | 1968 | J. of The Mech.and Phys. of Solids. vol 16, pp 1-12. |
| Rice, J. R., Tracy, D. M., | 1973 | In Numerical and Computational Methods in Struct. Mech., Academic Press. New York. |
| Robinson, J. N., | 1976 | Int. J. of Fracture., vol 12, p 723. |
| Rooke, D.P., Cartwright., D. J., | 1976 | Compendium of Stress Intensity Factors., London., H.M.S.O. |

| | | |
|---|---|---|
| Sham, T. L., | 1989 | Dept of Mech Eng., Aero. Eng. and Mech., Internal report, Troy, New York, 12180-3590, U.S.A. |
| Shih, C. F., and German, M. D., | 1981 | Int. J. of Fracture, vol 17, pp 27-43. |
| Shih, C.F., and Hutchinson, J. W., | 1986 | J. App. Mech., vol 53, pp 271-277. |
| Sih, G. C., | 1973 | Handbook of Stress Intensity Factors, Bethlehem, Pennsylvania, Lehigh University. |
| Sumpter, J. D. G., | 1973 | Ph.D Thesis, University of London Press. |
| Sumpter, J. D. G., and Hancock, J. W., | 1990 | Canadian Fracture Conference. ( C.F.C 21), Halifax, Nova Scotia. |
| Tada, H., Paris, P | 1973 | The Stress Analysis of Cracks Handbook, Hellertown, Pennsylvania, Del. Research Corporation. |
| Turner, C. E., | 1973 | Mat. Sci. Eng., vol 11, pp 275-282. |
| Wells, A. A., | 1961 | Crack Propagation Symposium, Cranfield. pp 210. |
| Wells, A. A., | 1963 | British Welding Research Ass. Rep. M13. |
| Williams, M. L., | 1957 | J. App. Mech., vol 24, pp 111-114. |

Westergaard, H. M., 1939 — J. App. Mech., vol 61, pp 449-453.

Westergaard, H. M., 1952 — Theory of Elasticity and Plasticity, Cambridge, Mass., Harvard University Press, New York.